UNIVERSITÉ DE MONTRÉAL

PRODUCTION OF CHITOSAN-BASED NON-WOVEN MEMBRANES USING THE ELECTROSPINNING PROCESS

MEHDI PAKRAVAN LONBANI

DÉPARTEMENT DE GÉNIE CHIMIQUE

ÉCOLE POLYTECHNIQUE DE MONTRÉAL

THÈSE PRÉSENTÉE EN VUE DE L'OBTENTION

DU DIPLÔME DE PHILOSOPHIAE DOCTOR

(GÉNIE CHIMIQUE)

JUILLET 2012

UNIVERSITÉ DE MONTRÉAL

ÉCOLE POLYTECHNIQUE DE MONTRÉAL

Cette thèse intitulée:

PRODUCTION OF CHITOSAN-BASED NON-WOVEN MEMBRANES USING THE ELECTROSPINNING PROCESS

présentée par: PAKRAVAN LONBANI, Mehdi
en vue de l'obtention du diplôme de: Philosophiae Doctor

a été dûment acceptée par le jury d'examen constitué de:

M. DUBOIS Charles, Ph.D., président

Mme. HEUZEY Marie-Claude, Ph.D., membre et directrice de recherche

M. AJJI Abdellah, Ph.D., membre et codirecteur de recherche

M. CARREAU Pierre, Ph.D., membre

M. HATZIKIRIAKOS Savvas, Ph.D., membre

DEDICATION

“To my lovely wife, cheerful son, and beloved family mom, dad, sister and brother”

AKNOWLEDGEMENTS

I vividly remember the day I received the letter of PhD program scholarship from faculty of chemical engineering, Ecole Polytechnique de Montreal, and still recall all the mixed feelings; the joy of stretching out my wings and the sorrow of leaving loved ones behind.

Today I am all again filled with emotions; the excitement of accomplishment and the bliss of contentment. I am certainly blessed to be surrounded by mentors, supervisors, supporters, friends and family who enlightened my growth path and disclosed new horizons ahead. I am grateful and in depth with them all, specially:

Dr. Marie-Claude Heuzey, for supervising my PhD research program, believing in me, supporting and challenging me; my sincere appreciation to you, your patience, enthusiasm toward scientific research and all the productive discussions.

Dr. Abdellah Ajji, my other supervisor for his insightful suggestions, guidance, constructive remarks and sharing his invaluable experience in experimental research. Thank you.

Prof. Pierre J. Carreau, for all his comments and discussion on my work presented in routine rheology meetings and *Prof. Basil Favis* for his inspiring polymer blend course and knowledge.

My special gratitude to the staff and technicians of Ecole Polytechnique de Montreal, chemical engineering department, Industrial Material Institute (IMI), and FPInnovations, for their contribution to this work.

Ladies: Mélina Hamdine, Weawkamol Leelapornpisit, Claire Circlé and Sylvie St. Amoure

Gentlemen: Robert Delisle, Daniel Dumas, Jacques Dufour, Alexis Laforges, and Vincent Darras

My heartfelt thanks to my close friends: Farhad, Amir Hossein, Abbas, Nima, Hesam, Marie, Afra, Shant, Fatemeh and Ahmad.

My beloved parents, Nayereh and Reza for their eternal caring open heart, open arms and their full presence regardless of distance.

Maryam, my love, wife, best friend, and encourager and our little son, Emaad who his charm made it possible throughout the tough times.

And you, the infinite cognition of the existence.

RÉSUMÉ

Le chitosane est un polymère naturel modifié produit à partir de la chitine, un des matériaux organiques le plus abondant dans la nature. Les applications biomédicales du chitosane tels que les échafaudages en génie tissulaire et les pansements d'aide à la cicatrisation ont beaucoup attiré l'attention ces derniers temps en raison de l'origine naturelle du chitosane et ses propriétés exceptionnelles telles que la biodégradabilité, la biocompatibilité et la non-toxicité. Les mats nanoporeuses de chitosane présentent les propriétés physico-chimiques spécifiques du matériau de base et bénéficient aussi des caractéristiques physiques de ces membranes en raison de leur morphologie et de grande surface spécifique. Réaliser ces structures en satisfaisant à des exigences essentielles telles que la flexibilité et une porosité élevée reste toujours difficile. L'électrofilage est une nouvelle technique développée récemment pour générer des fibres de polymères de taille nanométrique. Grâce à cette technique, des mats non-tissés poreux ayant une surface nettement élevée par rapport à la masse (généralement de 40 à 100 m^2/g) sont produits. Toutefois, la capacité d'électrofiler le chitosane est limitée principalement en raison de sa nature polycationique et de sa structure chimique rigide. Plusieurs démarches entreprises pour préparer des nanofibres électrofilées de chitosane n'ont pas réussi car les membranes préparées sont facilement dissoutes dans des solvants aqueux neutres et faibles acide, les propriétés des nanofibres sont affaiblies à cause de l'importante quantité de l'agent de co-électrofilage ou parce que les procédés utilisant des solvants nocifs dont les résidus peuvent se retrouver dans le produit final sont des préoccupations importantes.

Le but de ce travail est de fabriquer des membranes microporeuses non-tissées à base de nanofibres de chitosane pour des pansements de cicatrisation et pour filtrer les ions métalliques lourds de l'eau potable. Par conséquent, la préparation de nanofibres à haute teneur en chitosane à partir de solutions aqueuses est un objectif à atteindre pour ces applications. Dans cette thèse, deux approches ont été utilisées pour préparer les nanofibres à base de chitosane: l'électrofilage d'un mélange d'une solution de chitosane avec une solution facilement électrofilable telle qu'une solution aqueuse d'oxyde de polyéthylène (PEO) – et l'électrofilage co-axial des deux solutions.

Par conséquent, l'interprétation du comportement des phases et la miscibilité des solutions aqueuses acides de chitosane et de PEO et leurs mélanges est d'une importance cruciale,

puisqu'une séparation de phases ayant lieu pendant le procédé d'électrofilage change grandement la morphologie et les propriétés physico-mécaniques des produits finaux.

Premièrement, l'approche rhéologique a été utilisée sur une solution aqueuse de PEO bien caractérisée pour élaborer le protocole expérimental. En comparant les points critiques observés avec ceux obtenus par d'autres techniques expérimentales, nous avons montré que des mesures rhéologiques peuvent détecter de manière sensible les stades précoces de séparation de phases. Par conséquent, le procédé a été appliqué à des solutions de PEO, de chitosane ou du mélange des deux à différents ratios, dilués dans une solution d'acide acétique à 50% en masse. Ces solutions ont montré une température critique de solubilité inférieure (LCST) sur le diagramme de phase, qui est attribuée à l'existence de liaisons hydrogène entre les groupes actifs du chitosane, la chaîne principale du PEO et le solvant. Les températures de séparation de phase critiques des points binodaux et spinodaux ont été estimées à partir d'expériences isochrones en balayage de température. Les températures binodales obtenues confirment que les solutions de chitosane / PEO sont miscibles et stables à des températures modérées et que la séparation de phases a lieu à des températures plus élevées de 60 – 75 °C.

Alors, nous voulions comprendre de manière approfondie les propriétés de la solution chitosane / PEO qui permet d'obtenir un électrofilage réussi, c'est à dire continu et stable, et qui produit des nanofibres sans défaut et uniformes, des fibres sans relief ou non-perlées. Les effets de la composition du mélange et de la concentration en acide acétique sur les propriétés telles que la tension de surface et la conductivité, sur la possibilité d'électrofiler ces solutions ont été étudiés. Un chitosane fortement désacétylé (DDA = 97,5%) dans une solution d'acide acétique à 50% a été utilisé, c'est le degré le plus élevé de désacétylation du chitosane pour lequel il a été signalé que la préparation de nanofibres de chitosane était possible. Les caractéristiques rhéologiques de la solution de chitosane et de PEO, étant des paramètres importants du procédé d'électrofilage, ont été examinées et leurs relations avec la possibilité d'électrofiler ou non sont été évaluées. Comme nous avons montré que les solutions chitosane / PEO sont miscibles et stables à des températures modérées, un dispositif modifié pour électrofiler à des températures modérées (25-70 °C) a été conçu, permettant d'atteindre une quantité maximale de 90% en masse de chitosane dans des nanofibres non-perlées de chitosane / PEO ayant des diamètres de 60-80 nm de diamètre. Il a également été constaté que l'augmentation du rapport chitosane /

PEO de 50/50 à 90/10 a conduit à une réduction remarquable du diamètre des nanofibres de 123 à 63 nm à température ambiante.

En outre, nous avons constaté que des températures de procédé modérées (40-70 °C) aident à stabiliser le processus électrofilage de ces solutions et à produire des nanofibres non-perlées. Cependant, à des températures plus élevées (70-80 °C), le jet électrofilé est devenu instable et des fibres avec une morphologie perlée ont été obtenues. Ce phénomène a lieu dans une même gamme de températures que celle de la séparation de phases, déterminée précédemment par des études rhéologiques. Donc, la séparation de phases des solutions induite par la température est considérée comme à l'origine de cette observation. D'autre part, une étude par spectroscopie infra rouge à transformée de Fourier (FTIR) sur des films obtenu par évaporation du solvant et des nanofibres du mélange chitosane / PEO obtenues à la température ambiante a montré la présence d'interactions par liaison hydrogène entre le chitosane et le PEO. Ceci pourrait être une autre indication de la miscibilité entre ces deux polymères en solution à des températures modérées.

Enfin, afin d'éliminer l'étape de mélange, et pour réduire la quantité de chitosane utilisé et positionner le chitosane sur la surface extérieure des nanofibres en vue des applications visées, la technique d'électrofilage coaxial a été utilisée. En utilisant le procédé en une étape d'électrofilage coaxial, des nanofibres avec une structure cœur-enveloppe de PEO / chitosane ont pour la première fois été produites à partir de solutions aqueuses, le chitosane étant l'enveloppe (couche extérieure) et le PEO le cœur (couche intérieure). Des nanofibres uniformes et sans défauts de 100-190 nm de diamètre ont été produites. La nanostructure cœur-enveloppe et la présence de chitosane à la surface ont été confirmées par des images TEM obtenues avant et après le lavage à l'eau du PEO contenu. La présence du chitosane à la surface des nanofibres composites a aussi été confirmée par des analyses XPS. L'analyse de la composition, de manière générale ou locale, a été effectuée par thermogravimétrie (TGA) et par FTIR, respectivement, pour examiner l'homogénéité des nanofibres. De plus, il a été montré que les nanofibres de chitosane creuses ont pu être obtenues par l'extraction du PEO dans les nanofibres coaxiales de PEO / chitosane, ce qui pourrait être d'un grand intérêt dans des applications comme la purification du sang en hémodialyse.

ABSTRACT

Chitosan is a modified natural polymer mainly produced from chitin, one of the most abundant organic materials in the world. Highly porous chitosan mats present the specific physicochemical properties of the base material and also benefit from the physical characteristics of nanoporous membranes. Electrospinning is a novel technique developed long time ago and revisited recently that can generate polymeric fibers with nanometric size.

The ultimate purpose of this work is to fabricate microporous non-woven chitosan membranes for wound healing dressings and heavy metal ion removal from drinking water. In this dissertation, two approaches have been utilized to prepare chitosan-based nanofibers; blending and co-axial electrospinning of chitosan solution with a readily electrospinnable solution, i.e. an aqueous solution of polyethylene oxide (PEO).

Consequently, understanding the phase behavior and miscibility of aqueous acidic solutions of chitosan and PEO and their blends is of crucial importance, as any phase separation occurring during the electrospinning process greatly changes the morphology and physico-mechanical properties of the final products.

First we employed the rheological approach on a well-known aqueous PEO solution to develop the experimental protocol. By comparing these critical points with that obtained from other experimental techniques, we showed that rheological measurements can sensitively detect early stages of phase separation. Subsequently the method was applied to 50 wt% aqueous acetic acid solutions of PEO, chitosan and their blends at different ratios. These solutions showed a lower critical solution temperature (LCST) phase diagram that is attributed to the existence of hydrogen bonds between active groups on chitosan and PEO backbone and the solvent. Critical decomposition temperatures for binodal and spinodal points were estimated from isochronal temperature sweep experiments. The obtained binodal temperatures confirmed that chitosan/PEO solutions are miscible and stable at moderate temperatures and phase separate at higher temperatures of 60-75 °C.

Then, we intended to obtain a thorough understanding of chitosan/PEO solution properties that lead to a successful electrospinning process, i.e. continuous and stable, and which produces defect free uniform beadless nanofibers. The effect of blend composition and acetic acid

concentration on properties such as surface tension and conductivity and, ultimately, on electrospinnability were investigated. A highly deacetylated chitosan (DDA=97.5 %) in 50% acetic acid was used, which is the maximum deacetylated chitosan grade that has been reported for the preparation of electrospun chitosan-based nanofibers. The rheological characteristics of the chitosan/PEO solutions as a controlling parameter in the electrospinning process were examined and their relationships to electrospinnability presented. As we showed that chitosan/PEO solutions are miscible and stable at moderate temperatures, a modified electrospinning set up to electrospin at temperatures of 25-70 °C was designed to achieve content as high as 90 wt% of chitosan in beadless chitosan/PEO nanofibers of 60-80 nm in diameter. It was also found that increasing chitosan/PEO ratio from 50/50 to 90/10 led to a remarkable diameter reduction from 123 to 63 nm at room temperature.

Additionally, we found that moderate process temperatures help to stabilize the electrospinning process of these solutions and produce beadless nanofibers. However, at higher temperatures, the electrospun jet became unstable and beaded fiber morphology was obtained. This phenomena occurs closely at the temperature range of phase separation, previously determined by rheology studies. Therefore, temperature-induced phase separation of these solutions is considered as the reason for that observation. On the other hand, an FTIR study at room temperature on cast films and nanofibers of chitosan/PEO blends at room temperature showed the presence of hydrogen bonding interactions between chitosan and PEO that could be an another indication of miscibility between these two polymers in solution at moderate temperatures.

Finally, in order to remove the blending step, reducing the amount of chitosan used and also to put chitosan right on the outer surface of the nanofibers for further related applications, a co-axial electrospinning technique was employed. By using a one-step co-axial electrospinning process, for the first time core-shell structured PEO-chitosan nanofibers from aqueous solutions were produced in which chitosan is located at the shell (outer layer) and PEO at the core (inner layer). Uniform sized defect-free nanofibers of 100-190 nm diameter were produced. The core-shell nanostructure and existence of chitosan on the shell layer were confirmed by TEM images obtained before and after washing the PEO content with water. The presence of chitosan on the surface of the composite nanofibers was further supported by XPS studies. Bulk and local compositional analysis is performed by thermal gravimetry (TGA) and Fourier transform infra-red spectroscopy (FTIR) techniques, respectively, to examine the homogeneity of the nanofibers.

Additionally, it was shown that hollow chitosan nanofibers could be obtained by PEO washing of the co-axial PEO/chitosan nanofibers, which could also be of great interest in applications such as blood purification in hemodialysis.

TABLE OF CONTENTS

LIST OF TABLES

TABLE OF FIGURES

CHAPITRE 1

INTRODUCTION

Nanofibrous materials in the form of flat sheet membranes or three dimensional structures provide new solutions and vast opportunities to significantly improve current technologies and to create high value-added products and associated business development. Applications for nanofibers (defined as having diameter less than 0.5 μm) include tissue scaffolds, protective clothing, nanocatalysis, water and air filtration, nanosensors, separation membranes and health care products. Although there are other methods for fabricating nanofibers, none of them can be compared to electrospinning in terms of versatility, ease of fiber production and flexibility.

Electrospinning is a novel and simple technique to generate polymeric fibers with nanometric size. Using this technique, non-woven porous mats with distinctly high surface area to mass ratio (typically 40-100 m^2/g) are produced. The electrospinning technique is generally used to fabricate thin planar flat sheet mats with thickness of 50 to 200 μm. In this process a charged polymer solution flows out of a syringe/needle set up and accelerates toward a collector, mounted at a fixed distance from the needle. Then an electrostatically driven jet of polymer solution forms, elongates and whips until it is deposited on the collector, resulting in formation of non-woven random nanofibers. The prepared non-woven electrospun membranes exhibit remarkable characteristics such as distinctly high specific surface area, high porosity, small pores size and interconnected pore structure. Recent achievements in development of industrial scale electrospinning equipments have opened up the way to fabricate electrospun nanofibers for several applications. Therefore, nowadays research on electrospun nanofibers is not restricted only to academic research labs, but also different companies that are involved in the production of nanofibrous products for superior performance.

As for material selection in several biomedical applications, chitosan is among the most interesting due to its natural origin, non-toxicity, biocompatibility and biodegradability characteristics. Several methods such as phase inversion, phase separation and selective extraction have been used to produce porous chitosan morphologies. Lack of control over porosity and pore size dimensions and extracted phase and solvent residues in the final prepared structures are some negative aspects of these conventional methods. Therefore, microporous

chitosan structures obtained from the electrospinning process have gained much prominence recently. Highly porous electrospun chitosan-based mats present the specific physicochemical properties of the base material and benefit from the physical characteristics of nanoporous membranes because of their morphologies and large specific area. These materials show promising results in several applications such as wound healing dressings, anti-bacterial packaging films, drug delivery systems, scaffolds for tissue engineering and membranes for heavy metal ion absorption.

Chitosan is a modified natural polymer mainly produced from chitin, one of the most abundant organic materials in the world. Existence of $–NH_2$ groups on the chitosan backbone provides several unique properties such as solubility in acidic aqueous solvents, antifungal and antimicrobial properties and ability to chelate with heavy metal ions. However, chitosan is a challenging polymer to electrospin mainly due to its polycationic and rigid chemical structure in solution, and specific inter and intra- molecular interactions. The repulsive forces, arising from the protonation of $–NH_2$ groups, could also restrict the formation of sufficient chain entanglements needed for a successful electrospinning process.

Fabrication of chitosan-based electrospun nanofibers is a crucial step in order to produce the required structures for the above mentioned applications of interest. In this thesis, we aim to develop electrospun chitosan-based nanofibers with maximum chitosan content in stable electrospinning conditions, which can be used in various applications of interest, for example wound healing dressings and membranes for heavy metal ion removal from drinking water.

To achieve that goal, the first part of this thesis is dedicated to provide a clear understanding about miscibility range and phase separation behaviour of chitosan, PEO and their blend solutions for further electrospinning process. To do so, rheological measurements are employed.

Subsequently, electropsinnability of chitosan solutions in the presence of polyethylene oxide (PEO) as a co-spinning material was studied by performing a systematic study to obtain comprehensive knowledge about chitosan/PEO solution properties leading to a successful electrospinning process.

Finally, a one-step co-axial electrospinning set up is used to prepare a novel core/shell structured PEO/chitosan nanofibers with chitosan located on the outer layer.

This dissertation is based on three articles that have been published or submitted to scientific journals and comprised the following sections:

- **Chapter 2** provides a critical literature review considering the related issues and followed by the originality and main objectives of this dissertation.
- The summary and organization of the articles are described in **Chapter 3**.
- The main achievements of the thesis are given in the format of three scientific papers in **Chapters 4, 5 and 6**.
- **Chapter 7** presents a general discussion of the main results.
- Finally **Chapter 8** presents the final conclusions of this work and the recommendations for future work.

CHAPITRE 2

LITERATURE REVIEW

This chapter provides a comprehensive literature review covering many aspects of chitosan nanofiber fabrication which forms the backbone of this research. In Section 2.1 an overview of chitosan as a promising biopolymer that shows a great potential in many biomedical applications is discussed. Section 2.2 focuses on nanofibers and the electrospinning technique, developed a long time ago and revisited recently, to fabricate submicrometer fibers. Section 2.3 deals with nanofibrous chitosan membranes and the electrospinning of chitosan through different routes followed by some applications of chitosan nanofibrous mats. Section 2.4 focuses on phase behaviour of polymer solutions, specifically chitosan and PEO and different methods utilized to determine their phase separation temperatures. Finally, in Sections 2.5 and 2.6 the originality of the work and the main objectives of this dissertation are introduced.

2.1 Chitosan

Chitosan is a modified natural amino-polysaccharide derived from chitin, known as one of the most abundant organic materials in nature. Chitin is the major structural component in the exoskeleton of arthropods and cell walls of fungi and yeast (Pillai, Paul et al. 2009). Commercial chitin is mainly prepared from crab, lobster and shrimp shells which are the massive waste products of seafood industries (Kumar 2000; Rinaudo 2006). Applications for chitin are very limited because of its poor solubility in common solvents resulting mainly from its highly extended hydrogen-bonded semi-crystalline structure (Kumar, Muzzarelli et al. 2004; Pillai, Paul et al. 2009). Thus, chitin is often converted to its more deacetylated derivative called chitosan. Deacetylated form of chitin in nature only occurred in some fungi such as *Mucor Rouxi* that is identified as natural chitosan (Hudson and Jenkins 2001). Chitin is very similar to cellulose, except for the hydroxyl group at C-2 position that is replaced by the acetylamino group. These groups further transformed into aminogroups through the deacetylation process result in chitosan (Kumar 2000). Thus chitosan can be considered as a random copolymer; in addition the degree of deacetylation (DDA) is almost never 100%. The chemical structures of chitin, chitosan and cellulose are shown in Fig. 2-1. There is not a sharp border between chitin and chitosan in terms

of DDA. Some researchers defined chitosan as the copolymer with the DDA of larger than 50% (Brugnerotto, Desbrieres et al. 2001); however, some others believed that this limit should be defined as 75% (Knaul, Hudson et al. 1999). When the DDA reaches approximately 50%, chitin becomes soluble in aqueous acidic solutions (Brugnerotto, Desbrieres et al. 2001; Rinaudo 2006). Chitosan has an apparent pKa of 6.5 and is generally soluble at pHs below 6. This is related to the protonation of the free amino groups on its backbone. The amino groups on the chitosan molecule (Fig. 2-1) are identified as the main source of the unique properties of chitosan, after being protonated in acidic solvents resulting in a polyelectrolyte solution. Hence, beside molecular weight, DDA and the distribution of the amino groups along the polymer chain are the key factors affecting the final properties of chitosan.

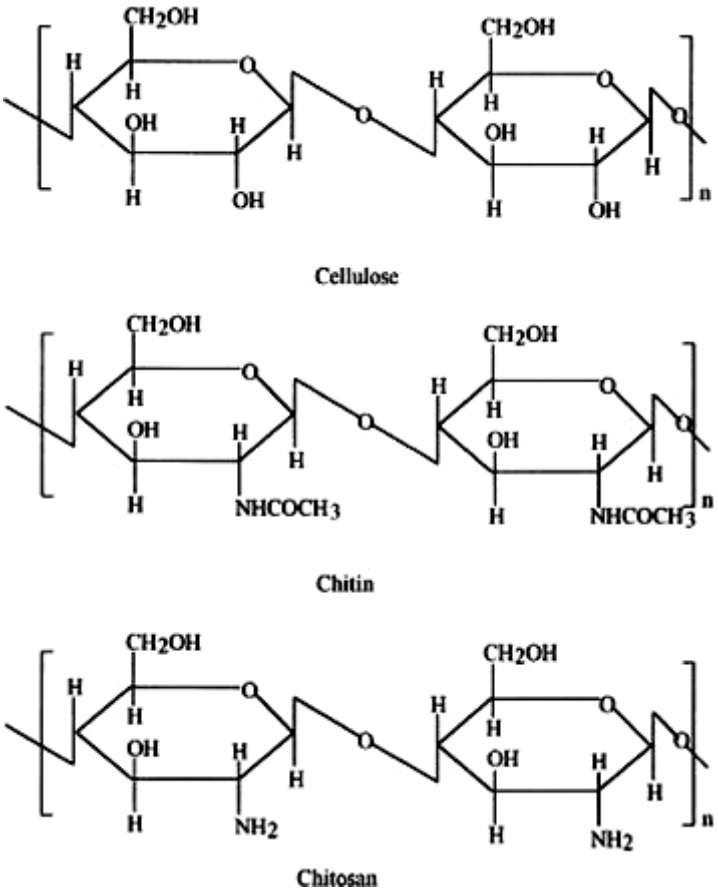

Figure 2-1: Chemical structure of cellulose, chitin and chitosan (Kumar 2000).

2.1.1 Chitosan solubility

While chitin is insoluble in most solvent systems, chitosan having at least 50% deacetylated groups is readily soluble in dilute acidic solutions below pH 6.0. At low pH, amine groups get protonated and become positively charged, which makes chitosan soluble and a cationic polyelectrolyte solution forms (Rinaudo, Pavlov et al. 1999; Pillai, Paul et al. 2009). Consequently, chitosan is known as the only semi-natural polycationic polymer in nature. The following equilibrium reaction describes the state of ionization:

$$\text{Chit–NH}_2 + \text{H}_3\text{O}^+ \leftrightarrow \text{Chit–NH}_3^+ + \text{H}_2\text{O}$$

Therefore, organic acids such as acetic, formic and lactic acids can dissolve chitosan (Hamdine et al. 2005, Hamdine et al. 2006). The most commonly used solvent is aqueous acetic acid solutions at different concentrations. Chitosan is almost insoluble in polyprotic acids such as sulfuric and phosphoric acid (Pillai, Paul et al. 2009, Hamdine et al, 2006).

2.1.2 Chitosan applications

Chitosan has been widely used in several applications due to its natural origin and exceptional properties such as biodegradability, biocompatibility, non-toxicity, and chelation of metal ions. Among them, scaffolds for tissue-engineering, wound healing dressings, water and waste water filtration and antibacterial films were among the interesting ones (Kumar 2000; Dutta, Dutta et al. 2004; Kumar, Muzzarelli et al. 2004; Rinaudo 2006; Dutta, Tripathi et al. 2009; Jayakumar, Menon et al. 2010). Table 2.1 shows the main application fields of chitosan.

Table 2.1: Main applications for chitosan (Rinaudo 2006)

Agriculture	Defensive mechanism in plants, Simulation of plant growth, Seed coating, Frost protection, Time release of fertilizers, and nutrients into the soil
Water and waste treatment	Flocculants to clarify water (drinking water, pools), Removal of metal ions, Ecological polymer (eliminate synthetic polymers), Reduce odors
Food & beverages	Not digestible by human (dietary fiber), Bind lipids (reduce cholesterol), Preservative, Thickener and stabilizer for sauces, Protective, fungistatic, Antibacterial coating for fruit
Cosmetics & toiletries	Maintain skin moisture, Treat acne, Improve suppleness of hair, Reduce static electricity in hair, Tone skin, Oral care (tooth paste, chewing gum)
Biopharmaceutics	Immunologic, Antitumoral, Hemostatic and anticoagulant healing, Bacterostatic

Table 2.2: Attractive properties of chitosan in relation to its use in biomedical applications (Rinaudo 2006)

Potential biomedical applications	Surgical sutures, Dental implants, Artificial skin, Rebuilding of bone, Corneal contact lenses, Time release drugs for animals and humans, Encapsulating material
Principal characteristics	Biodegradable, Biocompatible, Renewable, Film forming, Hydrating agent, Nontoxic, Biological tolerance, Hydrolyzed by lyzosyme, Wound healing properties, Efficient against bacteria, Viruses, Fungi

However, as it is found from literature, chitosan is more attractive and promising for biomedial applications as can be understood from Table 2.2, which summarizes the main properties of chitosan and their related potential biomedical applications.

In addition, chitosan is a good inhibitor against the growth of a wide variety of yeast, fungi and bacteria. It also exhibits gas and aroma barrier properties in dry conditions, which make it an interesting choice for anti-bacterial food packaging applications. This can improve the quality, security and storage stability of perishable foods (Begin and Van Calsteren 1999; No, Meyers et al. 2007; Zivanovic, Li et al. 2007; Dutta, Tripathi et al. 2009).

2.2 Nanofibers technology

Fibers play an important role in the everyday life of humans and have been long used since they were first produced. Nowadays, applications of fibers are not limited to textiles and woven products as newer fields of application opened up. A fiber is defined as a flexible, macroscopically homogenous material that is long and has small diameter, which is called high aspect ratio. Development of fiber industries proposed some newly enhanced technologies that can potentially produce ultra thin fibers, in the range of 1000-2000 nm, which are named microfibers. The electrospinning process was introduced later as a method to produce nanofibers with diameter range from few nm to μm (Ramakrishna, Fujihara et al. 2005). In electrospinning, unlike conventional fiber spinning technologies, an electrical force is used to elongate a polymer jet into nanometer-size fibers. The electrospinning process has attracted rapidly growing interest because of the large number of current and potential application for nanofibrous structures.

2.2.1 Nanotechnology

The term nanotechnology covers the activities related to the manufacturing and engineering of objects at the nano-scale level. Nanotechnology can be defined as the use of methods to fabricate nanoscale objects with unique properties. These unique characteristics are the key to a wide range of exciting applications that cannot be achieved by other methods. An exponential growth in the scientific research centers/institutes and publications were observed in the last decade in this area.

Accepted classification for nanoscale materials or nanomaterials defines them as materials with at least one dimension in the order of nanometers. Nanomaterials are categorized by their geometry, in zero, one and two dimensional materials (Huang, Zhang et al. 2003). Nanoparticles, nanofibers and nanofilms are examples of these structures, respectively. Conventional fiber drawing methods are limited to fibers in the range of several μm to mm and cannot be used to produce nanofibers. Short whiskers (single crystal nano rod), submicron steel and nickel fibers and carbon nanotubes are some examples of nanofibers. However, these fibers are short and available only in the form of chopped bundles;on the other hand , polymeric nanofibers can be long and continuous. Polymer nanofibers are expected to provide a number of distinctive and attractive properties. It is anticipated that a larger reduction in polymer fiber diameter improves further their properties (Reneker and Yarin 2008).

2.2.2 Electrospinning technique

Electrospinning or electrostatic spinning is the most convenient and scalable technique proposed for production of polymeric nanofibers. In recent years, this process has been used and scaled up to produce nanofibers industrially. Nanofibers with diameters in the range of 50-900 nm can be readily electrospun in the form of nonwoven mats. A 50 nm diameter polymer fiber has about 10^5 molecules passing any cross section of the fiber, each up to a length of 100 μm (Reneker and Chun 1996). At first glance, it seemed that electrospinning is very simple and thus an easily controlled method for the production of nanofibers. In a typical electrospinning experiment, the minimum set of equipment required is as follows:

a. A thin nozzle with an inner diameter of about 100 μm through which a polymer solution or melt is pumped via a special metering pump or gas pressure;
b. A collector in the form of fixed plate or rotating drum to collect the produced nanofibers, mounted at a distance of 10-25 cm from the nozzle;
c. A high voltage generator that applies a high electric field of 100-500 KV/m between the nozzle and collector.

A simple set up for laboratory scale production of electrospun nanofibers is shown in Fig. 2-2.

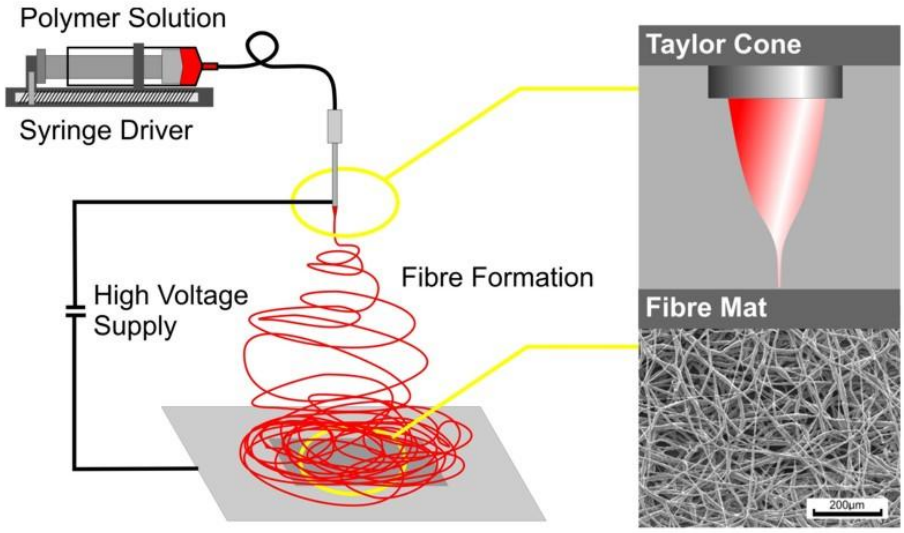

Figure 2-2: Schematic outline of a typical electrospinning set up.

Fig. 2-2 shows a vertical alignment of the nozzle and collector in the top to bottom geometry but it can be done in the bottom to top or horizontally. The electric current flow during electrospinning is in the range of a few hundred nano-amperes to micro-amperes. The electrospinning method is simple and does not require expensive equipments. In fact, a wide range of polymers can be electrospun into nanofibers at room temperature and atmospheric pressure. Electrospun nanofibers are considerably thinner than a human hair (Fig. 2-3).

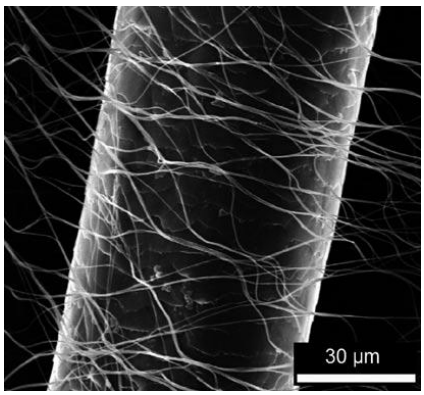

Figure 2-3: SEM image of electrospun nanofibers and human hair (Greiner and Wendorff 2007).

Moreover, electrospun nanofibers can be produced in a wide range of diameters small enough to be compared with nanoscale objects of biological systems such as proteins, viruses and bacteria. A comparison of nanofibers diameter with other nanoscale objects is illustrated Fig. 2-4.

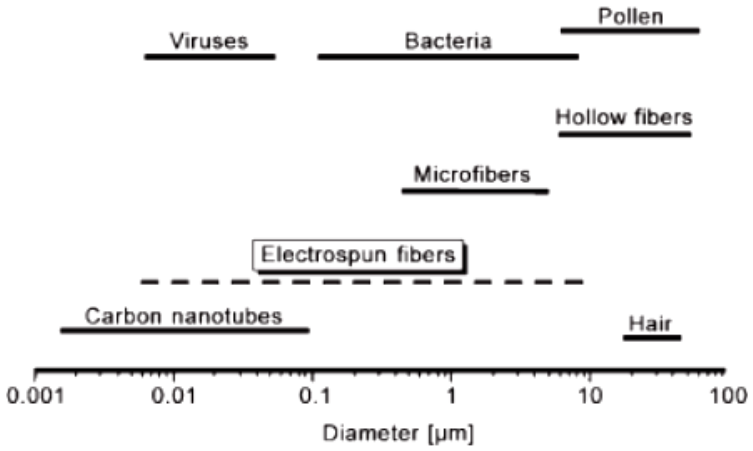

Figure 2-4: Comparison of the diameter of electrospun nanofibers with nanoscale biological and technological objects (Greiner and Wendorff 2007)

2.2.2.1 Description of the electrospinning technique

In the electrospinning process, a high voltage is applied between a syringe filled with polymer solution and a collector mounted at a fixed distance. The resulting powerful electric field causes a pendant drop of polymer solution to be electrified, and the induced charges distributes over its surface. At this stage, two forces act on the droplet; repulsive force between the surface charge and coulombic force exerted by the external electrical field on the droplet. Further increase in the applied voltage deforms the drop into a conical shape commonly known as Taylor cone (Reneker and Chun 1996). Evolution of the pendant droplet at the tip of a needle by increasing the applied voltage is displayed in Fig. 2-5. If higher voltages are applied, the strength of the applied electrical field can overcome the surface tension of the polymer solution and a liquid jet is ejected from the deformed drop at the nozzle (Fig. 2-5) (Reneker, Yarin et al. 2000; Koombhongse, Liu et al. 2001; Han, Yarin et al. 2008; Reneker and Yarin 2008). This electrical jet then undergoes a stretching and whipping process towards the counter electrode on the collector. During this step, the liquid jet is elongated and the solvent is evaporated, leading to a large reduction in the jet

diameter from hundreds of micrometers to as small as tens of nanometers, and is then deposited with high velocities of 1-10 m/s on the collector (Reneker, Yarin et al. 2000; Yarin, Koombhongse et al. 2001; Yarin, Koombhongse et al. 2001; Thompson, Chase et al. 2007; Han, Yarin et al. 2008; Reneker and Yarin 2008).

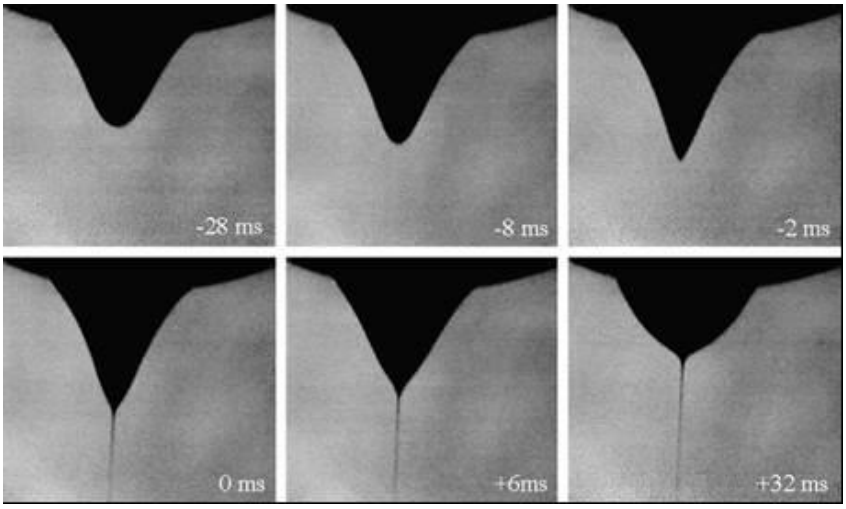

Figure 2-5: Evolution of Taylor Cone by increasing the electrical field (Reneker and Yarin 2008).

The charged fiber often deposits as a randomly oriented, non-woven mat on the collector. Depending on the polymer solution used and the electrospinning conditions, other morphologies such as beads, beaded fibers or ribbon-type fibers can be obtained instead. Typical examples of these morphologies are shown in Figs. 2-6 to 2-8.

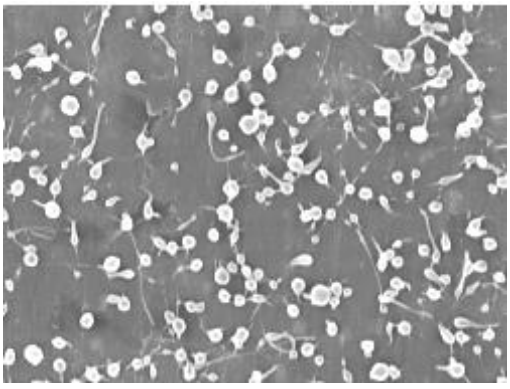

Figure 2-6: SEM image of beads produced by electrospinning of 1 wt% PEO (900 kDa) solution in water, the horizontal edge of image is 20 μm long. (Fong et al. 1999).

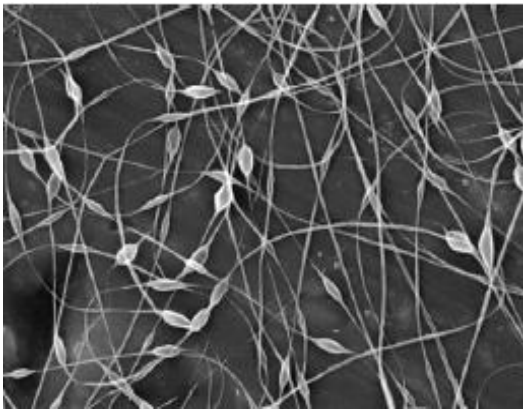

Figure 2-7: SEM image of beaded fiber morphology obtained from electrospinning of 2.5 wt% PEO (900 kDa) solution in water, the horizontal edge of image is 20 μm long (Fong et al. 1999).

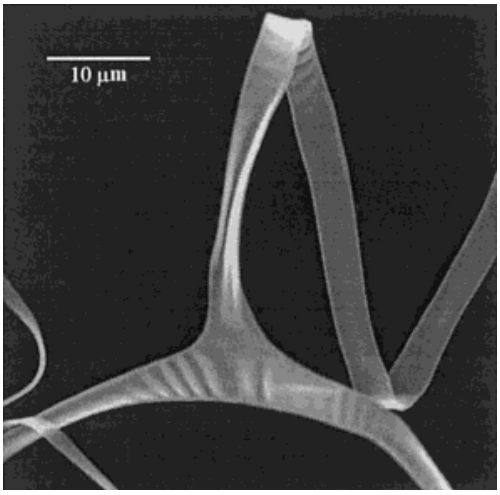

Figure 2-8: SEM image of ribbon fiber morphology prepareded by electrospinning of 10% Poly (etherimide) (Theron et al. 2004).

2.2.2.2 Electrospinning development

Electrical liquid droplets and jets have been studied for more than hundred years. These works provide the fundamental basis for electrospraying and electrospinning. Stability of the jet is the main difference between these two processes. In electrospraying the electrical jet breaks into droplets due to capillary instability, but if there is enough entanglements in the fluid, it will be stabilized and make a continued jet in the form of thin filaments resulting in the electrospinning

process (Ramakrishna, Fujihara et al. 2005). Cooley (Cooley 1902; Cooley 1903) and Morton (Morton 1902) issued the first patents on the electrostatic spinning of polymer solutions. They used cellulose nitrate in acetone and proposed a method of dispersing fluids that is similar to electrospinning and spraying. From 1934 to 1944, Formhals (Formhals 1934; Formhals 1943) published a sequence of patents on an improved version of the electrospinning process and apparatus. Sir Taylor in 1960s (Taylor 1964) fundamentally investigated the deformation of a droplet into a conical geometry in an electrical field. Baumgarten (Baumgarten 1971) produced acrylic fibers with diameter less than 1 μm from DMF solution. He studied the effect of solution viscosity (concentration) and electrical field on the diameter of fibers. Larrondo and Manley (Larrondo and Manley 1981) produced electrospun fibers of PE and PP by melt electrospinning. Although these studies prepared the basics for the electrostatic spinning process, the present knowledge is mainly due to more recent work, especially the ones carried out in the last 10-15 years. From 1993 to 1996, Reneker and coworkers reexamined the process to produce nanofibers (Doshi and Reneker 1995; Reneker and Chun 1996) and they coined the term “electrospinning” instead of electrostatic spinning for the first time. Recent scientific attempts also contributed well toward better understanding of electrospinning and its effective parameters to develop industrial applications. Consequently, nowadays research on electrospun nanofibers is not restricted only to academia, but also different companies such as Donaldson, Elmarco, Finetex Tech and Amsoil Ea are involved in the development/production of nanofibrous products for superior performance for several industrial applications and nanofiber production equipments.

2.2.2.3 Mechanism of electrospinning

Electrospinning looks simple but a closer inspection shows that this process is very complex. For instance, the jet only follows a direct path for a certain distance and after that, it changes its behavior considerably. The jet moves laterally and then splays into a number of jets, forming a cone shape towards the collector. Figure 2-9 shows a typical photograph of a jet during the electrospinning process on its way from a needle to the collector, taken at two different capture times (Shin, Hohman et al. 2001).

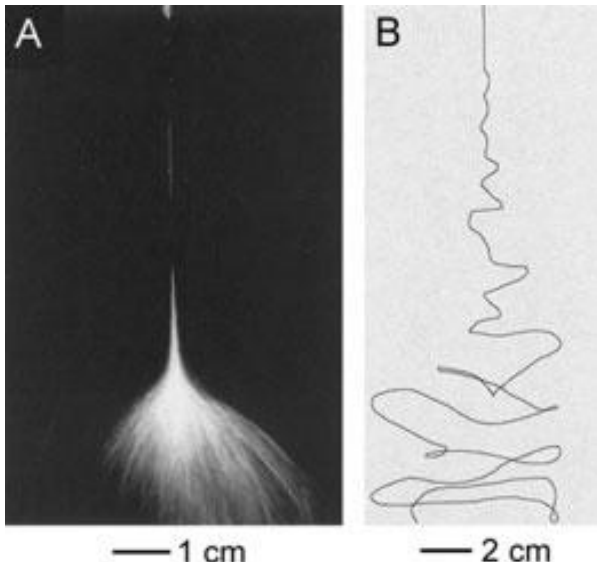

Figure 2-9: Photographs of a jet of PEO solution during electrospinning with two different capture times: A) 1/250 s, B) 18 ns (Shin, Hohman et al. 2001).

Before 1999, splitting or splaying the electrified jet due to the repulsion forces between surface charges was thought to be the main reason of nanofiber formation during the electrospinning process (Reneker and Chun 1996; Li and Xia 2004). However, more experimental observations showed that the thinning of a jet by the electrospinning process is mainly caused by the bending instability associated with the electrified jet (Reneker, Yarin et al. 2000; Yarin, Koombhongse et al. 2001). This concept was concluded further by experiments done by Yarin et al. (Yarin, Koombhongse et al. 2001; Yarin, Koombhongse et al. 2001), and Shin et al. (Shin, Hohman et al. 2001) in 2001. By using high-speed photography, they found that the conical envelope in the electrospinning jet contains only a single, rapidly bending or whipping thread (Fig.2-9B), even though it appears that the cone shaped region is composed of multiple jets. In some cases, splaying of the jet is also observed, but it is not the dominant process during electrospinning (Reneker, Yarin et al. 2000; Shin, Hohman et al. 2001; Yarin, Koombhongse et al. 2001; Yarin, Koombhongse et al. 2001; Li and Xia 2004). The frequency of whipping is so high that conventional photography cannot properly show what happens exactly, giving the impression of jet splaying into multiple jets toward the collector (Li and Xia 2004).

2.2.3 Applications of polymeric nanofibers

The special geometry of electrospun nanofibers makes them attractive options for various applications in the field of nanostructured materials and design. Figure 2-10 illustrates the potential applications of polymer nanofibers in different fields.

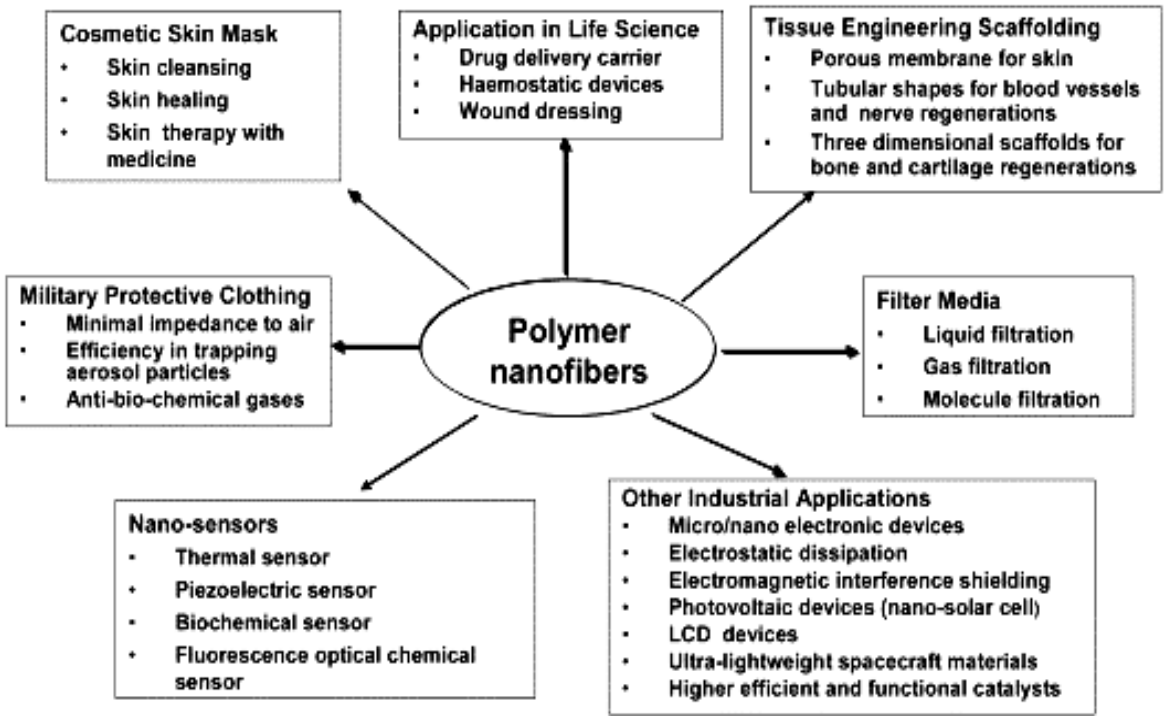

Figure 2-10: The diversity of application areas proposed for electrospun nanofibers (Huang, Zhang et al. 2003).

Nanofibrous mats have a high surface area to mass ratio (40-100 m^2/g). This unique characteristic is ideal for various membranes applications such as:

- Chemical membranes for removal of toxic products
- Protective clothing against chemical, biological or environmental attacks
- Ultrafine filters for air filtration in medicine, military devices, food processing and electronic industries to absorb tiny particles
- Highly breathable membranes due to high absorption capability and high porosity.

Two third of U.S. patents published on nanofibers are related to biological and medical applications. However, the first completely industrialized application of nanofibers was introduced in filtration due to its huge market. Electrospun mats as filter media provide advantages of high filtration efficiency, absorbance of fine particles and low air resistance resuling in lower pressure drop. Nanofibers are also attractive materials for nano sensor applications because their high specific area provides the ability to absorb or react rapidly with low levels of chemicals.

2.3 Nanofibrous chitosan membrane

There has been a growing interest for the fabrication of chitosan membranes with micro and nanoporous morphologies recently. Such chitosan mats can not only present the specific physicochemical properties of chitosan but can also benefit from the physical characteristics of microporous membranes. Several methods have been used to fabricate porous chitosan structures such as phase separation (Gu, Xue et al. 2001; Mi, Wu et al. 2003), phase inversion (Li, Gu et al. 1999; Mi, Shyu et al. 2001) and selective dissolution (Zeng, Fang et al. 2004). After successful development of the electrospinning technique to fabricate polymeric nanofibers, many researchers tried to employ this method to prepare chitosan microporous mats (Duan, Dong et al. 2004; Min, Lee et al. 2004; Ohkawa, Cha et al. 2004; Ohkawa, Minato et al. 2006). Fabrication of chitosan-based nanofibers in the form of non-woven mats is very desirable, as it can provide novel possibilities to develop applications of chitosan in various fields (Torres-Giner, Ocio et al. 2008). However, it was soon found that chitosan electrospinning is challenging. It is more likely due to its polycationic nature in solution, rigid chemical structure and specific inter and intra-molecular interactions (Duan, Dong et al. 2004; Li and Hsieh 2006; Desai, Kit et al. 2008). Formation of strong hydrogen bonds prevents the free movement of polymeric chain segments exposed to the electrical field, leading to jet break up during the process (Geng, Kwon et al. 2005; Li and Hsieh 2006; Desai, Kit et al. 2008). Additionally, the repulsive forces between ionic groups on the polymer molecules is expected to hinder the formation of sufficient chain entanglements to allow continuous fiber formation during jet stretching, whipping and bending, generally resulting in nanobeads instead of nanofibers (Min, Lee et al. 2004). In fact, it has been

shown on many occasions that sufficient chain entanglement in polymer solution is crucial for a successful electrospinning process (McKee, Wilkes et al. 2004; McKee, Park et al. 2005; Shenoy, Bates et al. 2005; Woerdeman, Shenoy et al. 2007).

2.3.1 Electrospinning of chitosan

In spite of all aforementioned difficulties in electrospinning of chitosan, its valuable properties and prospective applications are attractive enough to convince different research groups to work on this subject. Since 2004 several methods and approaches have been used with varying degrees of success to prepare electrospun nanofibers based on chitosan.

2.3.1.1 Electrospinning of neat chitosan

Neat electrospun chitosan nanofibers have been prepared by dissolving chitosan in trifluoroacetic acid (TFA) (Ohkawa, Minato et al. 2006) and its mixtures with dichloromethane (DCM) and trichloromethane (TCM) (Schiffman and Schauer 2007). TFA forms stable salts with the amino groups of chitosan which can efficiently hinder the intermolecular interactions between chitosan chains and facilitate electrospinning (Ohkawa, Minato et al. 2006). A highly concentrated aqueous acetic acid solution (80-90%) was also reported by some research groups as another successful solvent for the fabrication of neat chitosan nanofibers, using chitosan grades with DDA of 54 (Geng, Kwon et al. 2005) and 75-85% (Homayoni, Ravandi et al. 2009). It is believed that decreasing the surface tension of the solution by increasing the acetic acid content can help the electrospinnability of chitosan (Geng, Kwon et al. 2005). Applications of electrospun chitosan nanofibers using TFA-based solvents are however limited, as the prepared membranes can easily dissolve in neutral and weak basic aqueous solvents (Sangsanoh and Supaphol 2006), due to the high solubility of the TFA-chitosan salt residues. Additionally, working with toxic and harmful solvents and the possible presence of their residues in the final membranes always raise major concerns.

2.3.1.2 Electrospinning of chitosan blends with synthetic polymers and proteins

Blending chitosan with materials that facilitate its processing is another approach to make chitosan electrospinnable. The co-spinning agent should have excellent fiber forming

characteristics in order to create entanglements and physical bonds with chitosan, and act as a carrier in the electrospinning process. Various synthetic polymers have been successfully blended with chitosan to produce chitosan-based composite nanofibers such as: polyethylene oxide (PEO) (Bhattarai, Edmondson, et al. 2005; Desai, Kit et al. 2008; Klossner, Queen et al. 2008), polyvinyl alcohol (PVA) (Li and Hsieh 2006; Jia, Gong et al. 2007; Zhou, Yang et al. 2008), polylactic acid (PLA) (Ignatova, Manolova et al. 2009), nylon-6 (Zhang, Wu et al. 2010) and polycaprolactone (PCL) (Zhang, Venugopal et al. 2005). Moreover, chitosan blends with proteins such as: silk fibroin (Cai, Mo et al. 2010; Sionkowska 2011), zein (Torres-Giner, Ocio et al. 2009) and collagen (Mi, Shyu et al. 2001) have been electrospun productively. Generally the content of the co-spinning agent varies from 20 to 80 wt%. The presence of this second phase can however affect the properties of the nanofibers by decreasing the chitosan content located at the surface. This influences properties such as biocompatibility and mechanical integrity, and may be hard to rectify by an extraction process.

2.3.1.3 Co-axial electrospinning of chitosan

The co-axial electrospinning method provides an alternative and effective way of fabricating chitosan-based nanofibers. In this technique, two different solutions are spun simultaneously through a spinneret composed of two co-axial capillaries to produce core-shell structured nanofibers. Sun et al. (Sun, Zussman et al. 2003) and Yu et al. (Yu, Fridrikh et al. 2004) employed co-axial electrospinning to prepare nanofibers from polymer solutions with limited electrospinnability. They co-electrospun these solutions as the core material, with a readily electrospinnable solution as the shell layer to make core-shell nanofibers of the two components. Only Ojha et al. (Ojha, Stevens et al. 2008) used co-axial electrospinning technique to prepare chitosan nanofibers. They fed PEO as a template sheath for the chitosan core in a co-axial electrospinning set up. This leads to a two-step process, as the PEO shell layer should be removed by water washing to expose the chitosan nanofibers.

2.3.2 Applications of electrospun chitosan nanofibers

Electrospun chitosan microporous structures have been sucessfully used for many applications in recent years. Among them the followings were more promising:

- Supports for enzyme immobilization (Ye, Xu et al. 2006; Wang, Wan et al. 2009)
- Anti-bacterial films (Ignatova, Starbova et al. 2006; An, Zhang et al. 2009; Son, Yeom et al. 2009)
- Membranes for metal ions removal (Desai, Kit et al. 2008; Desai, Kit et al. 2009; Haider and Park 2009; Horzum, Boyaci et al. 2010)
- Drug delivery systems (Ignatova, Manolova et al. ; Jayakumar, Menon et al. 2010; Jayakumar, Prabaharan et al. 2010)
- Tissue engineering (Subramanian, Vu et al. 2005; Yang, Jin et al. 2008; Zhang, Venugopal et al. 2008; Wang, Itoh et al. 2009; Cooper, Bhattarai et al. ; Prabhakaran, Ghasemi-Mobarakeh et al. 2011)
- Wound healing dressings (Chen, Chang et al. 2008; Zhou, Yang et al. 2008; Ignatova, Manolova et al. 2009; Cai, Mo et al. 2010; Kang, Yoon et al. 2010)

2.4 Phase behavior of polymer solutions

Phase separation behavior of polymer solutions is of great interest in both scientific and industrial point of view. (Bae, Lambert et al. 1991; Dormidontova 2002; Hammouda, Ho et al. 2004; Shetty and Solomon 2009) Aqueous PEO solutions exhibit an inverse solubility-temperature relationship that leads to a phase separation upon heating. Therefore, a low critical solution temperature (LCST) that depends on the molecular weight is observed for high molecular weight PEO grades in water. Such extraordinary properties are seen only in highly polar systems that have strong molecular interactions such as hydrogen bonding.(Polic and Burchard 1983; Bae, Lambert et al. 1991; Fischer and Borchard 2000)

Aqueous acidic solutions of chitosan also exhibit great solubility, similarly to aqueous PEO solutions, due to the presence of strong hydrogen bonds between the solvent and the polymer owing to the presence of hydroxyl, acetylamine and amino groups on the chitosan chain.

Therefore, the occurrence of an LCST in chitosan solutions is expected.(Bae, Lambert et al. 1991; Dormidontova 2002)

Therefore, having clear knowledge about the phase behaviour and miscibility of solutions of chitosan and PEO and their blends is of crucial importance, as any phase separation occurring during the electrospinning process greatly changes the morphology and properties of the final products.

Several methods have been used to study the onset of phase separation in polymer systems. Simple visual observation of turbidity (Fischer, Borchard et al. 1996), thermo-optical analysis (TOA) (Bae, Lambert et al. 1991), light scattering (Polic and Burchard 1983; He, Liu et al. 1991; Shetty and Solomon 2009) and small angle neutron scattering (SANS) (Hammouda, Ho et al. 2002; Hammouda, Ho et al. 2004) are frequently used to determine the early stages of liquid-liquid phase separation in polymer solutions.

Rheometry represents a powerful tool to study the phase behaviour of polymeric systems. Near the phase separation temperature, the linear viscoelastic response is influenced by the critical concentration fluctuations and exhibits a thermorheological complexity, i.e. enhancement of elasticity in the vicinity of phase separation.(Kapnistos, Hinrichs et al. 1996; Niu and Wang 2006) Ajji and Choplin(Ajji and Choplin 1991) quantified this phenomenon for polymer blends by extending the mean field theories of Fredrickson and Larson (Fredrickson and Larson 1987) developed for copolymers. It was shown that this approach can determine both the spinodal (Kapnistos, Hinrichs et al. 1996; Niu and Wang 2006; Yeganeh, Goharpey et al. 2010) and binodal (Sharma and Clarke 2004; Niu and Wang 2006) temperatures by carrying out a dynamic temperature sweep test on the blend and tracking the evolution of rheological material functions G' and G''. This method was successfully employed for different polymer pairs and the obtained data agreed well with that from other techniques such as optical microscopy (Ajji, Choplin et al. 1991; Yeganeh, Goharpey et al. 2010), light scattering (Vlassopoulos, Koumoutsakos et al. 1997) and inverse gas chromatography. (Bousmina, Lavoie et al. 2002)

2.5 Originality of the work

According to the literature review, although considerable research has been conducted on the electrospinning of chitosan, there is still a great deal of uncertainty about the most influencing parameters leading to the achievement of electrospun chitosan nanofibers. Therefore, a comprehensive study is still required to clarify the relationships between chitosan-based solution properties and their success in the electrospinning process. Understanding the phase behavior of polymer solutions is also of crucial importance for any forming process, including electrospinning. To the best of our knowledge there is no published work that has examined the phase separation behavior of chitosan and its blend solutions with temperature. Furthermore, even if several methods have been used to study the onset of phase separation in polymer solutions, utilizing rheological measurements for this purpose have not been reported yet. Finally, even though the co-axial electrospinning technique is very promising for the preparation of nanofibers from polymers with limited electrospinnability, there is no published work on the fabrication of core-shell structured PEO-chitosan nanofibers with chitosan located on the surface by using a single-step co-axial electrospinning method.

2.6 Objectives

In view of the interesting features of highly porous chitosan structures and their huge potential for several biomedical applications, the well-established capability of the electrospinning process to produce non-woven nanofibrous structures, and considering the various drawbacks arising from the previous undertaken approaches to fabricate electrospun chitosan nanofibers, the main objective of this study is:

"To fabricate chitosan-based microporous non-woven membranes from aqueous solutions using the electrospinning process"

To achieve this main objective, two approaches are employed to prepare chitosan-based nanofibrous structures with high chitosan content, blending and co-axial electrospinning of chitosan with a readily electrospinnable solution, i.e. an aqueous solution of polyethylene oxide (PEO). The specific objectives of the current work are summarized as follows:

- To fabricate chitosan-based electrospun mats with maximum chitosan content through blending with PEO in aqueous solution.
- To investigate the phase behaviour and miscibility range of chitosan/PEO solutions as function of temperature.
- To establish a fundamental understanding of chitosan/PEO solution properties that lead to successful electrospinning.
- To produce PEO/chitosan nanofibers with chitosan located on the outer layer through a single step co-axial electrospinning process.

CHAPITRE 3

SUMMARY OF ARTICLES

The main achievements of this research project are presented in the form of three scientific papers in the following three chapters:

Chapter 4 presents the results of the first paper: "*Determination of phase behaviour of poly (ethylene oxide) and chitosan solution blends using rheometry"* that has been submitted to *Macromolecules*. In this work, small amplitude oscillatory shear and steady shear rheological measurements are used to study the miscibility range and phase behaviour of PEO/chitosan solutions. It is shown that information on the phase separation of polymer solutions such as binodal and spinodal temperatures can be estimated directly through rheological measurements. In addition, the results of isochronal dynamic temperature sweep experiments are used to calculate key macromolecular and thermodynamic parameters such as correlation length and Flory-Huggins interaction parameter.

Chapter 5 presents the second article "*A fundamental study of chitosan/PEO electrospinning"* that has been published in *Polymer* (Vol. 52, 2011, 4813-4824). In this work a thorough quantitative analysis of chitosan/PEO solution characteristics that lead to successful electrospinning is performed. Various properties such as surface tension, conductivity, viscosity and acetic acid concentration are considered in this study. Those fundamental findings allow us to prepare defect free chitosan-based nanofibers with high chitosan content. The effects of solution temperature and blend composition on morphology and fiber diameter of electrospun nanofibers are also investigated. In addition, an FTIR investigation is conducted to examine the presence of hydrogen bonding interactions between chitosan and PEO.

Chapter 6 presents the third paper "C*ore-shell structured PEO-chitosan nanofibers by coaxial electrospinning"*that has been published in *Biomacromolecules* (Vol. 13, 2012, 412-421). In this work, a single step co-axial electrospinning process is employed to prepare core-shell structured PEO/chitosan nanofibers with the possibility of producing chitosan hollow nanofibers through a subsequent PEO water washing step. Presence of chitosan on the outer layer is suggested by TEM images obtained before and after washing the PEO content with water, and also confirmed by XPS analysis. Bulk and local compositions of the prepared nanofibers are evaluated by TGA

and FTIR experiments, respectively, which confirms the homogeneity and uniformity of the nanofibers.

CHAPITRE 4

DETERMINATION OF PHASE BEHAVIOUR OF POLY (ETHYLENE OXIDE) AND CHITOSAN SOLUTION BLENDS USING RHEOMETRY[1]

Mehdi Pakravan, Marie-Claude Heuzey and Abdellah Ajji

4.1 Abstract

Aqueous solutions of PEO exhibit a lower critical solution temperature (LCST) phase diagram. In this work, phase separation behaviour of PEO/water solutions was investigated using small amplitude oscillatory shear and steady shear rheological measurements. Binodal decomposition temperatures were determined from the sudden changes in the slope of the dynamic temperature sweep of storage modulus and loss tangent. The spinodal decomposition points were also estimated by a mean field theoretical approach. Comparing the obtained critical points with other conventional methods revealed that rheological measurements are powerful and sensitive to detect even the early stage of phase separation of PEO solutions. This successful method was employed to investigate phase separation and miscibility of chitosan/PEO solutions at different compositions in aqueous acetic acid solutions that have already showed anomalous behaviour in a forming process. Lower critical solution temperature (LCST) phase behaviour was observed for chitosan/PEO solution blends. Phase separation temperature, miscibility range and correlation length of the solutions were determined from isochronal dynamic temperature sweep experiments. Effect of chitosan/PEO ratio on the binodal and spinodal decomposition temperatures was studied. Finding phase separation information on polymer solutions through rheological measurement is very promising. Isothermal steady shear rheological measurements were also carried out on chitosan/PEO solutions over a temperature range in which phase separation occurs. Viscosity increase at low shear rates above but in the vicinity of phase separation temperature was observed, which confirms the validity of the theoretical approach

[1] Submitted to Macromolecules, June 2012

employed to determine the critical temperatures through dynamic rheological measurements. Finally, the Flory-Huggins interaction parameters were estimated from critical solution temperature and concentration results.

4.2 Introduction

PEO is a water soluble, hydrophilic, non-toxic and biocompatible polymer that has been widely used for biomedical and biomimetics applications.[1-3] Phase separation behaviour and solubility characteristics of aqueous solutions of polyethylene oxide (PEO) have been raising both scientific and industrial interests for more than four decades. [1, 3-9] Aqueous PEO solutions exhibit anomalous behaviour in contrast to other ordinary polymer solutions. They show an inverse solubility-temperature relationship that leads to a phase separation upon heating. At even higher temperatures the homogeneous state becomes stable again. Hence, a closed loop phase diagram is observed as one of the characteristic features of aqueous PEO solutions. However, for high molecular weight PEO grades i.e. more than 100 kDa, only a low critical solution temperature (LCST) that depends on the molecular weight is observed. [4, 6, 9] Such extraordinary properties are seen only in highly polar systems that exhibit strong orientation dependence of molecular interactions such as hydrogen bonding.[1, 4-6, 10] Clustering (also referred to as aggregation) is another unusual characteristic of PEO solutions dissolved in water (or other solvents) that has been studied intensively by several authors.[2, 3, 5, 7, 9] Clusters or aggregates form in concentrated aqueous PEO solutions associated with temperature increase (T > 30° C). The clustering effect is pervasive and has been observed in some other systems such as polyelectrolyte solutions and clay dispersions.[7, 11, 12] The basic origin of this cluster formation is not understood and remains an open question.[7, 13] The peculiar behaviour of aqueous PEO solutions is attributed to the existence of hydrogen bonds between ether groups in PEO and hydrogen in water molecule and how these bonds are affected by temperature.[1, 3, 7, 8]

Chitosan is a linear polysaccharide that is mainly produced from the partial deactetylation of chitin, one of the most abundant polysaccharides in nature.[14-18] Chitosan is the only pseudo-natural cationic polyelectrolyte. Aqueous acidic solutions of chitosan exhibit great solubility, similarly to aqueous PEO solutions, due to the presence of strong hydrogen bonds between the

solvent and the polymer owing to the presence of hydroxyl, acetylamine and amino groups on the chitosan chain. Therefore, the occurrence of an LCST in chitosan solutions is expected.[1, 6] The tendency of chitosan to form aggregates in solution, which is attributed to the hydrophobic interactions of residual acetylated groups,[16] has also been investigated extensively. [11, 12, 19]

Chitosan solutions and their blends with other synthetic polymers have recently attracted great attention [15, 20-22] due to the following facts:

- The fascinating features of chitosan including renewability, availability in nature, non-toxicity, biocompatibility, anti-bacterial and biodegradability,[14, 17, 18] which makes it a promising choice for biomedical and pharmaceutical applications such as drug delivery systems, wound healing dressings, tissue engineering scaffolds and anti-bacterial membranes.[18, 21, 23]
- The "wet route" as the only successful method to fabricate chitosan final products in different forms of films, porous membranes, fibers, particles or sponges.[15, 21-24] Chitosan should be processed in a solution state for all final applications. "Dry methods" such as melt processing, plasticization and kneading are still in early stages of research.[25-27]
- Blending of chitosan in the solution state with other hydrophilic polymers such as PEO[28-31], polyvinyl alcohol (PVA)[32, 33], polylactic acid (PLA)[25] and polycaproloctone (PCL)[34, 35] is a well known approach to facilitate its processing, improve final properties or to overcome the disadvantage of the loss in mechanical strength in the wet state.[29, 36]

PEO is a more attractive polymer for blending with chitosan due to its solubility in various aqueous solvents and biocompatibility.[30] Consequently, understanding the phase behaviour and miscibility of aqueous acidic solutions of chitosan and PEO and their blends is of crucial importance, as any phase separation occurring during the forming processes such as film casting, fiber spinning and solution electro-spraying greatly changes the morphology and physico-mechanical properties of the final products.

In a separate study, the present authors have described an incoherent behaviour of chitosan/PEO solutions in the electrospinning process at high temperatures.[29] We found that moderate process temperatures help to stabilize the electrospinning process of chitosan/PEO blend solutions and produce bead-less nanofibers. However, at higher temperature, the electrospun jet became unstable and beaded fibers morphology were obtained.[29] The relevance of this observation to the temperature-induced phase separation of these solutions was questioned. On the other hand,

results of transmission FTIR on cast films and nanofibers of chitosan/PEO blends at room temperature showed the existence of hydrogen bonding interactions between chitosan and PEO, an indication of miscibility of these two polymers.[29]

Several methods have been used to study the onset of phase separation in polymer systems. Simple visual observation of turbidity[37, 38], thermo-optical analysis (TOA)[6], light scattering [3, 5, 39, 40] and small angle neutron scattering (SANS)[7, 13] are frequently used to determine the early stages of liquid-liquid phase separation in polymer solutions. However, only improved scattering techniques yield more detailed information leading to both spinodal and binodal points (cloud points).[6, 39, 40] While the extensive studies were done to estimate the binodal (cloud points) temperatures, little work on spinodal point measurements of well-known PEO/water solutions have been published. The fact is, that by having binodal and spinodal points one can calculate the values of Flory-Huggins interaction parameter (χ), a fundamental characteristic of polymer solutions.[10, 41, 42]

Rheometry represents a powerful tool to study the phase behaviour of polymeric systems. Rheological measurements are sensitive to polymer chain reptation, diffusion and interfacial tension, and thus can be used to detect phase separation in rather early stages. Concentration fluctuations involving various mechanisms such as nucleation, diffusion, domain growth and coagulation are generally considered as the physical source of phase separation.[43, 44] Near the phase separation temperature, the linear viscoelastic response is influenced by the critical concentration fluctuations and exhibits a thermorheological complexity, i.e. enhancement of elasticity in the vicinity of phase separation.[44-47] Ajji and Choplin[48] quantified this phenomenon for polymer blends by extending the mean field theories of Fredrickson and Larson[49] developed for copolymers. It was shown that this approach can determine both the spinodal[44-47] and binodal[44, 45, 50] temperatures by carrying out a dynamic temperature sweep test on the blend and tracking the evolution of rheological material functions G' and G''. This method was successfully employed for different polymer pairs and the obtained data agreed well with that from other techniques such as optical microscopy[47, 51, 52], light scattering[46] and inverse gas chromatography.[43] Additionally, this quantitative technique allowed obtaining suitable results for both LCST [43, 45, 47, 50, 53] and UCST [44, 46] systems.

In this paper we demonstrate the usefulness of the rheological approach to investigate the phase behaviour of polymer solutions. To the best of our knowledge, it is the first time that this method is employed to study the liquid-liquid phase separation of a polymer solution. A PEO aqueous solution is selected as a model system to develop the experimental protocol, and subsequently the method is applied to aqueous acetic acid solutions of PEO, chitosan and their blends at different ratios. The results are expected to provide a clear understanding about the phase behaviour and miscibility of these blends, which is valuable for polymer forming processes in the solution state such as fiber spinning and film casting.

Additionally, crucial macromolecular and thermodynamic parameters of correlation length and Flory-Huggins interaction parameter (χ) of polymer solutions were estimated from isochronal dynamic temperature sweep experiments.

4.3 Theoretical background

4.3.1 Scaling analysis of dynamic rheological properties near phase separation

Observations of anomalous behaviour in dynamic rheological properties of block copolymer melts in the transitional regime of phase separation have been analysed by Fredrickson and Larson.[49] They used a mean field theory to derive the critical contribution of the concentration fluctuations to the viscoelastic properties of block copolymers near the critical point. After wave-vector integration, they obtained the following expressions for the dynamic storage (G') and loss moduli (G'') respectively:

$$G'(\omega) = \frac{k_B T \omega^2}{15\pi^2} \int_0^{k_0} \frac{k^6 S_0^2(k)}{\omega^2 + 4\bar{\omega}^2(k)} \left[\frac{\partial S_0^{-1}(k)}{\partial k^2}\right]^2 dk \qquad (4\text{-}1)$$

$$G''(\omega) = \frac{2k_B T\omega}{15\pi^2}\int_0^{k_0} \frac{k^6 S_0^2(k)\,\bar{\omega}(k)}{\omega^2 + 4\bar{\omega}^2(k)}\left[\frac{\partial S_0^{-1}(k)}{\partial k^2}\right]^2 dk \qquad (4\text{-}2)$$

Where $\bar{\omega}(k) = k^2 S_0^{-1}(k)\lambda(k)$, $S_0(k)$ is a static structure factor, $\lambda(k)$ is the Onsager coefficient for the polymeric system of interest, *k* defines the wave vector, ω is the angular frequency and k_B is the Boltzman coefficient. These equations are valid for both block copolymers and homopolymer blends. Hence G' and G'' can be calculated by using the appropriate expression of the static structure factor and the Onsager coefficient. Ajji and Choplin[48] extended Fredrickson and Larson's approach[49] to binary homopolymer blends after observing a similar behaviour[52, 54] in the evolution of their viscoelastic properties under oscillatory shear flow. They derived the previous equations (Eqs. 4-1 and 4-2) for homopolymer blends by using: 1) the static structure factor computed by de Gennes by a mean-field approach in the random phase approximation:

$$\frac{1}{S_0(k)} = \frac{1}{\phi N_1 g_1(k)} + \frac{1}{(1-\phi)N_2 g_2(k)} - 2\chi \qquad (4\text{-}3)$$

Where ϕ is the volume fraction of polymer 1, N_i is the number of statistical segments, and $g_i(k)$ is the Debye function, and 2) the expression for the Onsager coefficient, $\lambda(k)$, proposed by Binder:

$$\frac{1}{\lambda(k)} = \frac{1}{\phi a_1^2 W_1 g_1(k)} + \frac{1}{(1-\phi)a_2^2 W_2 g_2(k)} \qquad (4\text{-}4)$$

Where a_i is the statistical segment length of the species *i* and W_i is its rate of orientation defined by:

$$W_i = 3\pi k_B T/\zeta_i \qquad (4\text{-}5)$$

Where ζ_i is the monomeric friction coefficient.

Using Eqs. 4-3 to 4-5, Ajji and Choplin[48] integrated Eqs 4-1 and 4-2 by considering an expansion of the Debye function in the homogenous region near the critical point. More details of their development and discussion in the case of homopolymer blends can be found in reference [46]. Finally the following expressions for G' and G'' were derived in the terminal one-phase region near the critical point:

$$G'(\omega) = \frac{k_B T \omega^2}{1920\pi}\left[\frac{1}{3}\left\{\frac{R_{g1}^2}{\phi N_1} + \frac{R_{g2}^2}{(1-\phi)N_2}\right\}\right]^{1/2} \times \left[\frac{1}{\phi a_1^2 W_1} + \frac{1}{(1-\phi)a_2^2 W_2}\right]^2 [2(\chi_s - \chi)]^{-5/2} \quad (4\text{-}6)$$

$$G''(\omega) = \frac{k_B T \omega}{240\pi}\left[\frac{1}{3}\left\{\frac{R_{g1}^2}{\phi N_1} + \frac{R_{g2}^2}{(1-\phi)N_2}\right\}\right]^{-1/2} \times \left[\frac{1}{\phi a_1^2 W_1} + \frac{1}{(1-\phi)a_2^2 W_2}\right] [2(\chi_s - \chi)]^{-1/2} \quad (4\text{-}7)$$

Where χ_s is the value of the interaction parameter at the spinodal temperature, χ is the interaction parameter at temperature T and R_{gi} is the radius of gyration defined as $R_{gi}^2 = N_i a_i^2/6$.

Using Eqs 4-6 and 4-7 the ratio of $G'(\omega)/G''^2(\omega)$ can be calculated as follows, where the monomeric friction coefficient (ζ) is eliminated and there is no explicit dependency on angular frequency (ω):

$$\frac{G'}{G''^2} = \frac{30\pi}{k_B T}\left\{\frac{a_1^2}{36\phi} + \frac{a_2^2}{36(1-\phi)}\right\}^{3/2} (\chi_s - \chi)^{-3/2} \quad (4\text{-}8)$$

This expression is only valid for the terminal response (near the critical region), where G' and G'' have the scaling behavior of $G' \sim \omega^2$ and $G'' \sim \omega^1$, respectively. The expression for the correlation length of a binary polymer blend is:

$$\xi = \frac{a'}{6}[\phi(1-\phi)(\chi_s - \chi)]^{-1/2} \quad (4\text{-}9)$$

Where a' is the characteristic length which is defined based on the individual segment lengths in each phase, a_1 and a_2, using the following equation:

$$\frac{a'^2}{\phi(1-\phi)} = \frac{a_1^2}{\phi} + \frac{a_2^2}{(1-\phi)} \qquad (4\text{-}10)$$

Thus, the correlation length can be calculated near the critical point directly from the shear rheological data:

$$\xi = \left[\frac{k_B T}{30\pi}\frac{G'}{G''^2}\right]^{1/3} \qquad (4\text{-}11)$$

Assuming the following expression for the interaction parameter[55]:

$$X = A + B/T \qquad (4\text{-}12)$$

By substituting the interaction parameter in Eq. 4-8, one can find the following expression:

$$\left(\frac{G''^2}{TG'}\right)^{2/3} = \frac{B}{C}\left(\frac{1}{T_s} - \frac{1}{T}\right) \qquad (4\text{-}13)$$

where *C* is given by:

$$C = \left(\frac{5\pi}{36k_\beta}\right)^{2/3}\left[\frac{a_1^2}{\phi} + \frac{a_2^2}{1-\phi}\right] \qquad (4\text{-}14)$$

Hence, a linear dependence of $(G''^2/G'T)^{2/3}$ versus $1/T$ is predicted for the blends at the phase transitional region. The spinodal decomposition temperature (T_s) is then calculated from the intercept of the line with the $1/T$ axis.

4.3.2 Evaluation of Flory-Huggins interaction parameter for polymer solutions from their critical temperature and concentration data

In general, the Flory-Huggins expression for the molar Gibbs free energy of mixing of a binary polymer solution at temperature *T* is given by: [42]

$$\frac{\Delta G}{RT} = \frac{\phi_1 \, ln\phi_1}{r_1} + \frac{\phi_2 \, ln\phi_2}{r_2} + \chi\phi_1\phi_2 \qquad (4\text{-}15)$$

where ΔG is the free energy of mixing per unit volume, *R* is the universal gas constant, *T* is the absolute temperature, ϕ_1 and ϕ_2 and r_1 and r_2 are the volume fractions and relative molar volumes of component 1 and 2, respectively; $r_1 = 1$ for the solvent, and χ is the Flory-Huggins interaction parameter.

However, it has been shown in several works that χ depends both on temperature and polymer concentration.[41, 56] Hence, in Eq. 4-15, a more general interaction function, $g(T, \phi_2)$, is suggested as a semi-empirical form of χ. After replacing χ with $g(T, \phi_2)$, the Gibbs free energy function is written as Eq. 4-16 for describing the free energy of real systems: [10, 56, 57]

$$\frac{\Delta G}{RT} = \frac{\phi_1 \, ln\phi_1}{r_1} + \frac{\phi_2 \, ln\phi_2}{r_2} + g(T, \phi_2)\phi_1\phi_2 \qquad (4\text{-}16)$$

Different functions have been proposed for the dependency of $g(T, \phi_2)$ on temperature and concentration.[37, 41] It is shown that similar to several other polymer/solvent systems, for highly diluted PEO/water solutions interaction parameter, χ starts out at a high value which decreases continuously by increasing the concentration. The minimum is reached and stayed constant at moderate concentrations and then increases steadily at highly concentrated solutions. Results of Venohr et al.[58] and Michalczyk et al.[59] showed that χ is constant at volume concentrations of 0.04 to 0.5 for a 10 kDa PEO grade. It is speculated that our solution concentration in here,

6 wt% ≈ 4.76 vol% falls in this concentration range. Hence, the interaction parameter function, $g(T,\phi_2)$, is nearly independent of concentration, and Eq. 4-12 is applicable and leads to acceptable results. The spinodal decomposition temperature is the boundary between unstable and metastable mixtures. Thermodynamically, at the spinodal points the following Eq. is satisfied at a certain temperature ($T = T_s$):[56, 57]

$$\frac{\partial^2\left(\frac{\Delta G}{R}\right)}{\partial \phi_2^2} = 0 \qquad (4\text{-}17)$$

At the binodal point, a homogeneous polymer solution separates into two phases. The general condition for equilibrium between two co-existing phases is that the chemical potential of each component must be the same in both phases.[55] It is shown that these conditions are satisfied when the so-called binodal points have a common tangent line e.g. at ϕ_{2A} and ϕ_{2B}, in the plot of $\Delta G/RT$ versus ϕ_2.[55] Thus, at the binodal points (ϕ_{2A} and ϕ_{2B}) at $T=T_b$, the following equations must be satisfied:[60]

$$\left.\frac{\partial\left(\frac{\Delta G}{RT}\right)}{\partial \phi_2}\right|_A = \left.\frac{\partial\left(\frac{\Delta G}{RT}\right)}{\partial \phi_2}\right|_B \qquad (4\text{-}18)$$

$$\left.\left(\frac{\Delta G}{RT} - \frac{\partial\left(\frac{\Delta G}{RT}\right)}{\partial \phi_2} \times \phi_2\right)\right|_A = \left.\left(\frac{\Delta G}{RT} - \frac{\partial\left(\frac{\Delta G}{RT}\right)}{\partial \phi_2} \times \phi_2\right)\right|_B \qquad (4\text{-}19)$$

By applying first and second derivative on Eq. 4-16 and considering Eq. 4-12 for the interaction parameter, and inserting into Eqs. 4-17 to 4-19, three equations are obtained, containing three unknown parameters: *A*, *B* and ϕ_{2B}. Hence, an estimation of the Flory-Huggins interaction function can be obtained from the simultaneous solution of these equations and from the phase separation temperatures, Tb and Ts evaluated from rheological measurements. According to

Flory-Huggins theory of polymer solutions, *A* and *B* in Eq. 4-12 represent the entropic and enthalpic contributions of the interaction function, respectively.[42, 55]

4.4 Experimental section

4.4.1 Materials

A commercial chitosan grade in the form of fine powder was supplied by Marinard Biotech (Rivière-au-Renard, QC, Canada). The weight-average molecular weight of this chitosan was measured by size exclusion chromatography with multi-angle laser light scattering (SEC-MALLS) and was found to be 85 ± 5 kDa. The degree of deacetylation (DDA) (97.5%) was determined from ^{1}H-NMR spectroscopy.[29] More on the characterization of this chitosan grade can be found in reference [29]. PEO with a molecular weight of 600 kDa was obtained from Scientific Polymers Inc. (Ontario, NY, USA). Reagent grade acetic acid (99.7 %, Aldrich, WI, USA) and deionized Mili-Q water (conductivity at 25 °C < 18 $\mu S \cdot cm^{-1}$) were employed to prepare the aqueous solutions. All the materials were used as received.

4.4.2 Solutions preparation

A solution of PEO in water was prepared at a concentration of 6 wt%. In addition, aqueous solutions of chitosan and PEO in 50 wt% acetic acid were separately prepared at 4 wt% polymer concentration. Solution mixing was performed at room temperature using a laboratory magnetic stirrer (Corning Inc, MA, USA) for 18-24 h to ensure complete dissolution of the polymers and obtain homogeneous solutions. The prepared solutions were left to rest 4 h for degassing and kept in sealed containers at room temperature. Chitosan/PEO blend solutions at 20/80, 50/50 and 80/20 ratios were prepared by mixing the two solutions at a 4 wt% total polymer concentration.

4.4.3 Rheological measurements

Dynamic rheological properties of the solutions were characterized using a stress-controlled rotational rheometer (AR-2000, TA Instruments, DE, USA) with a Couette flow geometry with bob and cup radius of 14 and 15 mm, respectively. Low viscosity silicon oil was used to cover the surface of the sample solutions to prevent solvent evaporation during testing. The presence of the oil was shown not to impact the rheological measurements. The stability of the solutions as a function of time at 25 °C was examined in oscillatory shear tests under a low frequency of 1 rad/s and a small deformation of 0.1. The elastic and loss modulus decreased by less than 1 and 3 %, respectively, in more than one hour, demonstrating a good stability of the solutions.

Preliminary isothermal stress sweeps were carried out from 0.18-20 Pa at several fixed frequencies between 0.1 to 150 rad/s to determine the linear viscoelastic regime of the solutions. The effect of temperature on the viscoelastic response of the various solutions was studied by performing isochronal temperature sweep experiments. The storage and loss moduli were measured at a given frequency of 1 rad/s and a uniform rate of heating of 0.5 °C/min at a constant stress of 2 Pa. The temperature range of 25-80 °C was chosen to cover the whole region from homogeneous to phase-separated regions in the phase diagram. Isothermal oscillatory frequency sweeps in the range of 0.2-120 rad/s using stresses 0.5-2.5 Pa, hence well within the linear viscoelastic regime, were also performed.

Isothermal steady simple shear measurements were carried out on solutions by applying shear rates from 0.1-2000 s^{-1} over a temperature range of 25 to 80 °C. Possible fluid inertia effects at high shear rates were also examined by looking at values of the Reynolds number *Re*. In Couette flow geometry, this number is given by $Re = \rho\dot{\gamma}h^2/\eta$, where ρ is the density of the fluid, $\dot{\gamma}$ is the shear rate, h is the flow gap, and η is the viscosity of the solution.[61] The calculated *Re* values were of the order of 10^{-4} to 1 over the range of shear rates used in these tests, hence, the flow conditions were considered inertialess. The zero shear viscosity of the solutions was evaluated by using the Carreau-Yasuda[62] model to the shear viscosity data when applicable.

4.5 Results and discussion

4.5.1 Determination of solution critical points by oscillatory shear measurements

4.5.1.1 PEO/water solution

To assess the viability of using the rheological measurements to find out the thermodynamic phase separation data of the polymer solutions, a dynamic temperature sweep test was carried out on a 6 wt% PEO solution in water. This solution was chosen since the phase behaviour of PEO solutions in water has been widely reported in the literature[1, 3-9]Additionally, PEO at this content is concentrated enough to develop large torques during the rheological tests, which helps to improve the reliability of the data. Figure 4-1 shows the storage and loss moduli and tan δ as functions of temperature for a 6 wt% PEO/water solution at a fixed frequency of 1 rad/s and a stress of 2 Pa. The temperature was increased from 15 to 90 °C at a rate of 0.5 °C/min. The frequency of 1 rad/s was selected to make sure that the changes observed in the viscoelastic properties were only induced by phase separation rather than any other factors. Ajji et al.[52] showed that this frequency is small enough for this purpose. Figure 4-1 depicts that G' and G''decreases gradually with increasing temperature, which is due to the increase of PEO chain's mobility and lower intermolecular friction.[44, 51, 52] As temperature further increases, the storage modulus (G') increases considerably in the temperature range of 60 to 85 °C, and an obvious upturn appears. A modest increase in the loss modulus is also observed. On the other hand, tan δ shows a reverse trend: a gradual increase followed by a sudden reduction with increasing temperature. Based on the known LCST behaviour of PEO/water solutions, phase separation occurs in this temperature range. In the vicinity of phase separation, the thermodynamic forces emerge as a competing phenomenon to chain mobility. By approaching the solution segregation temperature, these forces dominate and control the viscoelastic behaviour of the solution. It is believed that the temperature range in which the viscoelastic behaviour is more influenced by the thermodynamic forces is related to the phase separation region.[45, 46, 50] For temperatures higher

than this temperature range, mobility forces control again the viscoelastic behaviour of the resulted phase separated blend and thus, storage and loss modulus decrease again.[47]

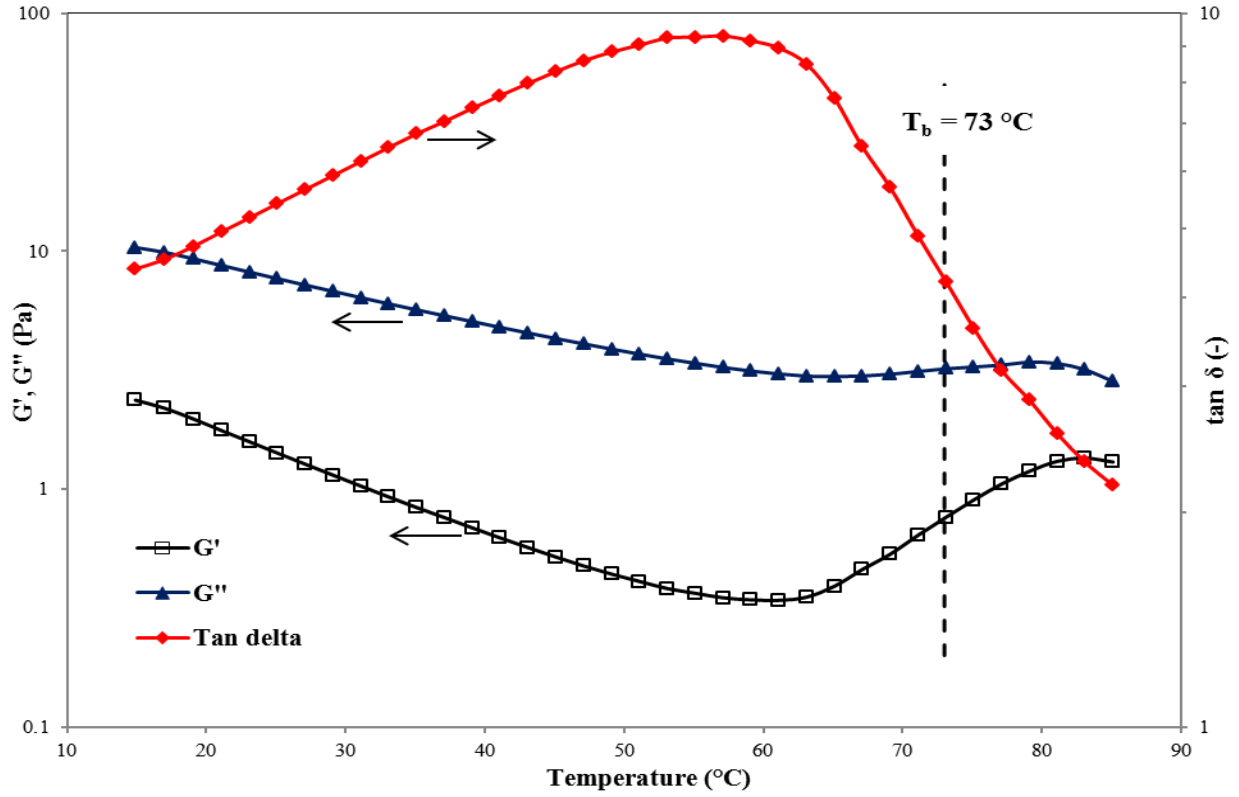

Figure 4-1**:** Isochronal dynamic temperature sweep of storage modulus (G'), loss modulus (G'') and tan δ for a solution of 6 wt % PEO in water. Measured at a fixed frequency of 1 rad/s, oscillatory stress of 2 Pa and heating rate of 0.5 °C/min.

The observed remarkable increase of the elasticity during the dynamic temperature sweep is most probably related to the morphology changes that occur during the phase separation of the solution. This elasticity enhancement originates mainly from two sources: concentration fluctuations resulting from coupling between chain mobility and thermodynamic forces [45, 46, 52], and formation of new interfaces during phase separation that brings in additional elasticity to the system.[43] PEO-rich domains may form during the segregation process, and the deformation and shape recovery of these domains may enhance the elasticity. This phenomenon can be considered as interfacial tension-driven elasticity, as seen in molten polymer blends.[44] Therefore, it is

predictable that the storage modulus, G', and loss tangent, tan δ, would be more sensitive to temperature changes since the stress induced to the system by the concentration fluctuations and the new interface formation have mostly an elastic origin that affect more the elastic modulus. The developed equations for G' and G'' (Eqs. 4-6 and 4-7 in Section 4-2) by Ajji and Choplin[48] also confirm this dependency.

Fig. 4-1 can be used to determine the binodal decomposition temperatures or cloud points. The temperature at the inflection point of G' or tan δ versus temperature, i.e. the temperature at the minimum dG'/dT, is assigned as the binodal temperature.[44, 45, 63] For the 6 wt% PEO water solution, a binodal temperature of 73 °C is obtained by this method, indicated by the dashed line in Fig. 4-1. The reported cloud point in the literature for PEO with similar molecular weight is around 85-90 °C. [4, 6, 10] The discrepancy between the binodal points obtained from rheometry with that measured by light scattering could be attributed to the aforementioned[7, 13] clustering effect in aqueous PEO solutions.

Formation of clusters at temperatures well below the phase separation temperature of PEO solution in water was investigated by several researchers using light and neutron scattering methods.[2, 5, 7, 9, 13] They showed that undissolvable aggregates increased when the PEO solution was heated to temperatures higher than 30 °C. They found that clusters concentration dramatically increased when the temperature was still 30 °C below the cloud point of the solution. A cluster size of 1.36 μm for a 4 wt% solution of 100 kDa PEO[7], and 740 nm for a very dilute (20 ppm) solution of 1000 kDa PEO[3] in water, has been reported in the literature. Clustering has been ignored in all proposed thermodynamic models for predicting PEO/water phase diagram and the phase separation behavior.[1, 7, 9] Only de Gennes [64] attempted to explain the clustering effect in aqueous PEO solutions by considering a novel second type of phase separation occurring well below the conventional LCST point, in which a very dilute solution of collapsed coils coexists with a dense polymer phase (i.e. clusters or aggregates).[9] It is speculated that the binodal temperature measured by rheological measurements in Fig. 5-1 is somehow associated with this phase separation phenomenon, as it is 10-20 °C below the reported cloud point for this sample, and hence in good agreement with cluster formation temperatures reported

in the literature.[5, 9, 64] The anomalous rheological behaviour of dilute PEO solutions was also ascribed to the presence of aggregates in PEO solutions.[3] PEO clusters mainly exist in solutions in two forms: high density spherulitic particles and low density aggregates of non-crystalline microgel particles [3, 5, 7], which both induce significant elasticity to the system. Moreover, it is worth noting that the binodal points obtained by optical methods are mainly measured in quiescent conditions, whereas in this study the phase separation point is measured under mild flow conditions. It was reported that shear flow can shift the binodal temperature by a few degrees, due to shear-induced demixing at low shear rates or lowering the chains entropy under applied rheological flow.[53, 65]

The spinodal decomposition temperature of the solution can be estimated by applying the quantitative Ajji and Choplin's [48] modified approach of Frederickson and Larson[49] theory (Section 4-2).

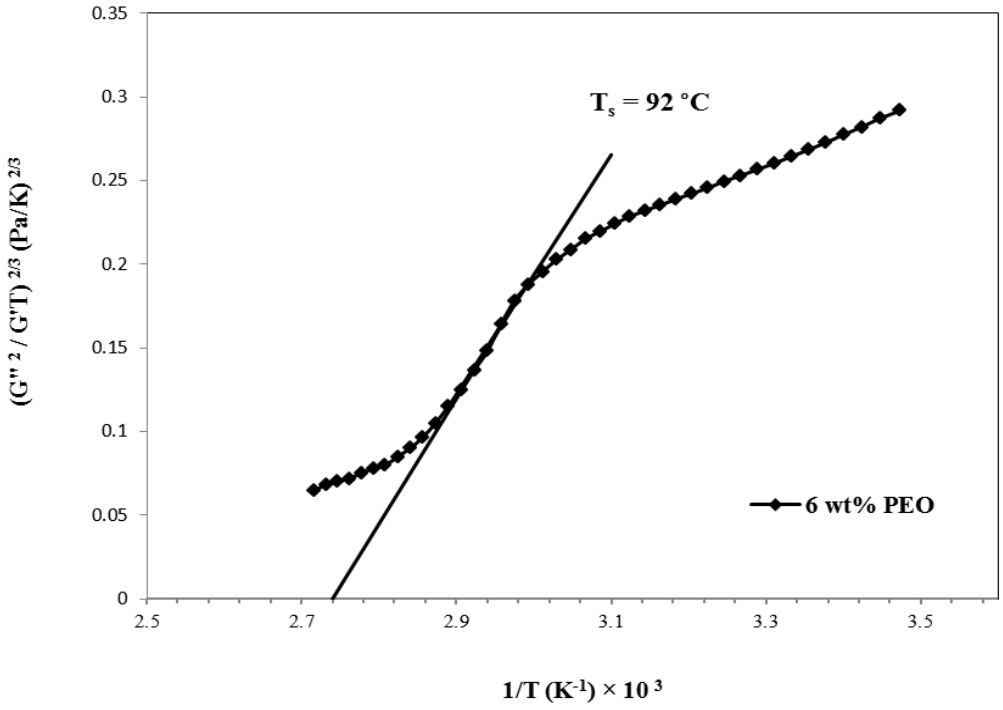

Figure 4-2: Estimation of spinodal temperature from the quantitative evaluation of the viscoelastic behaviour of a 6 wt% PEO in water near the phase boundary. The spinodal temperature is indicated in the figure by the intercept of the curve in the linear region.

Figure 4-2 displays $(G''^2/G'T)^{2/3}$ versus $1/T$ for the 6 wt% PEO solution in water. As mentioned in Section 4-2, the linear region in Fig. 4-2 corresponds to the one-phase region near the phase separation point. In this curve, the reciprocal of the intercept with the $1/T$ axis is assumed to be the spinodal temperature, T_s, that was calculated to be about 92 ± 3 °C for the PEO solution in Fig. 4-2. The error associated with the evaluation of the spinodal temperature is approximately ± 3 °C, based on the selection of the fitted line on the linear region of the curve. The obtained spinodal temperature by this method agrees well with the T_s points obtained by Hammouda and coworkers from SANS measurements. They reported spinodal temperatures of 105 °C and 95 °C for 4 wt% solutions of 50 and 100 kDa PEO in water, respectively. [7,13]

Figure 4-3 shows the changes in the correlation length, ξ of the PEO solution with temperature near the phase separation region. The data plotted in this figure were determined from Eq. 4-11 (Section 4-2), by using the rheological data of Fig. 4-1. The correlation length is related to concentration fluctuations. Significant changes in correlation length in the phase separation area represent the changes of the degree of local ordering and increased composition fluctuations during phase separation.[44] The order of magnitude of the correlation length obtained in this work through rheological measurements is almost the same as that reported by Hammouda et al.[13] obtained by the SANS method. They found correlation length of around 40-400 Å for a 4wt % solution of 100 kDa PEO in water.[13] This also validates again the rheological technique to find out thermodynamic properties. The binodal temperature is indicated in Fig. 4-3, and it is indeed located in the transition range, close to the inflection point.

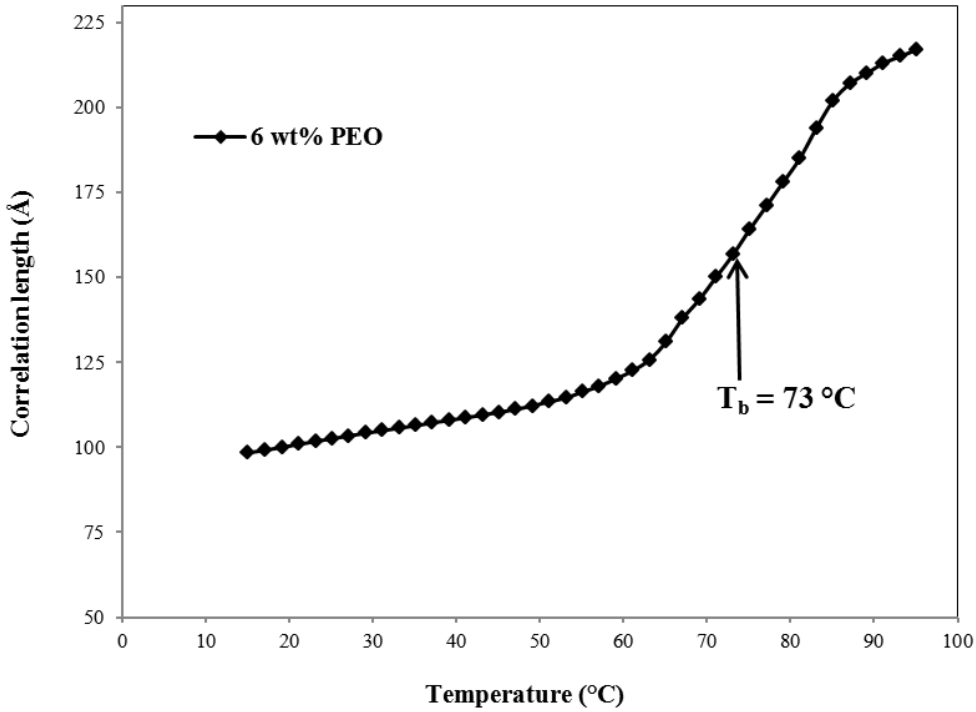

Figure 4-3: Temperature dependence of the correlation length, ξ for the 6 wt% PEO solution in water obtained quantitatively from Eqn 11 (Section 5-2) and isochronous dynamic temperature sweep data (Fig. 5-1).

4.5.1.2 Chitosan/PEO aqueous acetic acid solutions

After showing that rheological measurements can be employed successfully to determine the phase separation behaviour of a polymer solution, the same procedure is used for the solutions of interest here, i.e. chitosan, PEO and their blends in aqueous acidic solutions. As mentioned before, these solutions have shown anomalous behaviour during fiber electrospinning at elevated temperatures, [29] which was suspected to be due to phase separation during the process.

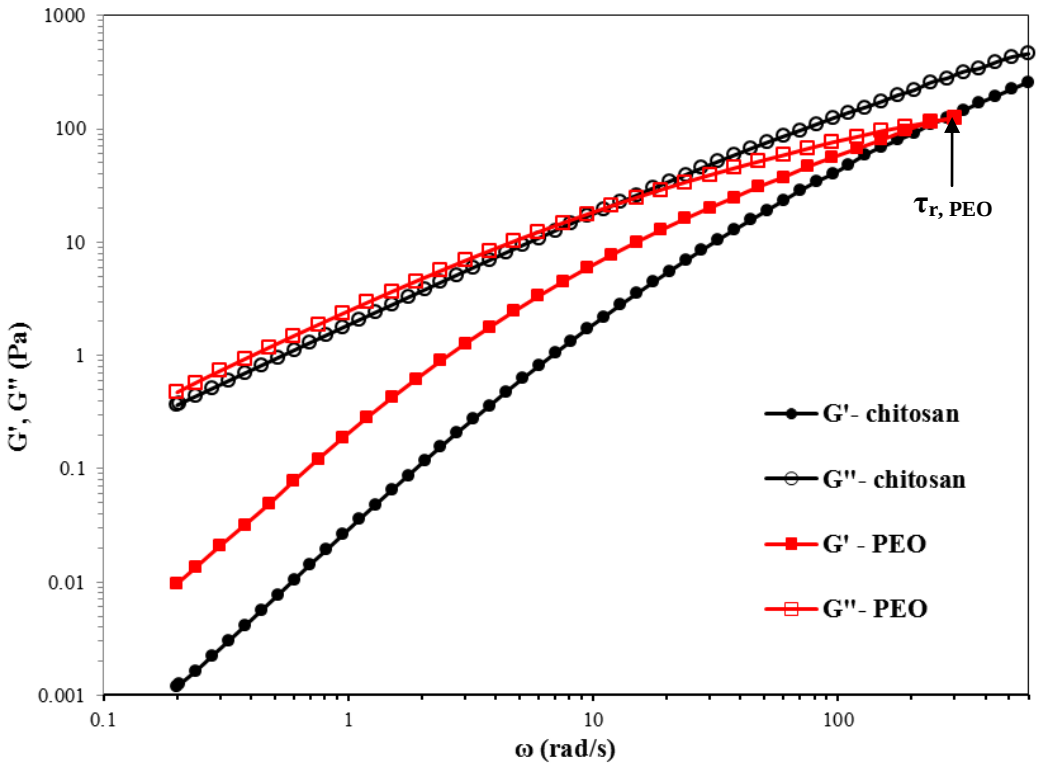

Figure 4-4: Frequency sweep plots of storage modulus, G', and loss modulus, G'', for 4 wt% solutions of neat chitosan and PEO in 50 wt% aqueous acetic acid at 25 °C.

Dynamic rheological properties of the neat solutions of chitosan and PEO in aqueous acetic acid were measured by isothermal frequency sweep experiments at 25 °C. The results are shown in Fig. 4-4. This figure depicts that the elastic modulus of PEO is higher than that of chitosan up to a frequency of 300 rad/s. The characteristic relaxation time, τ_r, obtained from the reciprocal of the frequency where $G' = G''$, (~ 5 ms) is longer for PEO than chitosan. In fact, this intersection point for chitosan falls outside the frequency range studied in this work and hence is shorter than ~ 1 ms. The characteristic relaxation time of the polymer chains is related to the monomeric friction coefficient or chain entanglements.[66] Lower elasticity and shorter relaxation time for

chitosan are probably due to repulsive forces between NH_3^+ groups formed in acidic media. This may reduce chain entanglements and result in a rigid rod-like chain conformation in the solution state.[15, 18]

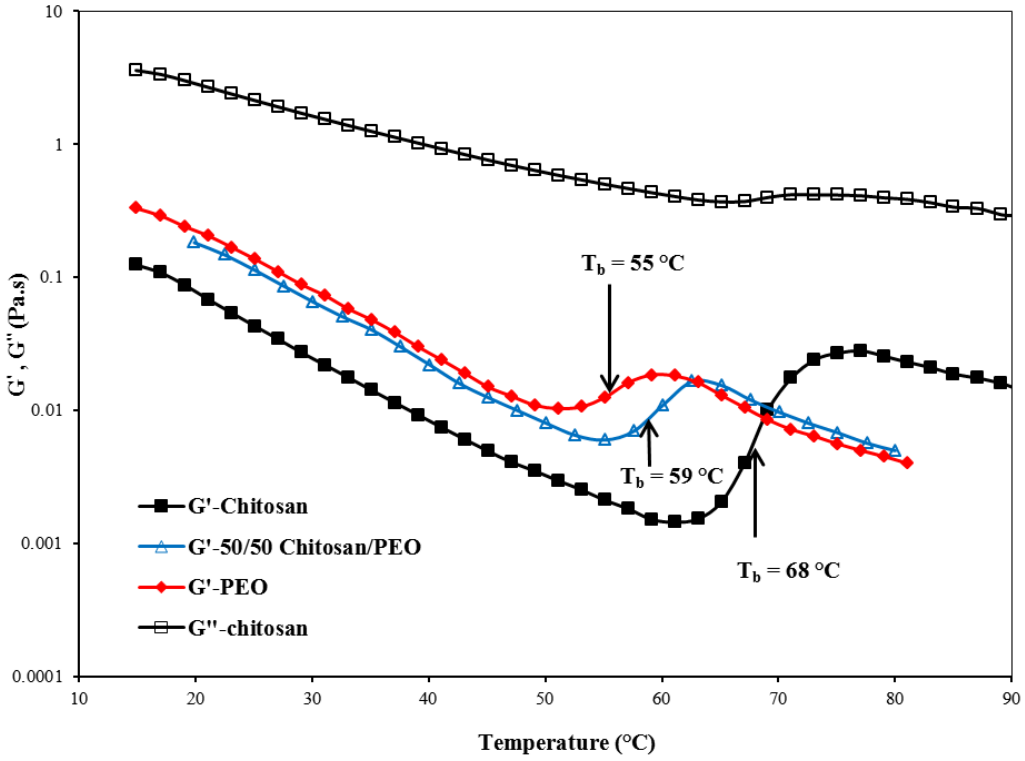

Figure 4-5: Isochronal dynamic temperature sweep of storage modulus (G') and loss modulus (G'') for 4 wt % solutions of chitosan, PEO and their 50/50 blend in 50 wt% aqueous acetic acid solution. Measured at a fixed frequency of 1 rad/s, oscillatory stress of 2 Pa and heating rate of 0.5 °C/min. Vertical lines show the rheologically determined binodal temperatures at the inflection points of G' vs. temperature curves.

To elucidate the phase behaviour of aqueous acetic acid solutions of chitosan and PEO with temperature, the method used above for PEO/water solution was applied. Dynamic isochronal

temperature sweep tests were carried out on the neat chitosan and PEO solutions and their blends at different composition ratios of 80/20, 50/50 and 20/80.

Figs. 4-5 and 4-6 present the evolution of the storage modulus (G') and tan δ, respectively, during dynamic temperature sweeps at a fixed frequency of 1 rad/s and oscillatory stress of 2 Pa for 4 wt% chitosan, PEO and their 50/50 blend solutions. Again the temperature was increased from 15 to 90 °C at a rate of 0.5 °C/min. Similar behaviours to that observed previously for the PEO/water solution (Fig. 4-1) can be depicted in Figs 4-5 and 4-6, i.e. a gradual decrease of G' with temperature along with a clear upturn at higher temperatures, and a reverse trend for the tan δ curves. Therefore it can be concluded that all these solutions also exhibit an LCST in their phase diagram, as they reveal phase separation behaviour with increasing temperature. This is attributed to the changes in specific interactions due to hydrogen bonds between hydroxyl groups of acetic acid/water solvent and ether groups in PEO, and hydroxyl and amino groups in chitosan.[14, 16, 29] It is well known that solutions with strong solvent/polymer interactions show an LCST phase diagram.[1, 3, 8]

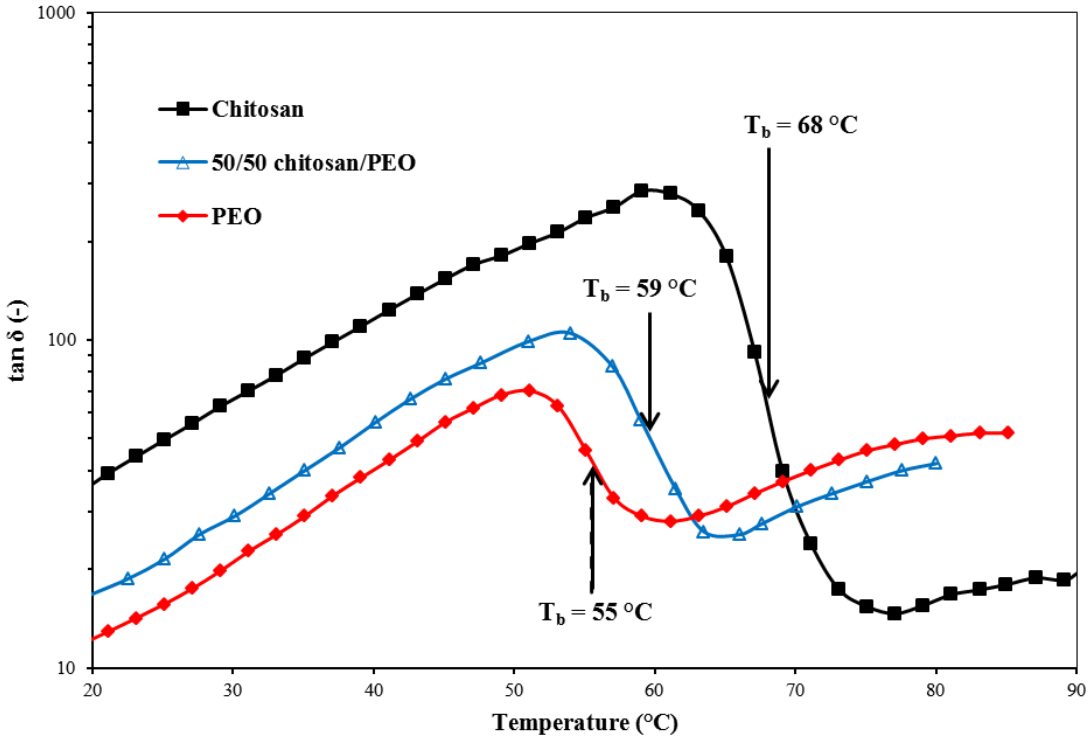

Figure 4-6: Isochronal dynamic temperature sweep of loss tangent angle (tan δ) for 4 wt% neat chitosan, PEO and their 50/50 blend in 50 wt% aqueous acetic acid solution. Measured at a fixed frequency of 1 rad/s, oscillatory stress of 2 Pa and heating rate of 0.5 °C/min. Vertical lines show the rheologically determined binodal temperatures at the inflection points of tan δ vs. temperature curves.

It is interesting to note that, over the tested temperature range, the 50/50 blend solution exhibits a single peak located between the peaks of its neat polymer constituents. This indicates full miscibility of chitosan and PEO in the solution state, hence a homogeneous solution up to phase separation temperatures. Additionally, it is also apparent from Figs. 5-5 and 5-6 that not only the magnitude of the upturn and reduction of the storage modulus and loss tangent angle, respectively, strongly depend on solution composition, but also the temperature range over which the sharp changes occur. The binodal decomposition temperatures, T_b, of the solutions were estimated using the same approach as for the PEO/water solution (Fig. 4-1). Inflection points of

G' and tan δ curves versus temperature gave estimates of binodal temperatures of about 68, 55 and 59 °C for neat chitosan, neat PEO and their 50/50 blend solutions, respectively. These points are indicated by arrows in Figs. 4-5 and 4-6. The evaluations from G' and tan δ resulted in the same value of T_b for each composition. Similar results were obtained for the 20/80 and 80/20 solutions, but the corresponding curves are not shown for the sake of clarity. The binodal temperatures evaluated for these two blends are reported below.

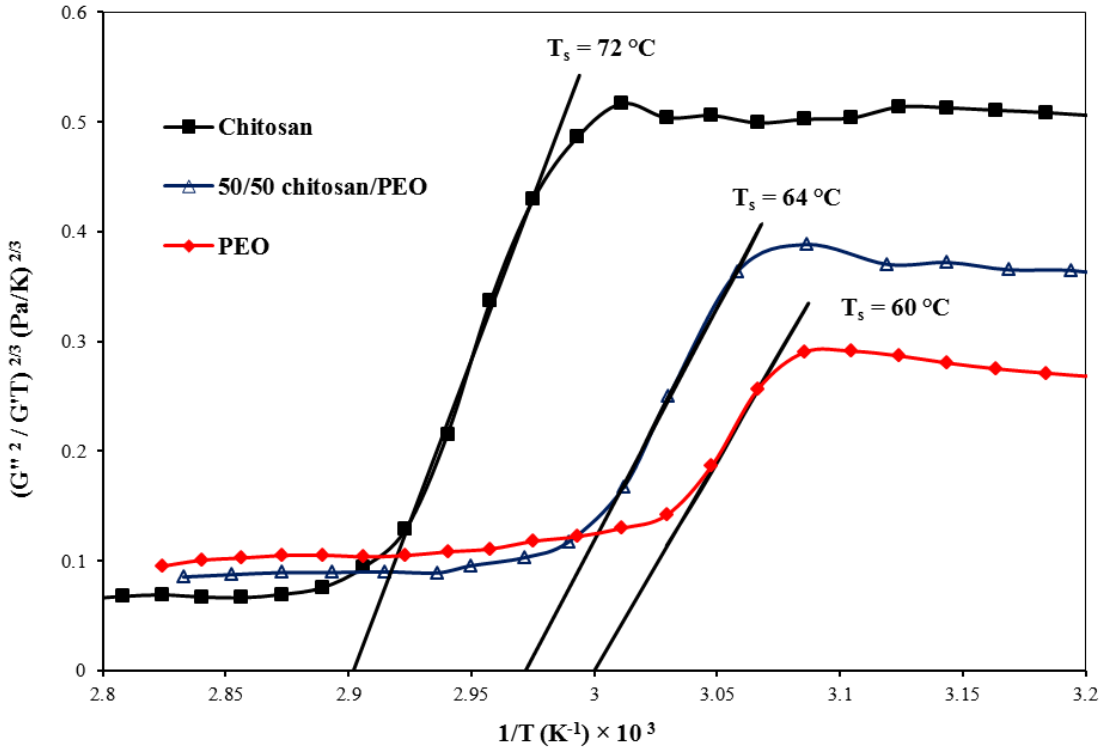

Figure 4-7: Estimation of spinodal temperature from the quantitative evaluation of the viscoelastic behaviour of neat chitosan, PEO and their 50/50 blend in 50 wt% aqueous acetic acid, near the phase boundary. The spinodal temperatures are indicated in the figure from the intercept of the curves in the linear region.

The approach taken in Fig. 4-2 was also employed to quantitatively evaluate the spinodal decomposition temperatures of PEO/chitosan solutions. Figure 4-7 presents $(G''^2/G'T)^{2/3}$ versus $1/T$ for the 4 wt% solutions of neat PEO, neat chitosan solution and their 50/50 blend in 50 wt% aqueous acetic acid solution. Spinodal temperatures T_s, were determined to be 72, 60 and 64 °C for neat chitosan, neat PEO and their 50/50 blend solutions, respectively. An error of about ± 2.5 °C is involved in these values.

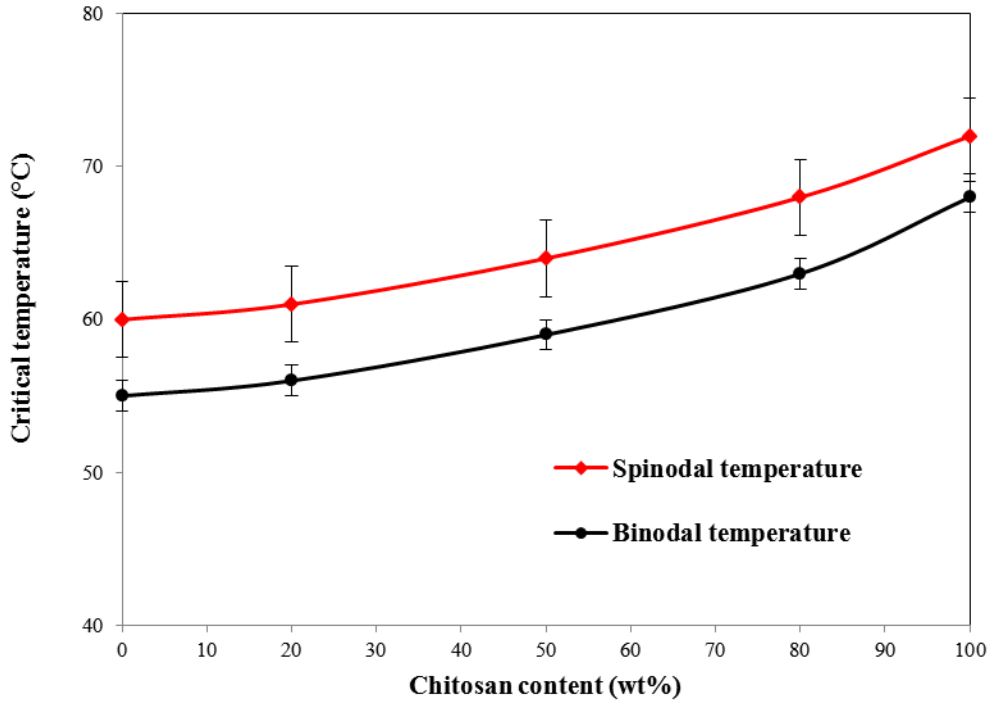

Figure 4-8: Binodal and spinodal phase separation temperatures of neat chitosan, neat PEO and their blends at different ratios in 50 wt% aqueous acetic acid (Total polymer concentration is 4 wt% for all solutions).

Binodal and spinodal decomposition temperatures of aqueous acetic acid solutions of chitosan and PEO and their blends, determined by temperature sweep experiments, are shown in Fig. 4-8

as functions of chitosan content. It depicts that, for the same 4 wt% total polymer concentration, chitosan has the higher LCST temperature. It means that chitosan in the aqueous acetic acid solvent has a larger one-phase homogeneous region as compared to PEO. It is known that LCST phase behaviour in polymer solutions is typical of systems that exhibit hydrogen bonds. Hydrogen bonds weakening or complete debonding occurs by a temperature increase.[1, 8, 9] Higher LCST in chitosan could be due to more intense interactions with the acetic acid/water solvent. While PEO can form hydrogen bonds only via its ether groups, chitosan has more active groups such as hydroxyl, acetylamine and amino groups to form hydrogen bonds.[14, 19] Therefore, temperature- induced disruption in polymer/solvent interactions affects more PEO and leads to an earlier phase separation lower critical temperature. Binodal and spinodal decomposition temperatures of chitosan/PEO blends are located between those of neat chitosan and PEO solutions, which is again an indication of their miscibility in the solution state prior to phase separation.

It is worth noting that both estimated binodal and spinodal temperatures for PEO in aqueous acetic acid solvent are about 15-20 °C lower than for PEO in water (Figs. 4-2 and 4-3). It indicates that the degree of association between PEO and the solvent in aqueous acetic acid solution is reduced earlier by increasing temperature. This is more likely due to weaker or fewer hydrogen bonds formed between acetic acid and PEO, as compared to PEO and water molecules. In PEO/water solution it is suggested that two water molecules are associated with each PEO monomer, that at the same time are in competition to form water-water hydrogen bonds with their neighboring water molecules.[1, 8] These prevailing hydrogen bonds are responsible for the unusual aforementioned characteristics of PEO solutions in water.

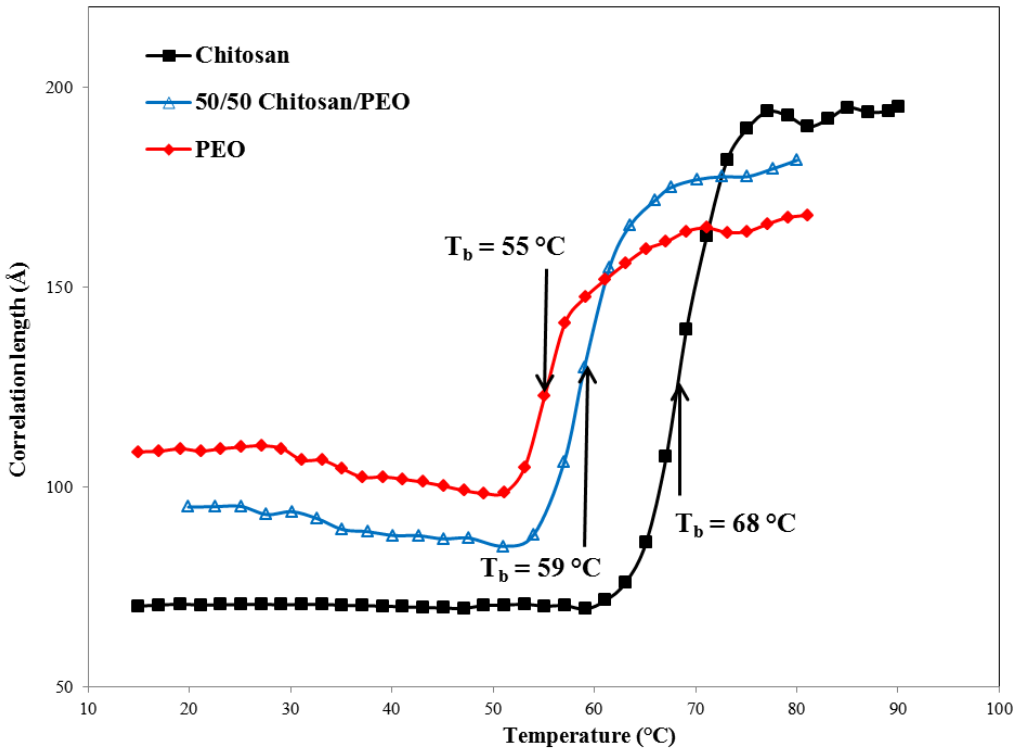

Figure 4-9: Temperature dependence of the correlation length, ξ for neat chitosan, neat PEO and their 50/50 blend in 50 wt% aqueous acetic acid obtained quantitatively from the rheological measurements.

Plots of the correlation length (ξ) evaluated from Eq. 4-11 (Section 4-2) as a function of temperature in the vicinity of phase separation for neat chitosan, PEO and their 50/50 blend are shown in Fig. 4-9. The order of magnitude of the correlation length of these solutions and PEO solution in water (Fig. 4-3) are almost the same. It reflects that concentration fluctuations and the process of phase separation in these polymer solutions are similar. Binodal decomposition temperatures are also indicated in Fig. 4-9 and are located in the transition range, close to the inflection point.

4.5.2 Isothermal steady shear viscosity results

Steady shear viscosity as a function of shear rate and temperature for solutions of 4 wt% neat chitosan and its 50/50 blend with 4 wt% PEO in 50 wt% aqueous acetic acid is shown in Fig. 10. The experiments were carried out from 25 to 70-80 °C over a shear rate range of 0.1 to 1000 s^{-1}. A typical shear-thinning behaviour with a well-developed plateau region is observed for neat chitosan solutions up to 60 °C (Fig. 5-10-A). This figure also shows that the magnitude of the zero-shear viscosity decreases with an increase of temperature up to 60 °C, and that the critical shear rate for the onset of shear-thinning increases as the temperature is raised. However, at a temperature of 70 °C, an enhancement in the viscosity is observed at low shear rates (Fig. 5-10-A). This temperature is near the phase separation point of this solution that was estimated to have a binodal temperature of 68 °C (Section 5-4-1). This enhancement in viscosity at low shear rates may be explained by Onuki's[67] interpretation of the viscosity of a phase separating two-component fluid near the critical point, and its similarity with a suspension of droplets in a fluid after the formation of phase-separated domains near the critical point.[67] The same behavior is also observed for the 50/50 blend of chitosan/PEO in aqueous acetic acid solution (Fig. 4-10-B). In this solution, the increase of viscosity at low shear rates is detected at temperatures as low as 60 °C, which is in agreement with its determined binodal phase separation temperature (59 °C). These results are in contrast with Sharma's [50] findings for a polymer blend system who reported that the overall behaviour of viscosity versus shear rate remains unchanged at temperatures before and after the phase separation point. This is more likely because Sharma tried to apply the Onuki's approach, developed for polymer solutions, to a molten polymer blend that is probably far from the emulsion behaviour observed in here.

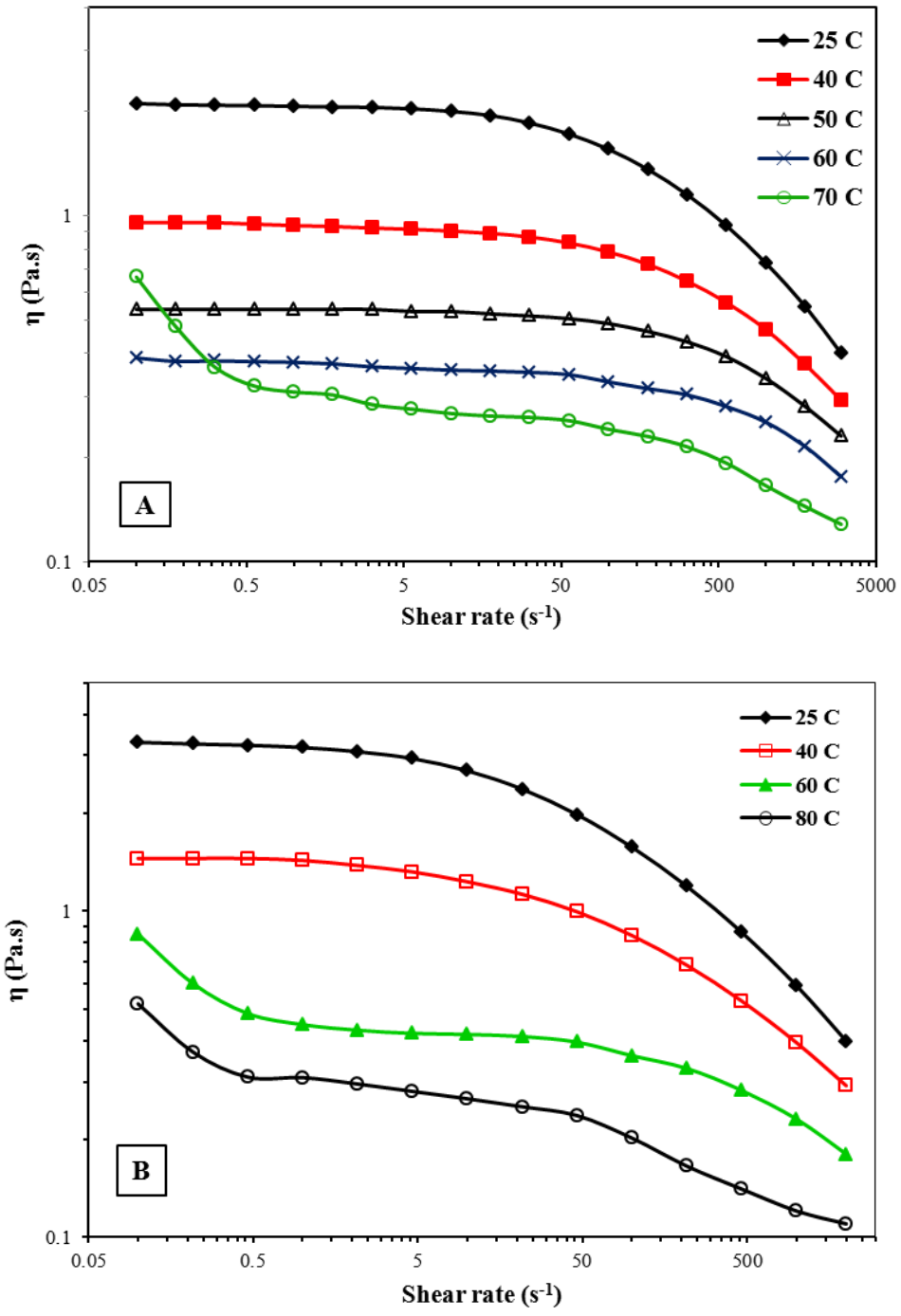

Figure 4-10: Plot of isothermal shear viscosity versus shear rate for A) 4 wt% neat chitosan solution and B) its 50/50 blend with 4 wt% PEO over the temperature range covering homogeneous to the two-phase regimes of the solutions phase behaviours, all in 50 wt% aqueous acetic acid solvent.

4.5.3 Flory-Huggins interaction parameter from rheological data

The temperature dependence of the Flory-Huggins interaction parameter, χ of the solutions investigated was evaluated from the basic thermodynamic approach described in Section 5-2-2 and the binodal and spinodal points estimated from rheological measurements (Section 4-4-1). The computed *A* and *B* coefficients (Eq. 4-12) and interaction parameter at certain temperatures are reported in Table 4.1. Absolute values of χ at given temperatures and the related coefficients, *A* and *B*, in the case of the PEO/water solution, coincide well with results reported in the literature obtained by light scattering, gas chromatography and vapour pressure osmometry techniques. The negative value of *B* confirms the existence of LCST phase diagrams in the PEO/chitosan solutions.

Table 4.1: *A* and *B* coefficients of Flory-Huggins interaction parameter, Eq. 4-12, and values of the interaction parameter, χ, at given temperatures obtained by using different experimental methods

Reference	Method	Solvent	Polymer	*A*	*B (K)*	T(°C)	Interaction parameter (χ)
This paper	Rheometry	Water	PEO, 600 kDa	0.8	-100	25	0.4644
Venohr et al[58]	Dynamic and static light scattering	Water	PEO, 20 kDa	0.8	-108	----	----
Venohr et al[58]	Dynamic and static light scattering	Water	PEO, 100 kDa	----	----	20	0.4653
Polik and Borchard[5]	Static light scattering	Water	PEO, 17 kDa	0.51	-3	25	0.5
Michalczyk and Borchard[59]	Vapor pressure osmometry	Water	PEO, 100 kDa	0.66	-71	----	----
Fischer[37]	Turbidity observation	Water	PEO, 6 kDa	2.41	-730.5	----	----
Bae et al[56]	Vapor sorption	Water	PEO, 8 kDa	----	----	30	0.349
Safranov & Zubarev[68]	Calculation of enthalpy of dilution	0.3 M acetic acid	Chitosan, 88% DDA	----	----	25	-0.01
This work	Rheometry	50 wt% acetic acid	PEO, 600 kDa	0.85	-120	25	0.4404
This work	Rheometry	50 wt% acetic acid	Chitosan, 98% DDA	0.9	-150	25	0.388

4.6 Conclusions

In this work a systematic rheological investigation of the well-known LCST polymer solution of PEO in water was conducted. We showed that the phase separation temperature of this solution could be assessed directly by rheological measurements. Binodal points were estimated from dynamic temperature sweep experiments and spinodal points were quantitatively calculated on the basis of a mean field theory. Comparing these critical points with that obtained from other experimental techniques showed that rheological measurements can sensitively detect rather early stages of phase separation.

This approach was then employed on our solutions of interest: chitosan/PEO at different ratios in aqueous acetic acid. These solutions showed a LCST phase diagram as well, originating mainly from the existence of hydrogen bonds. Knowledge of phase separation temperature of chitosan-based solutions is crucial for chitosan wet route formation processes. Additionally, occurrence of a viscosity enhancement in isothermal steady shear measurements right after phase separation confirms the validity of the aforementioned approach to determine solution critical points. The Flory-Huggins interaction parameter was calculated from the binodal and spinodal points estimated by the rheological measurements. The obtained results agreed well with reported data in the literature for aqueous PEO solution which validate further the rheometry-based approach used in this work. Additionally, this parameter was estimated for the first time for PEO/chitosan solutions in 50 wt% aqueous solution. Therefore, rheology provides a powerful and simple technique to assess the phase separation behaviour of polymer solutions.

4.7 Acknowledgements

The authors acknowledge the financial support of this work by NSERC (National Science and Engineering Research Council of Canada) and FRQNT (Fonds de recherche du Québec - Nature et technologies).

4.8 References

1. Dormidontova, E. E. Macromolecules 2002, 35, (3), 987-1001.
2. Duval, M.; Sarazin, D. Polymer 2000, 41, (7), 2711-2716.
3. Shetty, A. M.; Solomon, M. J. Polymer 2009, 50, (1), 261-270.
4. Saeki, A.; Kuwahara, N.; Nakata, M.; Kaneko, M. Macromolecules 1976, 17, 685-689.
5. Polic, W. F.; Burchard, W. Macromolecules 1983, 16, 978-982.
6. Bae, Y. C.; Lambert, S. M.; Soane, D. S.; Prausnitz, J. M. Macromolecules 1991, 24, (15), 4403-4407.
7. Hammouda, B.; Ho, D. L.; Kline, S. Macromolecules 2004, 37, (18), 6932-6937.
8. Dormidontova, E. E. Macromolecules 2004, 37, (20), 7747-7761.
9. Bekiranov, S.; Bruinsma, R.; Pincus, P. Physical Review E 1997, 55, (1), 577-585.
10. Fischer, V.; Borchard, W. Journal of Physical Chemistry B 2000, 104, (18), 4463-4470.
11. Esquenet, C.; Buhler, E. Macromolecules 2002, 35, (9), 3708-3716.
12. Esquenet, C.; Buhler, E. Macromolecules 2001, 34, (15), 5287-5294.
13. Hammouda, B.; Ho, D.; Kline, S. Macromolecules 2002, 35, (22), 8578-8585.
14. Rinaudo, M. Progress in Polymer Science 2006, 31, (7), 603-632.
15. Pillai, C. K. S.; Paul, W.; Sharma, C. P. Progress in Polymer Science 2009, 34, (7), 641-678.
16. Schatz, C.; Viton, C.; Delair, T.; Pichot, C.; Domard, A. Biomacromolecules 2003, 4, (3), 641-648.
17. Kumar, M. Reactive & Functional Polymers 2000, 46, (1), 1-27.
18. Kumar, M.; Muzzarelli, R. A. A.; Muzzarelli, C.; Sashiwa, H.; Domb, A. J. Chemical Reviews 2004, 104, (12), 6017-6084.
19. Philippova, O. E.; Volkov, E. V.; Sitnikova, N. L.; Khokhlov, A. R.; Desbrieres, J.; Rinaudo, M. Biomacromolecules 2001, 2, (2), 483-490.
20. Dash, M.; Chiellini, F.; Ottenbrite, R. M.; Chiellini, E. Progress in Polymer Science 2011, 36, (8), 981-1014.

21. Riva, R.; Ragelle, H.; des Rieux, A.; Duhem, N.; Jerome, C.; Preat, V. Advances in polymer science 2011, 244, 19-44

22. Jayakumar, R.; Menon, D.; Manzoor, K.; Nair, S. V.; Tamura, H. Carbohydrate Polymers 2010, 82, (2), 227-232.
23. Dutta, P. K.; Tripathi, S.; Mehrotra, G. K.; Dutta, J. Food Chemistry 2009, 114, (4), 1173-1182.
24. Jayakumar, R.; Prabaharan, M.; Nair, S. V.; Tamura, H. Biotechnology Advances 2010, 28, (1), 142-150.
25. Correlo, V. M.; Boesel, L. F.; Bhattacharya, M.; Mano, J. F.; Neves, N. M.; Reis, R. L. Materials Science and Engineering a-Structural Materials Properties Microstructure and Processing 2005, 403, (1-2), 57-68.
26. Epure, V.; Griffon, M.; Pollet, E.; Averous, L. Carbohydrate Polymers 83, (2), 947-952.
27. Mir, S.; Yasin, T.; Halley, P. J.; Siddiqi, H. M.; Nicholson, T. Carbohydrate Polymers 2011, 83, (2), 414-421.
28. Zivanovic, S.; Li, J. J.; Davidson, P. M.; Kit, K. Biomacromolecules 2007, 8, (5), 1505-1510.
29. Pakravan, M.; Heuzey, M. C.; Ajji, A. Polymer 2011, 52, 4813-4824.
30. Kuo, Y. C.; Ku, I. N. Biomacromolecules 2008, 9, (10), 2662-2669.
31. Mucha, M.; Piekielna, J.; Wieczorek, A. Macromolecular Symposia 1999, 144, 391-412.
32. Islam, A.; Yasin, T. Carbohydrate Polymers 88, (3), 1055-1060.
33. Chuang, W. Y.; Young, T. H.; Yao, C. H.; Chiu, W. Y. Biomaterials 1999, 20, (16), 1479-1487.
34. Sarasam, A.; Madihally, S. V. Biomaterials 2005, 26, (27), 5500-5508.
35. Sarasam, A. R.; Krishnaswamy, R. K.; Madihally, S. V. Biomacromolecules 2006, 7, (4), 1131-1138.
36. Sionkowska, A. Progress in Polymer Science 2011, 36, (9), 1254-1276.
37. Fischer, V.; Borchard, W.; Karas, M. Journal of Physical Chemistry 1996, 100, (39), 15992-15999.
38. Ataman, M. Colloid and polymer science 1987, 265, 19-25.
39. He, M. J.; Liu, Y. M.; Yi, F.; Ming, J.; Han, C. C. Macromolecules 1991, 24, (2), 464-473.
40. Lal, J.; Bansil, R. Macromolecules 1991, 24, (1), 290-297.
41. Koningsveld, R.; Kleintjens, L. A. Macromolecules 1971, 4, (5), 637-641.
42. Flory, P. J., Principles of polymer chemistry. Cornell University Press: Ithaca, NY, 1953.
43. Bousmina, M.; Lavoie, A.; Riedl, B. Macromolecules 2002, 35, (16), 6274-6283.
44. Niu, Y. H.; Wang, Z. G. Macromolecules 2006, 39, (12), 4175-4183.
45. Kapnistos, M.; Hinrichs, A.; Vlassopoulos, D.; Anastasiadis, S. H.; Stammer, A.; Wolf, B. A. Macromolecules 1996, 29, (22), 7155-7163.
46. Vlassopoulos, D.; Koumoutsakos, A.; Anastasiadis, S. H.; Hatzikiriakos, S. G.; Englezos, P. Journal of Rheology 1997, 41, (3), 739-755.
47. Yeganeh, J. K.; Goharpey, F.; Foudazi, R. Macromolecules 2010, 43, (20), 8670-8685.
48. Ajji, A.; Choplin, L. Macromolecules 1991, 24, (18), 5221-5223.
49. Fredrickson, G. H.; Larson, R. G. Journal of chemical physics 1987, 86, (3), 1553-1560.
50. Sharma, J.; Clarke, N. Journal of Physical Chemistry B 2004, 108, (35), 13220-13230.
51. Gharachorlou, A.; Goharpey, F. Macromolecules 2008, 41, (9), 3276-3283.

52. Ajji, A.; Choplin, L.; Prudhomme, R. E. Journal of polymer science: Part B: polymer physics 1991, 29, 1573-1578.
53. Madbouly, S. A.; Ougizawa, T. Macromolecular Chemistry and Physics 2004, 205, (9), 1222-1230.
54. Ajji, A.; Choplin, L.; Prudhomme, R. E. Journal of polymer science: Part B: polymer physics 1988, 26, 2279-2289.
55. Gedde, U. W., Polymer physics. Chapman & Hall: London, 1995.
56. Bae, Y. C.; Shim, J. J.; Soane, D. S.; Prausnitz, J. M. Journal of Applied Polymer Science 1993, 47, (7), 1193-1206.
57. Qian, C. B.; Mumby, S. J.; Eichinger, B. E. Macromolecules 1991, 24, (7), 1655-1661.
58. Venohr, H.; Fraaije, V.; Strunk, H.; Borchard, W. European Polymer Journal 1998, 34, (5-6), 723-732.
59. Michalczyk, A.; Borchard, W. European Polymer Journal 1989, 25, (9), 957-959.
60. Kim, S. S.; Lloyd, D. R. Polymer 1992, 33, (5), 1047-1057.
61. Yosick, J. A.; Giacomin, J. A.; Stewart, W. E.; Ding, F. Rheologica Acta 1998, 37, (4), 365-373.
62. Carreau, P. J.; De Kee, D.; Chabra, P. R., Rheology of polymeric systems: principles and applications. Hanser Publishers: Munich, 1997.
63. Patel, A. J.; Balsara, N. P. Macromolecules 2007, 40, (5), 1675-1683.
64. de Gennes, P. G. C.R. Academie Des Sciences Serie II 1991, 313, (10), 1117-1122.
65. Pang, P.; Englezos, P. Fluid Phase Equilibria 2002, 194, 1059-1066.
66. Doi, M.; Edward, S. F., The theory of polymer dynamics. Oxford press: New York, 1986.
67. Onuki, A. Physical Review A 1987, 35, (12), 5149-5155.

CHAPITRE 5

A FUNDAMENTAL STUDY OF CHITOSAN/PEO ELECTROSPINNING[2]

Mehdi Pakravan, Marie-Claude Heuzey and Abdellah Ajji

5.1 Abstract

A highly deacetylated (97.5%) chitosan in 50% acetic acid was electrospun at moderate temperatures (25-70 °C) in the presence of a low content of polyethylene oxide (10 wt% PEO) to beadless nanofibers of 60-80 nm in diameter. A systematic quantitative analysis of the solution properties such as surface tension, conductivity, viscosity and acid concentration was conducted in order to shed light on the electrospinnability of this polysaccharide. Rheological properties of chitosan and PEO solutions were studied in order to explain how PEO improves the electrospinnability of chitosan. Positive charges on the chitosan molecule and its chain stiffness were considered as the main limiting factors for electrospinability of neat chitosan as compared to PEO, since surface tension and viscosity of the respective solutions were similar. Various blends of chitosan and PEO solutions with different component ratios were prepared (for 4 wt% total polymer content). A significant positive deviation from the additivity rule in the zero shear viscosity of chitosan/PEO blends was observed and believed to be a proof for strong hydrogen bonding between chitosan and PEO chains, making their blends electrospinnable. The impact of temperature and blend composition on the morphology and diameter of electrospun fibers was also investigated. Electrospinning at moderate temperatures (40-70 °C) helped to obtain beadless nanofibers with higher chitosan content. Additionally, it was found that higher chitosan content in the precursor blends led to thinner nanofibers. Increasing chitosan/PEO ratio from 50/50 to 90/10 led to a diameter reduction from 123 to 63 nm. Producing defect free nanofibrous mats from the electrospinning process and with high chitosan content is particularly promising for antibacterial film packaging and filtration applications.

---

[2] Published in Polymer 52, 2011, 4813-4824

5.2 Introduction

Polysaccharides are some of the most promising natural materials to substitute for synthetic polymers in a number of applications due to their abundance in nature. Chitin and chitosan polymers are not only natural aminopolysaccharides, but also provide specific properties owing to their unique structures. Chitosan has been widely used in several industries due to its natural origin and exceptional properties such as biodegradability, biocompatibility, non-toxicity and chelation with metals. Among them, biomedical applications including tissue-engineering scaffolds and wound healing dressings, along with water filtration applications using separation membranes, have attracted a lot of attention lately [1-3]. Moreover, chitosan is a good inhibitor against the growth of a wide variety of yeasts, fungi and bacteria, and also displays gas and aroma barrier properties in dry conditions. These characteristics, beside its ease of film formation, make chitosan an interesting choice for active anti-bacterial food packaging applications. Chitosan-based packaging films can improve the quality, security and storage stability of perishable foods [4-8].

Films and membranes with micro and nanoporous morphologies exhibit enhanced efficiency because of their large specific area; such individual layers can be combined with barrier and structural films to provide the required permeability and mechanical properties, respectively. Such chitosan mats can not only present the specific physicochemical properties of chitosan but can also benefit from the physical characteristics of nanoporous membranes. A number of different methods have been used to obtain porous chitosan membranes such as phase separation [9, 10], phase inversion [11] and selective dissolution [12]. More recently, electrospinning has been developed as a novel technique to generate polymeric fibers of nanometric size, resulting in non-woven three-dimensional porous mats with distinctly high surface area to mass ratio (typically 40-100 m^2/g) [13-15] .

The electrospinning process involves the application of a high voltage between a syringe filled with a polymer solution and a collector mounted at a fixed distance from the needle/syringe set-up. An electrical charge builds up on the surface of the solution that is attracted to the collector. The large potential difference overcomes the surface tension of the fluid droplet at the tip of the needle. Under specific conditions of voltage, flow rate and distance, a jet of fluid is ejected from the needle and subjected to whipping and splaying instabilities due to stresses from electrostatic

origin [16]. The solvent evaporates over the jet path, and polymer nanofibers are formed on the collector. Various factors affect the electrospinning process such as solution properties, process parameters (flow rate, voltage, distance,…) and ambient conditions; hence different requirements should be met in order to have an efficient process [13, 17].

The electrospinnability of chitosan is limited mainly because of its polycationic nature in solution, rigid chemical structure and specific inter and intra-molecular interactions [18-20]. Formation of strong hydrogen bonds prevents the free movement of polymeric chain segments exposed to the electrical field, leading to jet break up during the process [19-21]. Moreover, the repulsive force between ionic groups on the polymer backbone is expected to hinder the formation of sufficient chain entanglements to allow continuous fiber formation during jet stretching, whipping and bending, generally resulting in nanobeads instead of nanofibers [22].

Trifluoroacetic acid (TFA) is a well-known solvent for the electrospinning of chitosan. It can form stable salts with chitosan which prevents interchain interactions, and also has a low boiling point (71.8 °C as compared to 118.1 °C for acetic acid), which is beneficial for faster fiber formation in the evaporation region of the electrospinning process [23]. Some papers report the preparation of pure electrospun chitosan nanofibers using TFA or its mixtures with dichloromethane (DCM) and trichloromethane (TCM) [24, 25]. However, TFA is environmentally harmful, very toxic and corrosive, which makes its use very limited from an industrial point of view for food and biomedical applications. A highly concentrated acetic acid aqueous solution (90 wt %) was also reported by two research groups as a successful solvent for the electrospinning of neat chitosan, using samples with degrees of deacetylation (DDA) of 54 and 75-85%, respectively [21, 26]. Electrospinning of chitin followed by deacetylation of the prepared nanofibers [22, 24], and co-axial electrospinning of chitosan with polyethylene oxide (PEO) are alternative proposed methods [27], however they present their own difficulties such as solubility and electrospinnablity of chitin or controlling adequately the co-axial electrospinning process. Finally, chemically modified chitosan has also been electrospun by some researchers, such as hexanoyl chitosan [28, 29], carboxymethyl chitosan [30], carboxyethyl chitosan [31] and quaternized chitosan [32, 33]. Among all of these approaches, the most successful and easiest method to improve the electrospinnability of chitosan is blending it with a second natural or synthetic polymeric phase. This co-spinning agent is usually an easily electrospinnable polymer such as PEO [7, 18, 34-36], polyvinyl alcohol (PVA) [19, 37-39], polylactic acid (PLA) [25, 40,

41], polyacrylamide (PAM) [42, 43], zein [44, 45], silk fibroin [46, 47] and collagen [48], which are all biocompatible and biodegradable and will not constraint the final applications of chitosan nanofibers. Brief descriptions of these various approaches have been recently reviewed elsewhere [49-51].

Depending on the second polymeric phase, type, content and developed morphology, physical and mechanical properties of composite chitosan nanofibers vary greatly. Integrity and stability of the fibers in different working conditions is another concern that should be taken into account for the final applications of chitosan-based nanofibers [52]. Generally, due to the outstanding electrospinnability of the selected second phase, a higher content of the co-spinning polymer leads to further improvement of chitosan electrospinnability. Normally, the second phase is added in the range of 20 to 90 wt%. Obviously, for applications that require a particular property of chitosan, such as antimicrobial properties, the lowest amount of added polymer is preferable. Bhattarai et al. [34] could reach a low amount of 10 wt% PEO in chitosan nanofibers by using dimethyl sulfoxide (DMSO) and an aniogenic surfactant in an acetic acid aqueous solvent. Recently Zhang et al. [52] prepared chitosan-based nanofibers with 5 wt% of added PEO using ultra high molecular weight PEO along with DMSO as a co-solvent. Desai et al. also reported the formation of composite chitosan nanofibers having 5 wt% PEO [20] and 10 wt% PAM [43] by utilizing a special designed hot air assisted electrospinning unit. Finally, even though the preparation of chitosan-based nanofibers at high chitosan content has been achieved in the past years, several of these studies have been based on the use of harmful solvents such as trifuoroacetic acide (TFA) and dimethyl sulfoxane (DMSO) [34, 52]. Obviously, there is much remaining to be improved and clarified in the electrospinning of chitosan.

In this work, chitosan-based nanofibers with high chitosan content are prepared from acetic acid aqueous solutions. In addition, a systematic analysis of chitosan solution properties that lead to successful electrospinning in the presence of polyethylene oxide (PEO) is presented for the first time. The effect of blend composition and acetic acid concentration on properties such as surface tension and conductivity and, ultimately, on electrospinnability are considered. An FTIR study is also performed to investigate the presence of hydrogen bonding interactions between chitosan and PEO. Since rheological characteristics have been shown to play an important role in electrospinning [53-55], the rheological behaviour of the chitosan solutions and their relationships to electrospinnability are investigated. For this aim, a highly deacetylated chitosan

(DDA=97.5 %) is used in the presence of PEO as a co-spinning agent. To the best of our knowledge this is the maximum DDA value that has ever been reported to successfully prepare electrospun chitosan nanofibers. Finally, a modified electrospinning set up is used to control the temperature of the solution being pumped through the syringe and needle to allow spinning at moderate temperatures. The influence of temperature on the electrospinnability of the chitosan solutions is also investigated.

5.3 Experimental

5.3.1 Materials

A commercial chitosan grade was supplied by Marinard Biotech (Rivière-au-Renard, QC, Canada). PEO with a molecular weight of 600 kDa was obtained from Scientific Polymers Inc. (Ontario, NY, USA). Reagent grade acetic acid (99.7 %, Aldrich, WI, USA) was employed to prepare the aqueous solutions. All the materials were used as received.

5.3.2 Chitosan characterization

5.3.2.1 Size exclusion chromatography

Size exclusion chromatography with multi-angle laser light scattering (SEC-MALLS) as described in reference [56] was used to evaluate the chitosan molecular weight. This method employs a GPC system consisting of a Shimadzu LC-20AD isocratic pump, a Dawn HELEOS II multi-angle laser light scattering detector (Wyatt Technology Co.), a Viscostar II (Wyatt Technology Co.), an Optilab rEX interferometric refractometer (Wyatt Technology Co.) and two TSK-GELPW columns (Tosoh Biosep, G4000 serial number F3373 and G3000 serial number H0012). In this procedure, a solvent of 0.15 M acetic acid/0.1 M sodium acetate and 0.4 mM sodium azide with a pH of 4.5 is used as the mobile phase in the column series. The chitosan sample was dissolved in that solvent at a concentration of 1.0 mg/mL. This solution was kept at room temperature for 24 h under gentle stirring and then filtered through a 0.45 μm membrane prior to the analysis. The injection volume, the flow rate and the temperature were 100 μL, 0.8 mL/min and 25 ºC respectively. Values of the specific refractive index, dn/dc, were measured using a Wyatt manual injector coupled with a Shimadzu LC-20AD pump and the Wyatt Optilab

rEX refractometer. The refractive indices of six solutions with different concentrations between 0 and 1 mg/mL (0, 0.1, 0.25, 0.5, 0.75 and 1 mg/mL) were recorded for calculation of d*n*/d*c*.

An average molecular weight of 85 ± 5 kDa was calculated from the observed elution time peaks (not shown here). Hence the chitosan sample used in this work is considered as a medium molecular weight grade.

5.3.2.2 Nuclear Magnetic Resonance (NMR) spectroscopy

A Bruker 500 MHz NMR spectrometer was used to obtain the ^{1}H-NMR spectrum of the chitosan sample. Solutions of chitosan (10 mg) in a mixture of D_2O and DCl (0.99/0.01 v/v) were prepared. Sixty four (64) scans of the chitosan solution were recorded with interscan delays of 6 s. In this method, the DDA is calculated using the integral of the peak of proton H1 of the deacetylated group (H1-D) and of the peak of the three protons of the acetyl group (H-Ac) from Eq. 5-1:

$$DDA(\%) = \left(\frac{H1-D}{H1-D+H-Ac/3}\right) \times 100 \qquad (5\text{-}1)$$

5.3.3 Solutions preparation

Chitosan and PEO solutions were prepared separately at 4 wt% concentration in 50 wt% aqueous acetic acid. The solution mixing was performed at room temperature using a laboratory magnetic stirrer (Corning Inc, MA, USA) for 18-24 h to ensure complete dissolution of the solutes and obtaining homogeneous solutions. The prepared solutions were left to rest 4 h for degassing and kept in a sealed container at room temperature. Chitosan/PEO blend solutions were then prepared by mixing the two solutions at 50/50, 70/30, 80/20 and 90/10 chitosan/PEO ratios.

5.3.4 Electrospinning

Electrospinning was performed using a horizontal set up containing a variable high DC voltage power supply (Gamma High Voltage Research, FL, USA) and a programmable micro-syringe pump (Harvard Apparatus, PHD 2000, USA). The solutions were poured into a 10 mL stainless steel syringe (Harvard Apparatus, USA) with Luer-Lock connection to a 20-gauge blunt tip needle (Cadence Science, NY, USA). The syringe was mounted with a grip on the micro-syringe

pump and grounded by use of an alligator clip. The schematic outline of the electrospinning set up is shown in Fig. 5-1. An electrical heater containing an aluminum shell, cartridge heaters and a temperature controller was designed to heat the polymer solution during the process. It was placed around the needle and syringe (see inset in Fig. 5-2) to set the solution temperature up to 80 °C. Fiber mats were collected on an aluminum foil attached to a drum collector that could be easily removed for subsequent characterization. The homemade designed drum has both controllable rotational and translational movement connected to the power supply and was placed 15 cm away from the needle (optimum distance based on preliminary tests). Samples were collected on the drum in both static and rotating conditions, based on the requirements of specific samples for different experiments. Typical flow rates of 0.1-2 mL/h and voltages between 15-35 kV were used as process parameters. All experiments were conducted at ambient pressure and relative humidity of 15-20%.

5.3.5 Film preparation

Thin films of chitosan were prepared by pouring and spreading approximately 10 g of a chitosan solution in a plastic Petri dish. Cast films were then vacuum dried at 40 °C overnight to completely evaporate the solvent. The dried films were peeled from the Petri dish and kept in a desiccator at room temperature until characterization.

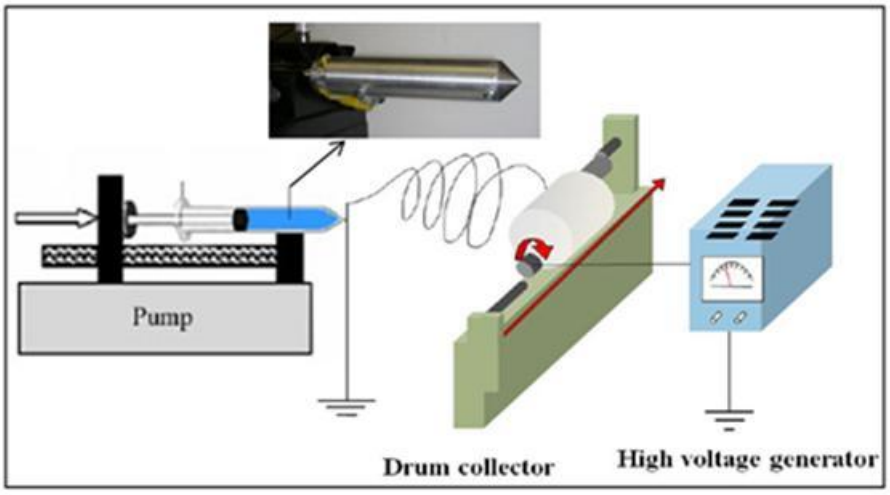

Figure 5-1: A schematic outline of the electrospinning set-up. Inset shows the heated syringe (inspired from Ref. [83]).

5.3.6 Rheological measurements

Dynamic and steady shear rheological properties of the solutions were characterized at 25 ºC and temperatures between 40 to 80 ºC with 10 ºC increment, using two different rotational rheometers: a highly sensitive strain-controlled rheometer ARES (Rheometric Scientific, NJ, USA) for low viscosity solutions, and a stress-controlled rheometer AR-2000 (TA Instruments, DE, USA) for more viscous solutions. In both cases a Couette flow geometry was used. A low viscosity silicon oil was used to cover the surface of the sample solutions to prevent evaporation of the solvent during the tests. The presence of the oil was shown not to impact the rheological measurements. The stability of the solutions was examined as a function of time in oscillatory shear tests under a frequency of 1 rad/s and a deformation of 0.1. After an hour the elastic and loss modulus decreased by less than 1 and 3 %, respectively, showing the solutions to be stable. The linear viscoelastic (LVE) regime was determined at various frequencies from the maximum strain or stress (depending on the instrument) at which the elastic modulus, as a function of strain (stress), did not deviate by more than 5% from its low strain (stress) value. The oscillatory measurements were carried out by applying frequency sweeps from 0.0625 to 100 rad/s in the linear viscoelastic regime at temperatures between 25 to 80 °C. The zero-shear viscosity of the solutions were evaluated from the application of the Carreau-Yasuda model [57] to the shear viscosity and complex viscosity data.

Additionally, the specific viscosity of chitosan and PEO solutions was determined using rheometry and viscosimetry to set the limits of their respective concentration regimes. For viscosimetry, the specific viscosity was measured using a Cannon-Fenske dilution capillary viscometer (diameter = 0.78 mm, Cannon-Fenske, Canada) at various concentrations. A water bath (model BT 15, Cole-Parmer, IL, USA) was used to control the temperature at a constant value of 25 ºC.

5.3.7 Fiber diameter characterization

The surface morphology of electrospun nanofibers was characterized by a Hitachi S-4700 field emission scanning electron microscope (FESEM) operating at 5-10 kV. Samples cut from an electrospun mat on the aluminum foil and mounted on aluminum stubs were coated by an ultrathin layer of platinum for better conductivity during imaging. The samples were observed at

magnifications between 100 and 40,000 times their original sizes to visually evaluate the electrospinnability and existence of beads and droplets. Fiber diameters were also determined using Image-J (National Institutes of Health (NIH), http://rsb.info.nih.gov/ij/) image processing software. For each electrospun mat, at least 100 fibers were considered from three different images to calculate the average diameter.

5.3.8 Surface tension

Surface tension of the various prepared solutions was measured using a dynamic Wilhelmy plate tensiometer DCAT 21 (Dataphysics Instruments GmbH, Germany). The measurements were carried out at 20 ºC and repeated five times on different samples for each solution.

5.3.9 Electrical conductivity

Electrical conductivity of different solutions was tested in a conductivity meter Infolab® Cond 750 (WTW GmbH, Germany). The measurements were performed at 25 ºC and reported after five times replication.

5.3.10 FTIR spectroscopy

Transmission FTIR spectra were measured at room temperature on the as-cast chitosan film and as-spun PEO and chitosan/PEO blend nanofibrous mats using a Perkin Elmer 65 FTIR-ATR instrument. A total of 128 scans were accumulated for the signal-averaging of each IR spectral measurement to ensure a high signal-to-noise ratio with a 4 cm^{-1} resolution. The spectra of the samples were recorded over a wavenumber range of 600-4000 cm^{-1}.

5.4 Results and discussion

5.4.1 Material characterization

The degree of deacetylation (DDA) is an important chitosan physico-chemical characteristic for anti-microbial properties. Since it increases the active amino groups on the chitosan backbone, a high DDA chitosan has a stronger ability to act against bacteria as compared to a lower DDA molecular chain of the same size [2, 58]. In this work a recently established liquid phase ^{1}H-NMR procedure proposed by Lavertu [59] has been used. It is a more reliable and precise

method than FTIR [60] to characterize high DDA chitosan. The advantage of this technique is that there is no need for a reference sample or calibration curve. Moreover, impurities and moisture content in chitosan do not overlap with chitosan peak signals [59]. The ^{1}H-NMR spectrum of the grade used in this work is shown in Fig. 2. Based on this curve the DDA was calculated to be 97.5 %.

5.4.2 Solution characterization

Chitosan is soluble in a wide range of acetic acid concentrations, and some reports show that highly concentrated acetic acid can help chitosan electrospinnability by decreasing the solution surface tension [21]. The high DDA chitosan grade used in this work was soluble in aqueous solutions of 3 to 90 wt% acetic acid and could form homogeneous solutions up to a polymer concentration of 5 wt% concentration, above which the solution resulted in a gel. Preliminary tests depicted that the optimum concentrations for chitosan and PEO in terms of electrospinnability was 4 wt%.

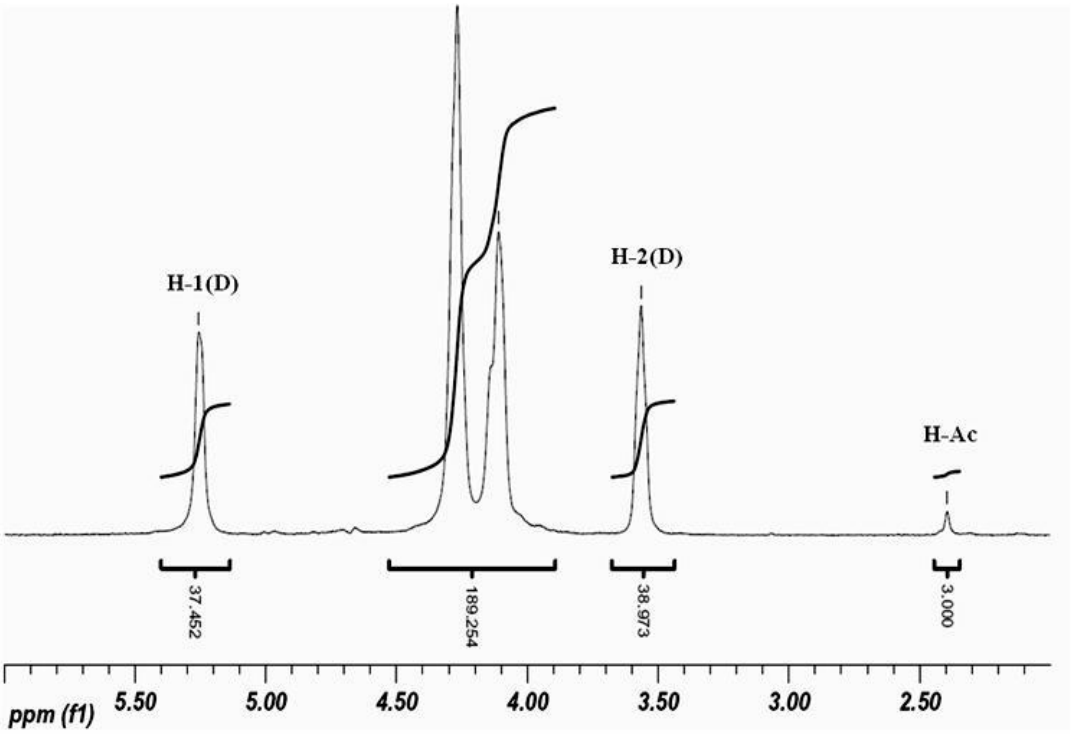

Figure 5-2: Chitosan 1H-NMR spectrum at 70 ºC.

After preparation, the solutions were immediately used in the electrospinning process in order to avoid aging effects. Aging is a well known phenomenon for chitosan solutions and originates mainly from conformational change, aggregation and some enzymatic chain scission [61, 62]. PEO chains are also easily subjected to mechanical degradation and can likely undergo solution aging. Additionally, phase separation can also take place in these blends, for example a remarkable drop in viscosity (between 15-60%) has been observed after three days of storage (data not shown here). Similarly to previous works [54, 63], it was observed that aged solutions of the neat polymers or their blends lost their ability to be electrospun mainly due to phase separation, complexation, polymer degradation or change in polymer conformation.

5.4.2.1 Surface tension and electrical conductivity

The effects of acetic acid concentration and temperature on surface tension of aqueous acetic acid solutions are presented in Fig. 5-3. The curve at 20 ºC is obtained in the present study while the other curves, i.e. at 35 ºC and 50 ºC, are adapted from reference [64]. Surface tension decreases from 73 mN/m for water to 28 mN/m for pure acetic acid at 20 ºC. It is also found that at 50 wt% acetic acid, 76% of this reduction is achieved. The electrical conductivity of different concentrations of aqueous acetic acid is also shown in Fig. 5-3. Increasing the acid concentration results in an increase of the electrical conductivity of the solution up to a maximum exhibited at 20 wt% acetic acid. At higher acid concentrations (e.g. 50 wt%), the electrical conductivity shows a descending trend due to a lack of water molecules to completely dissociate the acid molecules [65]. Our initial tests also showed that increasing acid concentration to more than 50 wt% in chitosan solutions led to a reduction in jet stability, as reported by other groups [54, 66]. This could be related to a reduction in the evaporation rate that delays the fiber formation step in the process. Therefore, a solution of 50 wt% acetic acid is a compromise between low surface tension, reduced evaporation rate and moderate electrical conductivity. The results of surface tension measurements for solutions of 4 wt % chitosan, 4 wt% PEO and their 50/50 blend in 50 wt% acetic acid are superposed in Fig.5-3, indicating an identical surface tension at room temperature. Figure 5-3 also reveals that surface tension decreases by increasing temperature, for example a 50 wt% acetic acid solution undergoes a 8% reduction in surface tension of when temperature is increased from 20 ºC to 50 ºC, a result that is in favour of electrospinnability.

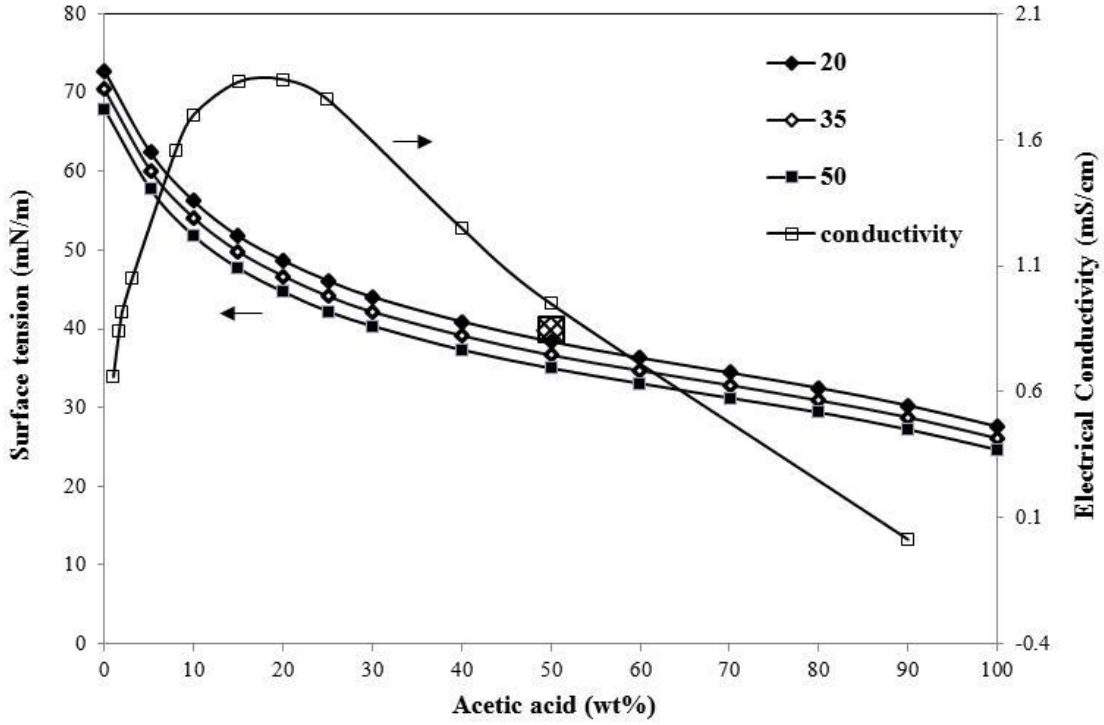

Figure 5-3: Effect of acetic acid concentration and temperature on surface tension of aqueous acetic acid solutions; 20 ºC: data from present study, 35 ºC & 50 ºC: data adapted from reference [64]. Surface tension of 4 wt% chitosan solution, PEO solution and their 50/50 blend overlie at 20 ºC, showing as a single point in the graph. The electrical conductivity of aqueous acetic acid solutions at 25 ºC is also shown (secondary y-axis).

5.4.2.2 Rheological behaviour

The rheological properties of chitosan and PEO solutions and their blends have been investigated to relate the effect of their flow behaviour on electrospinnability. Results in steady shear flow are shown in Fig.5-4. The zero-shear viscosity of 4 wt% neat PEO in 50 wt% acetic acid is 2 Pa.s, a value much higher (three times) than that of in water (0.7 Pa.s). This is probably due to the strong interactions between ether groups in PEO and hydroxyl groups in acetic acid, which may expand the PEO chains in an acidic environment, resulting in a remarkable increase of the shear viscosity [18] . The zero-shear viscosity of 4 wt% neat chitosan solutions in 50 and 90 wt% acetic acid is nearly the same (almost 2 Pa.s), however this value is only 1.2 Pa.s for the same concentration of chitosan in 3 wt% acetic acid. The repulsive forces between protonated $–NH_3^+$ groups of the chitosan molecules increase the solution viscosity due to an expansion of their hydrodynamic

volume. However, the viscosity of chitosan solutions remains constant at acetic acid concentrations higher that 50 wt% since the amine groups are fully protonated at this concentration and above. In Fig. 5-4, it is worth noting that the zero shear viscosities of chitosan and PEO solutions at the same concentration (4 wt%) in 50 wt% acetic acid are the same. The apparent shear rate at the needle wall was evaluated approximately by applying Eq. 5-2, considering the solution as a Newtonian fluid:

$$\dot{\gamma} = \frac{4Q}{\pi r^3} \qquad (5\text{-}2)$$

where $\dot{\gamma}$ is the shear rate at the needle wall, Q is the volumetric flow rate and r is the radius of the needle (300 µm in this work). The calculated shear rate is around 2 s^{-1} (for a typical flow rate), hence situated in the plateau (zero-shear viscosity) region.

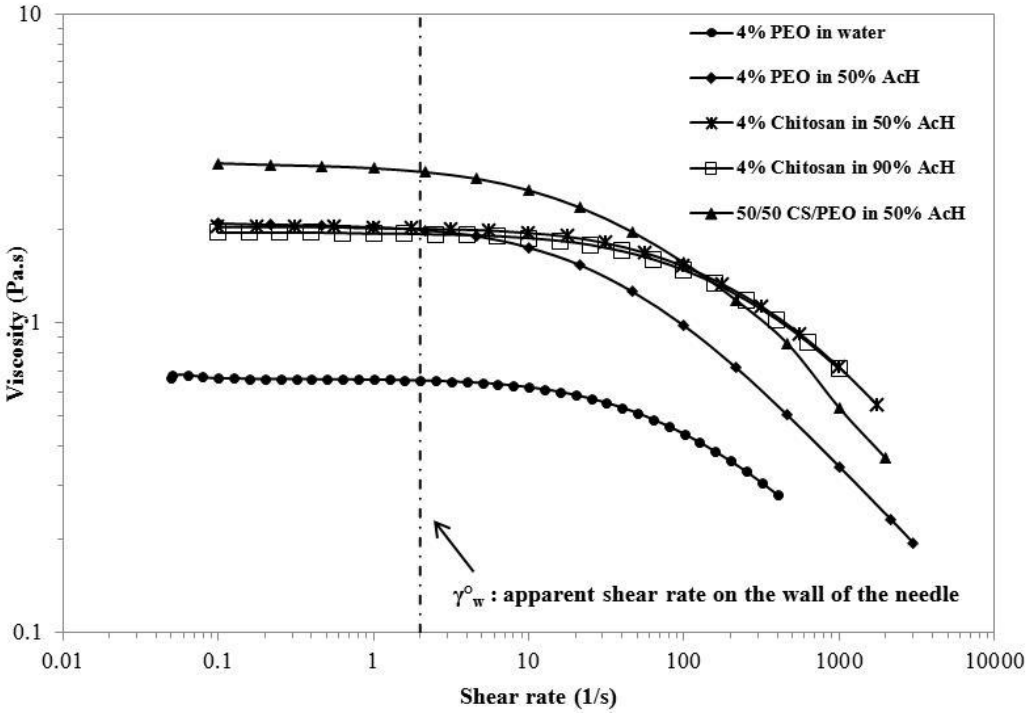

Figure 5-4: Viscosity as a function of steady shear rate for chitosan, PEO and chitosan/PEO solutions in various solvents (total polymer concentration of 4 wt%).

Interestingly, a 50/50 mixture of chitosan/PEO with total polymer concentration of 4 wt% exhibits a higher viscosity than both of its precursor solutions. The effect of chitosan/PEO content on the zero-shear viscosity of solutions is shown in Fig. 5-5. Viscosity of the blends shows a strong positive deviation from the additivity rule, indicating strong interactions between PEO and chitosan chains. Strong hydrogen bonds between hydroxyl and amino groups on chitosan molecules and ether groups in PEO, schematically illustrated in Fig. 5-6, are believed to be the main reason for this observation [18, 63]. Further investigation of hydrogen-bonding interactions between chitosan and PEO in the nanofibers is presented in the next section. In contrast, in some previous works PEO was added to decrease the viscosity of chitosan solutions and it was believed that it could work as a plasticizer by breaking down the inter and intra molecular interactions of chitosan chains through new interactions with PEO [34, 67]. Flexible and small PEO chains can lie down along the rigid chitosan macromolecules facilitating their flow and decreasing the viscosity of the blends. However, the distinctive behaviour observed in this work is attributed to the size and conformation of the PEO molecules in 50 wt% acetic acid solution. Large expanded PEO chains in solution can make strong entanglements with chitosan chains leading to an opposite trend [68].

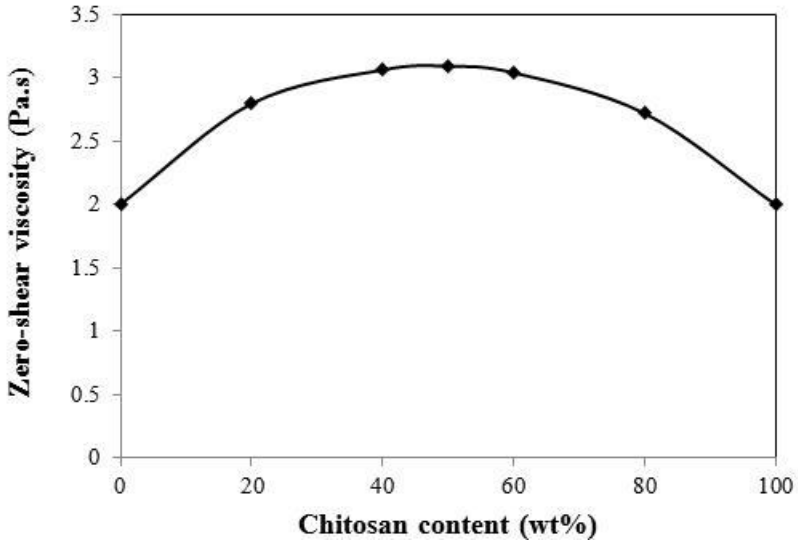

Figure 5-5: Effect of chitosan content on zero-shear viscosity of chitosan/PEO blends. A 4 wt% chitosan solution is mixed with a 4 wt% PEO solution in a 50 wt% acetic acid solvent (total polymer concentration of 4 wt%).

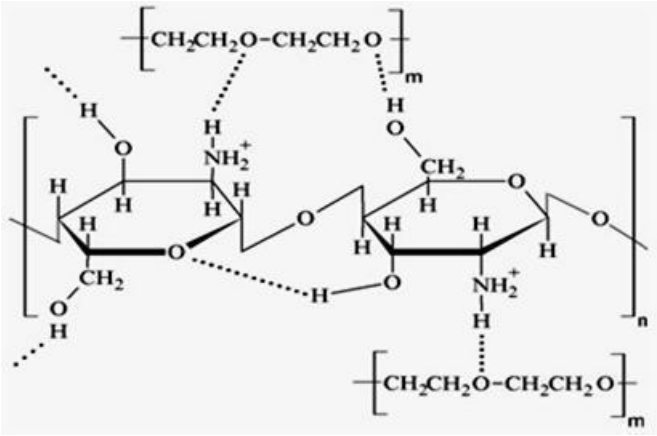

Figure 5-6: Proposed hydrogen bonding interactions between chitosan and PEO molecules [63].

5.4.3 FTIR spectra

Hydroxyl, carbonyl (C=O-NHR), amine (NH2) and ether groups in chitosan form intra/inter chain hydrogen bonds [69]. As shown in Fig. 5-6, polyether groups in PEO may also form hydrogen bonds with chitosan. Figure 5-7 shows the FTIR spectra obtained for neat PEO and chitosan/PEO blend nanofibers at various chitosan/PEO contents. The absorption peak observed at 1112 cm^{-1} is typical of the vibration stretching of the ether (C-O-C) group [18, 70]. This peak, indicated by the arrow, gradually shifts to lower wavenumbers by increasing the chitosan content in the nanofibers. As for the case of nanofibers containing 90% chitosan, this peak is shifted by almost 29 cm^{-1} unit.

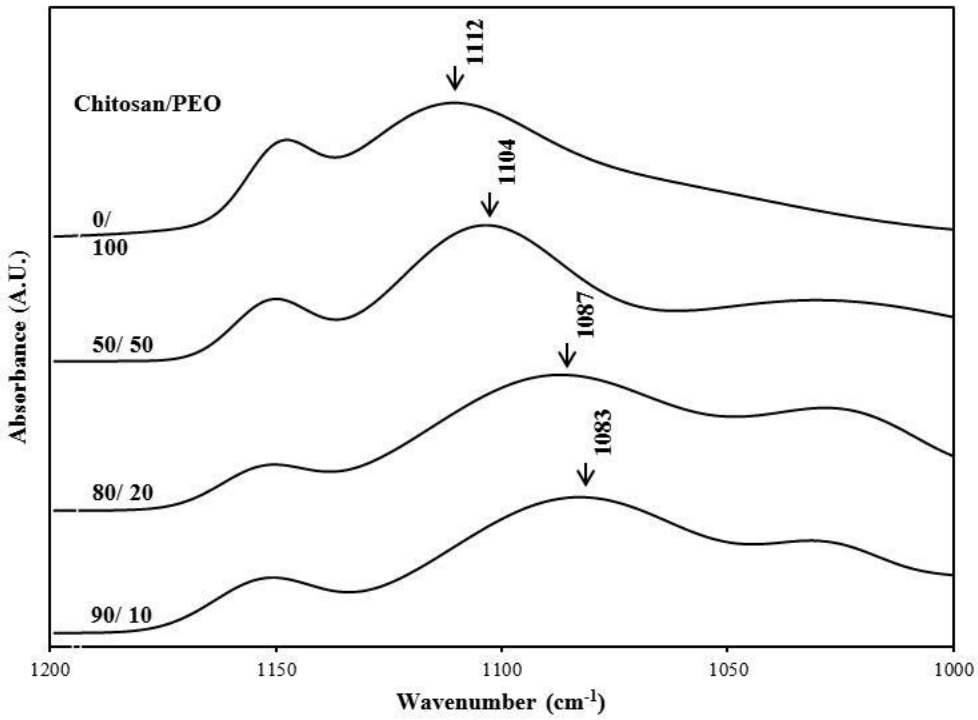

Figure 5-7: Normalized transmission FTIR spectra recorded at room temperature in the ether (C-O-C) region for neat PEO film and as-spun chitosan/PEO nanofibers.

The FTIR spectra obtained at room temperature for neat chitosan and chitosan/PEO blend nanofibers at various chitosan/PEO contents in the amine (NH_2) stretching region are shown in Fig. 5-8. The strong peak observed at 1555 cm^{-1} is attributed to the amine band in chitosan [3, 71]. This peak is gradually shifted to higher wavenumbers by increasing the PEO content in the nanofibers. The amine peak is shifted by almost 39 cm^{-1} unit after the addition of 50 wt% PEO in the nanofibers. The same trend was also observed in the hydroxyl/amine region (2000-4000 cm^{-1}), where the peak attributed to chitosan shifted to lower wavenumbers after the addition of PEO (data not presented). The shift in ether (Fig. 5-7), amine (Fig. 5-8) and hydroxyl bands in the chitosan/PEO nanofibers may be attributed to the formation of hydrogen bonds between polyether oxygen and amino hydrogen in PEO and chitosan, respectively [72, 73]. Therefore, strong interactions between chitosan and PEO may prevail from the formation of these hydrogen bonds.

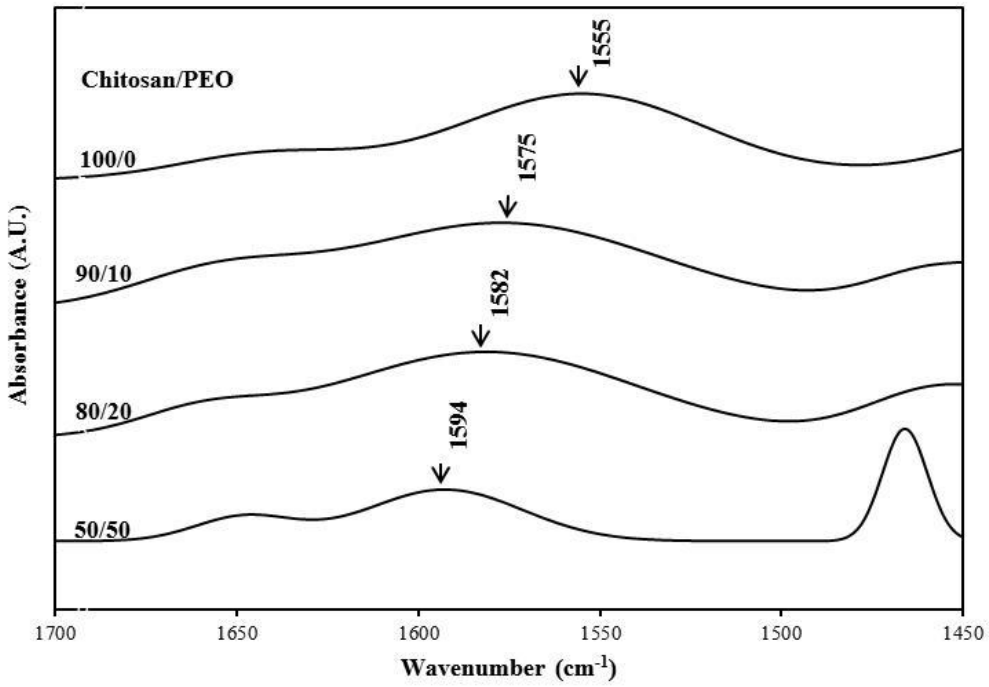

Figure 5-8: Normalized transmission FTIR spectra recorded at room temperature in the amine (NH2) region for neat chitosan film and as-spun chitosan/PEO nanofibers.

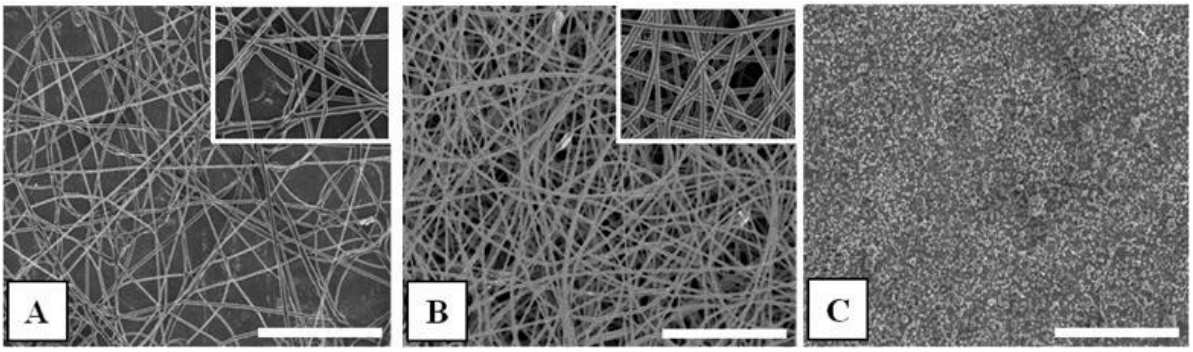

Figure 5-9: Electrospun solutions: A) 4 wt% PEO in 50 wt% acetic acid, B) 4 wt% PEO in water (tip to collector distance = 15 cm, flow rate = 0.5 mL/h, voltage = 15 kV), C) 4 wt% chitosan in 50 wt% acetic acid at 25 °C, (tip to collector distance = 15 cm, flow rate = 0.5 mL/h, voltage = 30 kV). Scale bars represent 10 µm.

5.4.4 Morphology of electrospun nanofibers and concentration regimes

Figure 5-9 shows FESEM images of fibers electrospun from a 4 wt% PEO in 50 wt% acetic acid solution and in water (Fig. 5-9-A and B, respectively), and from a 4 wt% chitosan in 50 wt% acetic acid (Fig. 5-9-C). PEO can produce defect free nanofibers in both solvents; however it loses some of its electrospinnability in aqueous acetic acid mainly due to its higher viscosity (Fig. 5-4) and to the lower evaporation rate of the solvent. This loss of electrospinnability has been concluded from a less stable jet (intermittent spinning) and the large reduction of collected nanofibers for the same electrospinning conditions and deposition time (Fig. 5-9-A and B). The results for chitosan are completely different; only nano beads and droplets in the range of 100-150 nm are obtained (Fig. 5-9-C). For chitosan, typically a droplet is formed at the tip of the needle, is elongated very slowly with vibrations and then splayed around by an explosion-like behaviour. In the best conditions, a jet could be formed for only a fraction of a second, leading to beads on the collector.

The electrospinnability of neat PEO and chitosan need to be explained by other criteria than shear viscosity (Fig. 5-4) and surface tension (Fig. 5-3), since these properties show the same values for both solutions in typical electrospinning conditions. For example, chain entanglement is another solution physico-chemical characteristic that may affect electrospinnability. McKee et al. [53] showed that the minimum polymer concentration in solution to prepare defect free beadless electrospun nanofibers depends on the critical entanglement concentration (C_e) and polymer type, i.e. neutral or charged (flexible or stiff). C_e is the boundary between the semi-dilute unentangled and semi-dilute entangled regimes at which entanglements between polymer chains form and start constraining chain motions. They found that for neutral polymers, beaded nanofibers formed at C_e [53], while defects and droplets disappear at 2-2.5 C_e. However, these values change to 8-10 C_e for salt free polyelectrolytes [55]. Shenoy also studied the role of chain entanglements on fiber formation in the electrospinning process and concluded that for neutral polymers, stable fiber formation occurs roughly at more than 2.5 entanglements per chain, or as $C >> C^*$ (the critical overlap concentration) [74]. Rheological and viscometric measurements have been performed in this work to calculate C^* and C_e for chitosan and PEO dissolved in 50 wt% acetic acid. Figure 5-10 shows the viscosity as a function of shear rate for chitosan solutions at different concentrations. All solutions show a very well-developed plateau region that indicates the value

of the zero-shear viscosity (η_0). Moderate shear-thinning is observed at increasing chitosan content, due to more entanglements (hence disentanglements) between polymer chains.

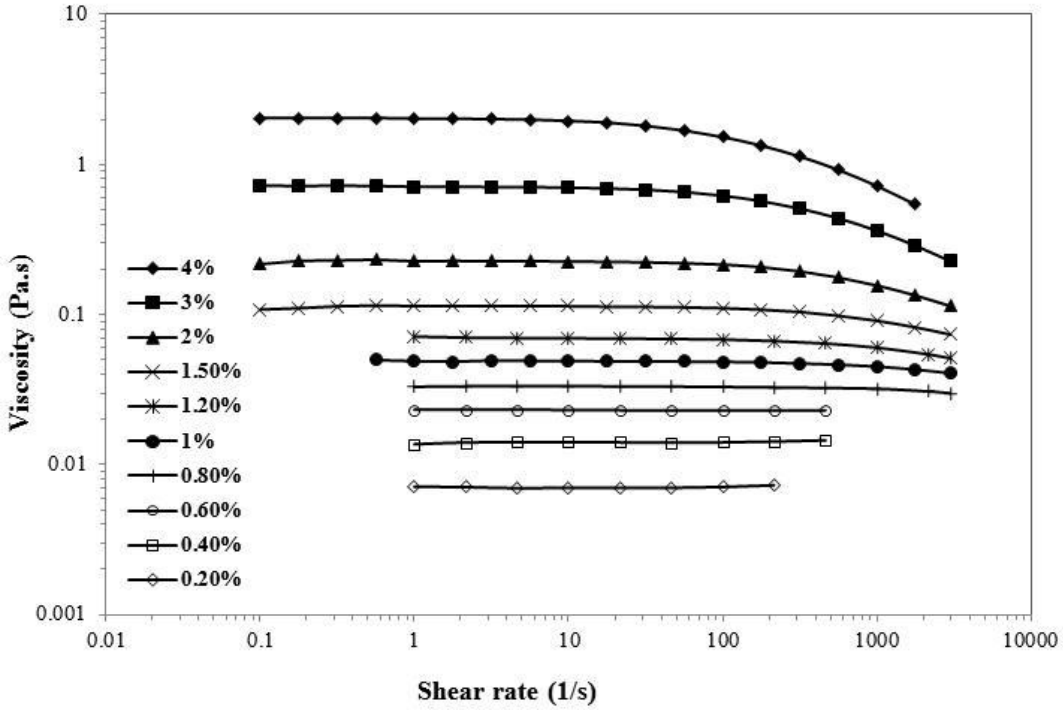

Figure 5-10: Dependence of viscosity on shear rate for chitosan solutions at various concentrations (50 wt% acetic acid at 25 °C).

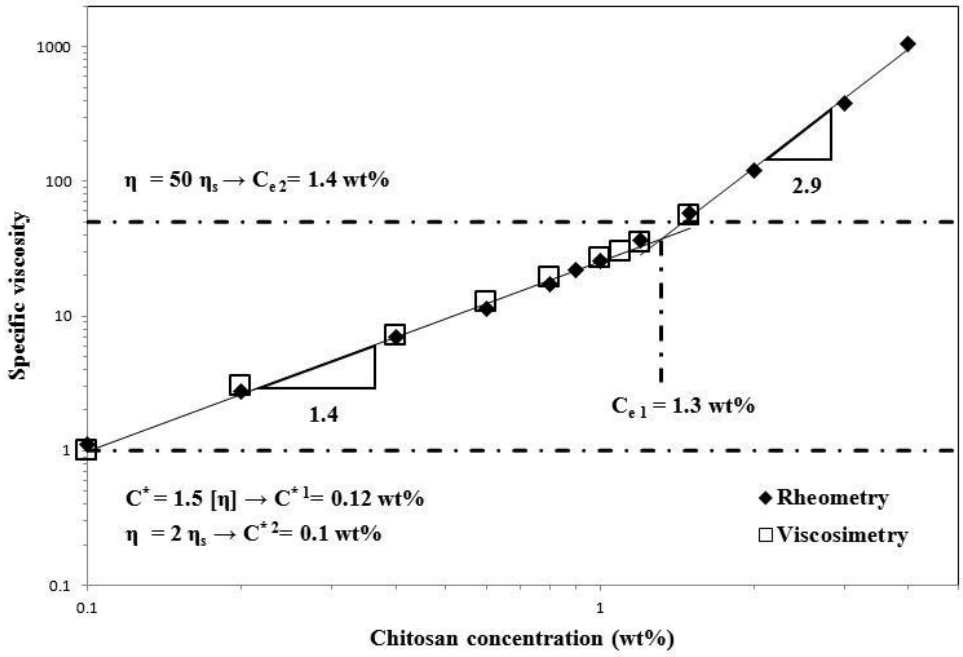

Figure 5-11: Dependence of specific viscosity on concentration for chitosan dissolved in 50 wt% acetic acid (T = 25 °C).

In this work C_e was evaluated using the method proposed by Colby [75]. In this method, the specific viscosity defined by Eq. 5-3 is plotted against concentration, then C^* and C_e are evaluated based on the onset points of changes in the slope.

$$\eta_{sp} = \frac{\eta_0 - \eta_s}{\eta_s} \qquad (5\text{-}3)$$

In Eq. 5-3 η_0 and η_s are the zero-shear viscosity of polymer solution and solvent, respectively. The specific viscosity of low concentration solutions was also measured by viscosimetry to validate results from rheometry, and both are shown overlapping in Fig. 5-11 for chitosan solutions. The value of C_e was determined to be 1.3 wt% for chitosan. Dobrynin [76] also defined C_e as the point at which the specific viscosity of a solution is 50 times that of the solvent. In this case, the calculated C_e from Fig. 5-11 is 1.4 wt% and agrees with the calculated C_e from Colby's method. The scaling theory of Rubinstein [77] predicts a change in the slope from 0.5 to 1.5 at C_e for polyelectrolytes in solution. It represents $\eta_{sp} \sim C^{0.5}$ for the semi-dilute unentangled regime and

$\eta_{sp} \sim C^{1.5}$ for the semi-dilute entangled regime, evidential of more associated polymer chains after C_e. The calculated scaling powers from Fig. 5-11 are higher than those predicted by the theory, i.e. 1.4 instead of 0.5, and 2.9 instead of 1.5. This illustrates a higher level of interactions between chitosan chains, resulting from strong intra and inter chain hydrogen bonds. It is also worth noting that the scaling relationship for concentrations higher than C_e in this work ($\eta_{sp} \sim C^{2.9}$) is lower than that measured previously by other researchers. For instance, Klossner [54], Hwang [67] and Cho [78] reported scaling values of 6.0, 3.94 and 4.1 respectively.

The critical overlap concentration (C^*) was also determined using two criteria; the first one was $C^* = 1.5[\eta]$ [79], and the second one was the point at which the viscosity of the solution is twice that of the related solvent [76, 77]. C^* was determined to be 0.12 wt% and 0.1 wt% using these two criteria, respectively, hence in good agreement.

The same procedure was used to measure the critical overlap (C*) and entanglement (C_e) concentrations for PEO (more detalis in appendix A). The obtained result indicated a C_e of 1.1 wt% and 1.5 wt% by applying the same methods as defined previously for chitosan. The C^* was also estimated to be 0.2 wt% at the point where $\eta = 2\ \eta_s$. Based on the above findings, the chitosan concentration used for electrospinning in this work, i.e. 4 wt% is nearly 40 times its C^* and 3 times its C_e. Therefore, according to McKee [55], this concentration is too low and consequently no chitosan nanofibers can be obtained (as shown in Fig. 5-9-C). In the case of PEO, 4 wt% is 20 times C^* and approximately 3-3.5 times C_e, and this is above the threshold for defect-free nanofibers for a neutral polymer [53]. Consequently, the totally different behaviour in electrospinning of chitosan as compared to PEO can be attributed to a significant difference in chain entanglements in solution.

Moreover, electrical conductivity of solutions is another factor affecting the electrospinning process. Figure 5-12 shows the electrical conductivity of different ratios of chitosan/PEO solutions in 50 wt% acetic acid. The value for a neat 4 wt% PEO solution is 0.73 mS/cm, and is very similar to that of the solvent (0.9 mS/cm) (Fig. 5-3). However, it is relatively lower than the electrical conductivity of a neat 4 wt% chitosan (3.4 mS/cm). Chitosan solutions are more conductive as compared to PEO due to the polycationic nature and positive charges on the polymer chains. This leads to more stretching during the whipping and bending motion of the solution in the strong electric field. On the other hand, these charges caused repulsive interactions

between chitosan chains, which destabilize the charged jet in the stretching region, resulting in splaying and explosion-like behaviour of the jet, making only droplets on the collector. Addition of PEO decreases the electrical conductivity of chitosan/PEO solutions, firstly by substituting a positive charged molecule by a neutral one, and secondly by reducing the amount of protonation due to hydrogen bonds formed between amino groups of chitosan and ether groups of PEO, as discussed in Section 5-3-3.

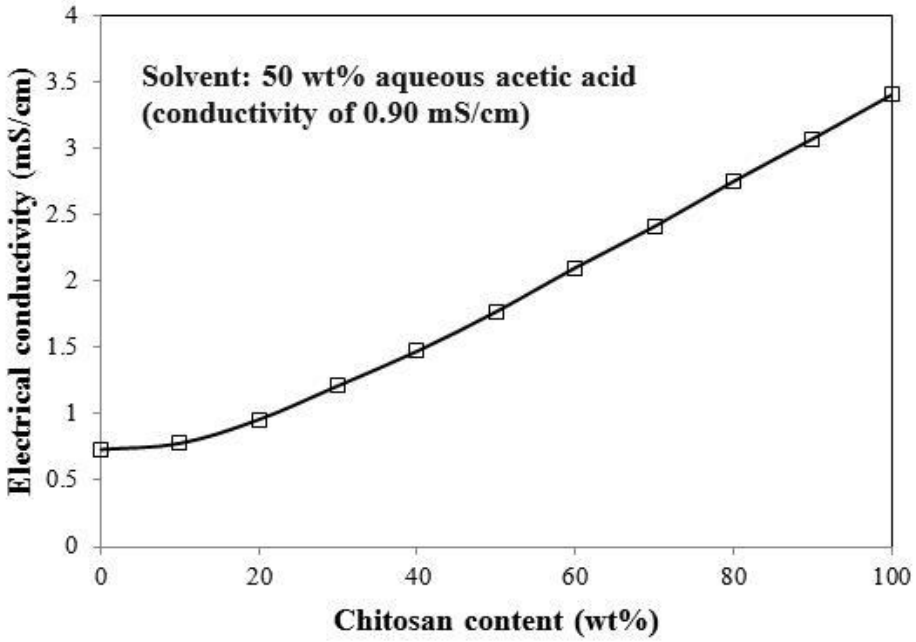

Figure 5-12: Effect of chitosan concentration on electrical conductivity of chitosan/PEO blends. A 4 wt% chitosan solution is mixed with a 4 wt% PEO solution in a 50 wt% acetic acid solvent.

5.4.5 Moderate temperature electrospinning

The effect of moderate temperature on the electrospinnability of chitosan solutions is shown in the SEM micrographs of Fig. 5-13 (A-D). As mentioned before, neat chitosan shows very poor electrospinnability at room temperature and only nanobeads and droplets are formed (Fig. 5-13-A). As temperature increases from 40 to 60 °C, fiber formation slightly improves and the morphology changes to a combination of beads and fibers (Fig. 5-13-B and C). However, at higher temperatures the number of beads rises again so that at 80 °C the result is almost the same than at room temperature (Fig. 5-13-D), with an only beaded morphology. This behaviour can be

explained by three competing phenomena at elevated temperatures: an increased rate of solvent evaporation, a decreasing surface tension (Fig. 5-3) and viscosity (Fig. 5-12). In Fig. 14 the viscosity of neat chitosan (2 Pa.s at 25 °C) and 50/50 blend of chitosan/PEO (3.1 Pa.s at 25 °C) is shown decrease to 0.5 Pa.s at 60 °C. The reduction in viscosity and surface tension may stabilize the jet in the spinning process, while faster solvent evaporation rate can cause faster drying of the whipping jet and increase chain entanglements, which overall improves spinnability. However at higher temperatures (70 to 80 °C), the jet may dry too fast without having enough time to be stretched by the electrical field and result in the disappearance of fibers and get back to a beaded morphology (Fig. 5-13-D).

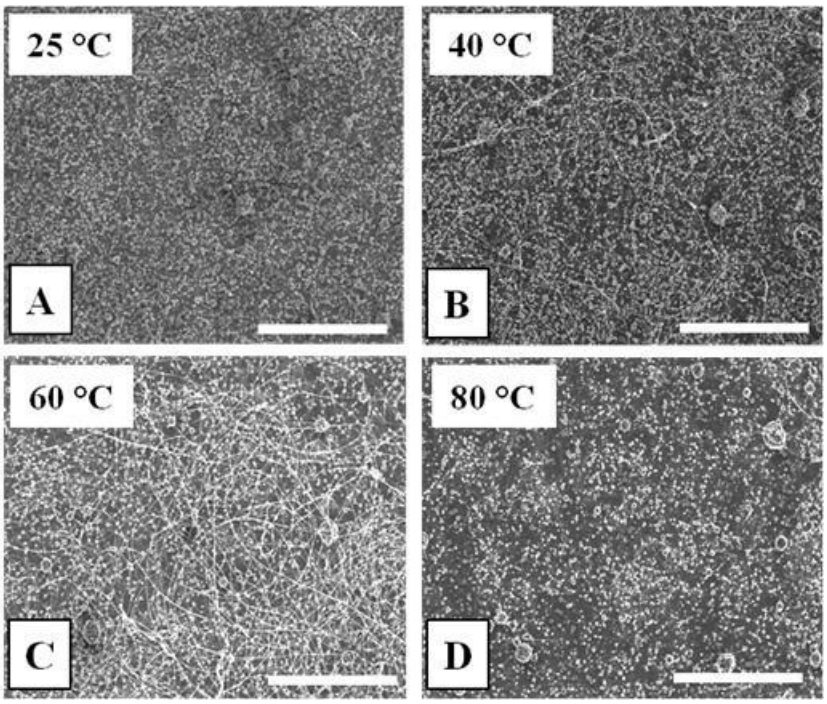

Figure 5-13: SEM micrographs of electrospun neat chitosan solutions at various temperatures (4 wt% chitosan in 50 wt% acetic acid), (tip to collector distance = 15 cm, flow rate = 0.5 mL/h, voltage = 30 kV). Scale bars represent 10 µm.

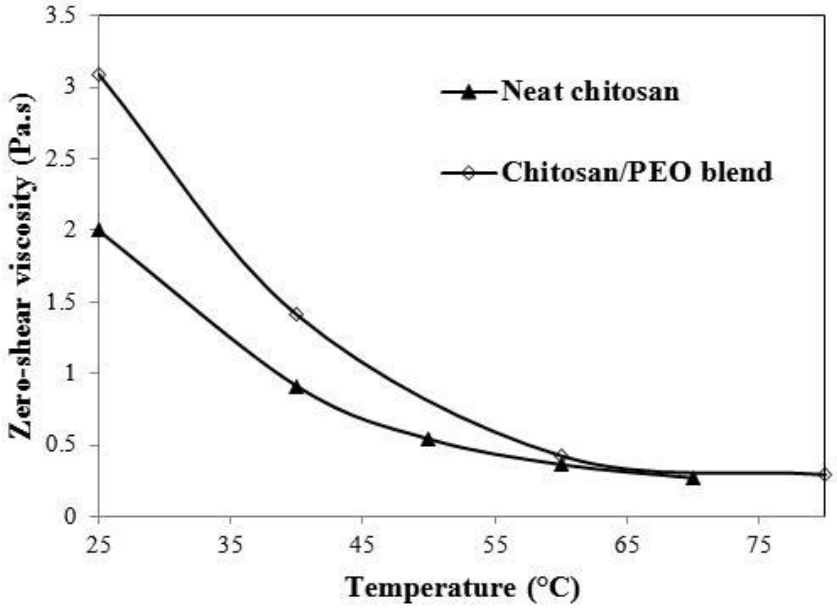

Figure 5-14: Effect of temperature on zero shear viscosity of 4 wt% neat chitosan and its 50/50 blend with 4 wt% PEO, all in 50 wt% acetic acid.

In order to obtain defect free nanofibers based on chitosan, 4 wt% PEO is added to a chitosan solution of the same concentration, both in aqueous solutions of 50 wt% acetic acid at different blend ratios (for a 4 wt% total polymer concentration). Micrographs of morphologies obtained for various polymer ratios are presented in Fig. 5-15. At room temperature (25 °C), beadless nanofibers can be obtained from mixtures of 50/50 to 80/20 of chitosan/PEO (Fig. 5-15-A, D). Higher chitosan content (90/10) results in a large presence of beads in the final microstructure (Fig. 5-15-G). These results demonstrate that the addition of PEO can greatly facilitate the electrospinning process of chitosan up to 80 wt% chitosan in the mixture at room temperature.

As discussed before, the formation of hydrogen bonds between PEO polyether oxygen and chitosan amino hydrogen may increase chain entanglements in solution and make chitosan more electrospinnable [19]. In fact, PEO chains may produce “links” between chitosan chains due to these hydrogen bonding interactions and carry them out in the jet toward the collector and hence facilitate fiber formation. These interactions probably still prevail at high temperature. Coleman and his coworkers have studied the effect of temperature on hydrogen bonds for several polymers

and blends in a series of publications (see for example [80]). They concluded that at higher temperature, the concentration of free N-H groups that must have increased as a result of destroyed hydrogen bonds did not change significantly over a temperature range of 30-210 °C. Therefore in the case of the chitosan/PEO blends examined here, it is expected that the hydrogen bonds would still exist at higher temperature (up to 80 °C).

Moreover, the addition of PEO decreases the electrical conductivity of chitosan solutions (Fig. 5-12), thus may help in obtaining a more stable jet and prevent jet splaying in the stretching region [18]. As for the effect of temperature, beadless morphologies and more stable jets during the spinning process are obtained from a 90/10 chitosan/PEO blend (Fig. 5-15-H, I). This can be attributed to a reduction in viscosity (Fig. 5-14) and surface tension (Fig. 5-3), and also to a faster solvent evaporation rate that helps the charged jet to be further stretched and stabilized [20]. In blend solutions, higher temperatures (70 to 80 °C) (Fig. 5-15-C, F, I) did not have the same effect as for chitosan alone (Fig. 5-13-D). That may be due to the presence of PEO chains which increase chain entanglements so that faster evaporation rate cannot change the morphology from fibers to beads. At higher chitosan content (95 wt %, results not shown), the number of beads increases even at high temperature due to the large content of chitosan in solution.

Finally, the effect of chitosan content and spinning temperature on the distribution of fiber diameters is shown in Fig. 4-16. It reveals that fiber diameter decreases with increasing chitosan content. For example, increasing chitosan/PEO ratio from 50/50 to 90/10 leads to a diameter reduction from 123 to 63 nm at room temperature, and a similar trend is observed at higher temperatures. The diameter reduction may be due to the decrease in viscosity (from the maximum in 50/50 to the steadily decreased value in 90/10, Fig. 5-5) and the larger conductivity of chitosan rich solutions (Fig. 5-12). Both effects results in higher stretching rate and subsequent thinner fibers. However, while no discernible trend is observed for fiber diameter with temperature, in most blends, as temperature increases, slightly larger values are observed. There are two opposing phenomena that may control the temperature effect on resulting fiber size: First, increasing temperature exponentially increases solvent evaporation rate, thus leading to larger fibers due to decreasing solidification time and lower stretching rate. On the other hand, viscosity and surface tension drop at higher temperatures, resulting in higher stretching rates and thinner fibers [81].Therefore depending on the dominant phenomena, different diameter-temperature trends can be observed. This has led to contradictory results in the literature; for example Wang

et al. [82] reported a fiber diameter reduction, while Desai and Kit [43] observed a diameter increase with electrospinning temperature.

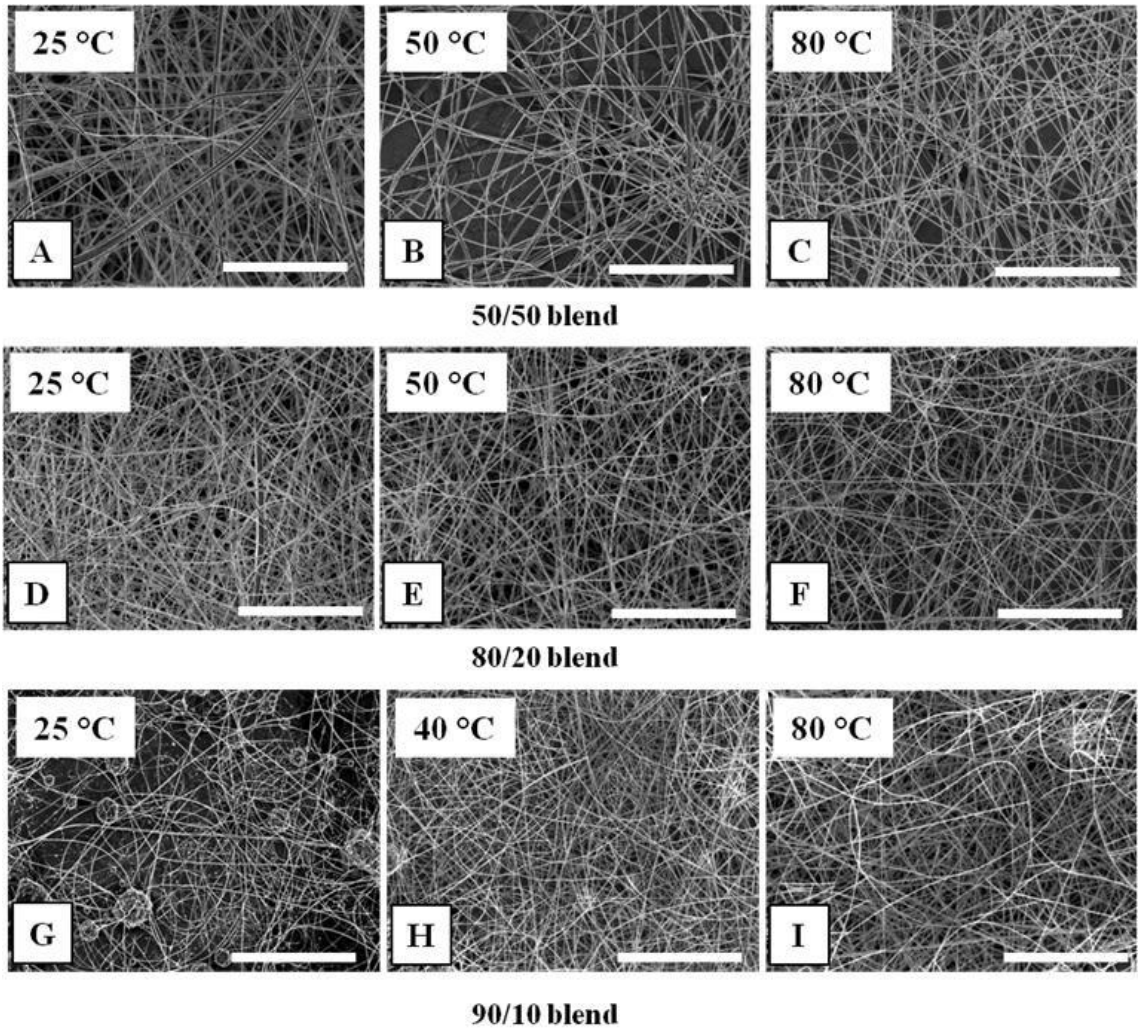

Figure 5-15: Effect of blend ratio (chitosan/PEO) and temperature on electrospun nanofibers (blends of 4 wt% chitosan and 4 wt% PEO in 50% acetic acid); (tip to collector distance = 15 cm, flow rate = 0.5 mL/h, voltage = 30 kV). Scale bars represent 10 μm.

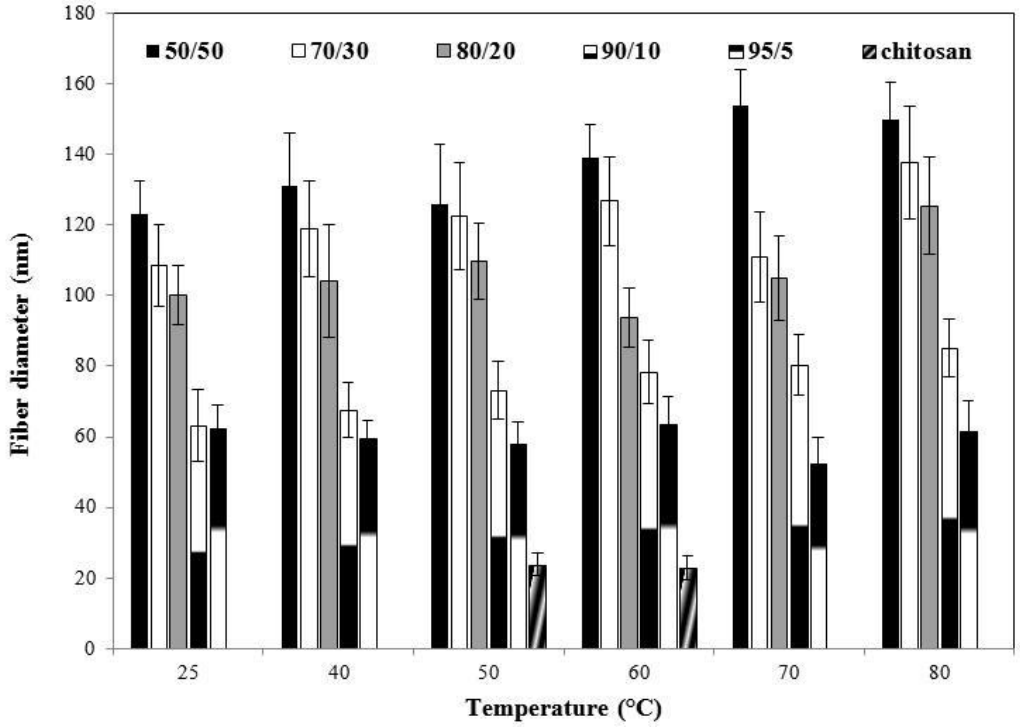

Figure 5-16: Effect of blend ratio (chitosan/PEO) and spinning temperature on fiber diameter, total polymer concentration = 4 wt% in 50 wt% acetic acid, (tip to collector distance = 15 cm, flow rate = 0.5 ml/h, voltage = 30 kV).

5.5 Conclusion

In this work, defect-free nanofibers with diameters of 60-120 nm were obtained from a highly deacetylated chitosan grade blended with PEO. A new set up designed to electrospin at moderate temperature was utilized to achieve content as high as 90 wt% of chitosan in the final chitosan/PEO nanofibers.

The different behaviour of chitosan and PEO in electrospinning was attributed to their intrinsic different nature in solution, i.e. a polyelectrolyte behaviour for chitosan and neutral for PEO, leading to higher electrical conductivity and lower entanglements in the chitosan solutions. The success of chitosan PEO-assisted electrospinning is believed to be the consequence of strong hydrogen bonds formed between ether groups in PEO and hydroxyl and amino groups in chitosan, as shown by FTIR. It is speculated that PEO may act as a "carrier" of chitosan in the electrospinning process via those physical bonds. Electrospinning at moderate temperature

(40-80 °C) also helped to stabilize the jet and improved the spinnability of chitosan solutions, so that higher chitosan content could be reached in the nanofibers (up to 90 wt%). Finally, it was found that increasing chitosan content in the blend solutions led to a significant reduction in nanofiber diameters (from 123 to 63 nm for 50/50 and 90/10 chitosan/PEO blends, respectively, at room temperature). This is likely related to a reduction in viscosity and increased conductivity when increasing the chitosan content from 50 to 90%.

5.6 Acknowledgements

The authors acknowledge the financial support of this work by NSERC (National Science and Engineering Research Council of Canada). We also thank Dr. Vincent Darras and staff of Canada Research Chair in Cartilage Tissue Engineering for kindly performing the ^{1}H-NMR and SEC-MALLS tests.

5.7 References

1. Kurita K. Polymer Degradation and Stability 1998;59(1-3):117-120.
2. Pillai CKS, Paul W, and Sharma CP. Progress in Polymer Science 2009;34(7):641-678.
3. Rinaudo M. Progress in Polymer Science 2006;31(7):603-632.
4. Begin A and Van Calsteren MR. International Journal of Biological Macromolecules 1999;26(1):63-67.
5. Tripathi S, Mehrotra GK, and Dutta PK. International Journal of Biological Macromolecules 2009;45(4):372-376.
6. No HK, Meyers SP, Prinyawiwatkul W, and Xu Z. Journal of Food Science 2007;72(5):R87-R100.
7. Zivanovic S, Li JJ, Davidson PM, and Kit K. Biomacromolecules 2007;8(5):1505-1510.
8. Dutta PK, Tripathi S, Mehrotra GK, and Dutta J. Food Chemistry 2009;114(4):1173-1182.
9. Gu ZY, Xue PH, and Li WJ. Polymers for Advanced Technologies 2001;12(11-12):665-669.
10. Mi FL, Wu YB, Shyu SS, Chao AC, Lai JY, and Su CC. Journal of Membrane Science 2003;212(1-2):237-254.
11. Mi FL, Shyu SS, Wu YB, Lee ST, Shyong JY, and Huang RN. Biomaterials 2001;22(2):165-173.
12. Zeng MF, Fang ZP, and Xu CW. Journal of Applied Polymer Science 2004;91(5):2840-2847.
13. Reneker DH and Yarin AL. Polymer 2008;49(10):2387-2425.
14. Li D and Xia YN. Advanced Materials 2004;16(14):1151-1170.
15. Greiner A and Wendorff JH. Angewandte Chemie-International Edition 2007;46(30):5670-5703.

16. Shin YM, Hohman MM, Brenner MP, and Rutledge GC. Applied Physics Letters 2001;78(8):1149-1151.
17. Shin YM, Hohman MM, Brenner MP, and Rutledge GC. Polymer 2001;42(25):9955-9967.
18. Duan B, Dong CH, Yuan XY, and Yao KD. Journal of Biomaterials Science-Polymer Edition 2004;15(6):797-811.
19. Li L and Hsieh YL. Carbohydrate Research 2006;341(3):374-381.
20. Desai K, Kit K, Li J, and Zivanovic S. Biomacromolecules 2008;9(3):1000-1006.
21. Geng XY, Kwon OH, and Jang JH. Biomaterials 2005;26(27):5427-5432.
22. Min BM, Lee SW, Lim JN, You Y, Lee TS, Kang PH, and Park WH. Polymer 2004;45(21):7137-7142.
23. Ohkawa K, Cha DI, Kim H, Nishida A, and Yamamoto H. Macromolecular Rapid Communications 2004;25(18):1600-1605.
24. Schiffman JD and Schauer CL. Biomacromolecules 2007;8(2):594-601.
25. Torres-Giner S, Ocio MJ, and Lagaron JM. Engineering in Life Sciences 2008;8(3):303-314.
26. De Vrieze S, Westbroek P, Van Camp T, and Van Langenhove L. Journal of Materials Science 2007;42(19):8029-8034.
27. Ojha SS, Stevens DR, Hoffman TJ, Stano K, Klossner R, Scott MC, Krause W, Clarke LI, and Gorga RE. Biomacromolecules 2008;9(9):2523-2529.
28. Neamnark A, Rujiravanit R, and Supaphol P. Carbohydrate Polymers 2006;66(3):298-305.
29. Peesan M, Rujiravanit R, and Supaphol P. Journal of Biomaterials Science-Polymer Edition 2006;17(5):547-565.
30. Du J and Hsieh YL. Nanotechnology 2008;19(12).
31. Zhou YS, Yang DZ, Chen XM, Xu Q, Lu FM, and Nie J. Biomacromolecules 2008;9(1):349-354.
32. Ignatova M, Manolova N, and Rashkov I. European Polymer Journal 2007;43(4):1112-1122.
33. Alipour SM, Nouri M, Mokhtari J, and Bahrami SH. Carbohydrate Research 2009;344(18):2496-2501.
34. Bhattarai N, Edmondson D, Veiseh O, Matsen FA, and Zhang MQ. Biomaterials 2005;26(31):6176-6184.
35. Subramanian A, Vu D, Larsen GF, and Lin HY. Journal of Biomaterials Science-Polymer Edition 2005;16(7):861-873.
36. An J, Zhang H, Zhang JT, Zhao YH, and Yuan XY. Colloid and Polymer Science 2009;287(12):1425-1434.
37. Duan B, Yuan XY, Zhu Y, Zhang YY, Li XL, Zhang Y, and Yao KD. European Polymer Journal 2006;42(9):2013-2022.
38. Jia YT, Gong J, Gu XH, Kim HY, Dong J, and Shen XY. Carbohydrate Polymers 2007;67(3):403-409.
39. Zhang YY, Huang XB, Duan B, Wu LL, Li S, and Yuan XY. Colloid and Polymer Science 2007;285(8):855-863.
40. Ignatova M, Manolova N, Markova N, and Rashkov I. Macromolecular Bioscience 2009;9(1):102-111.
41. Xu J, Zhang JH, Gao WQ, Liang HW, Wang HY, and Li JF. Materials Letters 2009;63(8):658-660.

42. Mincheva R, Manolova N, Paneva D, and Rashkov I. Journal of Bioactive and Compatible Polymers 2005;20(5):419-435.
43. Desai K and Kit K. Polymer 2008;49(19):4046-4050.
44. Torres-Giner S, Ocio MJ, and Lagaron JM. Carbohydrate Polymers 2009;77(2):261-266.
45. Song TY, Yao C, and Li XS. Chinese Journal of Polymer Science 2010;28(2):171-179.
46. Park WH, Jeong L, Yoo DI, and Hudson S. Polymer 2004;45(21):7151-7157.
47. Cai ZX, Mo XM, Zhang KH, Fan LP, Yin AL, He CL, and Wang HS. International Journal of Molecular Sciences 2010;11(9):3529-3539.
48. Chen ZG, Mo XM, and Qing FL. Materials Letters 2007;61(16):3490-3494.
49. Schiffman JD and Schauer CL. Polymer Reviews 2008;48(2):317-352.
50. Jayakumar R, Prabaharan M, Nair SV, and Tamura H. Biotechnology Advances 2010;28(1):142-150.
51. Lee KY, Jeong L, Kang YO, Lee SJ, and Park WH. Advanced Drug Delivery Reviews 2009;61(12):1020-1032.
52. Zhang YZ, Su B, Ramakrishna S, and Lim CT. Biomacromolecules 2008;9(1):136-141.
53. McKee MG, Wilkes GL, Colby RH, and Long TE. Macromolecules 2004;37(5):1760-1767.
54. Klossner RR, Queen HA, Coughlin AJ, and Krause WE. Biomacromolecules 2008;9(10):2947-2953.
55. McKee MG, Hunley MT, Layman JM, and Long TE. Macromolecules 2006;39(2):575-583.
56. Nguyen S, Winnik FM, and Buschmann MD. Carbohydrate Polymers 2009;75(3):528-533.
57. Carreau PJ, De Kee D, and Chabra PR. Rheology of polymeric systems: principles and applications. Munich: Hanser Publishers, 1997.
58. Knaul JZ, Hudson SM, and Creber KAM. Journal of Polymer Science Part B-Polymer Physics 1999;37(11):1079-1094.
59. Lavertu M, Xia Z, Serreqi AN, Berrada M, Rodrigues A, Wang D, Buschmann MD, and Gupta A. Journal of Pharmaceutical and Biomedical Analysis 2003;32(6):1149-1158.
60. Kasaai MR. Journal of Agricultural and Food Chemistry 2009;57(5):1667-1676.
61. Sorlier P, Viton C, and Domard A. Biomacromolecules 2002;3(6):1336-1342.
62. Mironov AV, Vikhoreva GA, Kil'deeva NR, and Uspenskii SA. Polymer Science Series B 2007;49(1-2):15-17.
63. Martinova L and Lubasova D. Research Journal of Textile and Apparel 2008;12:72-79.
64. Alvarez E, Vazquez G, SanchezVilas M, Sanjurjo B, and Navaza JM. Journal of Chemical and Engineering Data 1997;42(5):957-960.
65. Ivanov AA. Russian Journal of Inorganic Chemistry 2008;53(12):1948-1963.
66. Homayoni H, Ravandi SAH, and Valizadeh M. Carbohydrate Polymers 2009;77(3):656-661.
67. Hwang JK and Shin HH. Korea-Australia Rheology Journal 2000;12:175-179.
68. Nikolova A, Manolova N, and Rashkov I. Polymer Bulletin 1998;41:115-121

69. Roberts GAF. Chitin chemistry. London: Mac Millan Press, 1992.
70. Kriegel C, Kit KM, McClements DJ, and Weiss J. Polymer 2009;50(1):189-200.
71. Kasaai MR. Carbohydrate Polymers 2008;71(4):497-508.
72. Guo LH, Sato H, Hashimoto T, and Ozaki Y. Macromolecules 2010;43(8):3897-3902.

73. Deyao K, Tao P, Goosen MFA, Min JM, and He YY. Journal of Applied Polymer Science 1993;48(2):343-354.
74. Shenoy SL, Bates WD, Frisch HL, and Wnek GE. Polymer 2005;46(10):3372-3384.
75. Colby RH, Fetters LJ, Funk WG, and Graessley WW. Macromolecules 1991;24(13):3873-3882.
76. Dobrynin AV, Colby RH, and Rubinstein M. Macromolecules 1995;28(6):1859-1871.
77. Rubinstein M, Colby RH, and Dobrynin AV. Physical Review Letters 1994;73(20):2776-2779.
78. Cho JY, Heuzey MC, Begin A, and Carreau PJ. Journal of Food Engineering 2006;74(4):500-515.
79. Krause WE, Bellomo EG, and Colby RH. Biomacromolecules 2001;2(1):65-69.
80. Coleman MM, Lee KH, Skrovanek DJ, and Painter PC. Macromolecules 1986;19(8):2149-2157.
81. De Vrieze S, Van Camp T, Nelvig A, Hagstrom B, Westbroek P, and De Clerck K. Journal of Materials Science 2009;44(5):1357-1362.
82. Wang C, Chien HS, Hsu CH, Wang YC, Wang CT, and Lu HA. Macromolecules 2007;40(22):7973-7983.
83. Laforgue A, Robitaille L. Synthetic Metals 2008;158(14):577-84

CHAPITRE 6

CORE-SHELL STRUCTURED PEO-CHITOSAN NANOFIBERS BY COAXIAL ELECTROSPINNING[3]

Mehdi Pakravan, Marie-Claude Heuzey, Abdellah Ajji

6.1 Abstract

Core-shell structured PEO-chitosan nanofibers have been produced using a co-axial electrospinning set-up. PEO and chitosan solutions, both in an aqueous acetic acid solvent, were used as the inner (core) and outer (shell) layer, respectively. Uniform sized defect-free nanofibers of 100-190 nm diameter were produced. In addition, hollow nanofibers could be obtained subsequent to PEO washing of the membranes. The core-shell nanostructure and existence of chitosan on the shell layer were confirmed by TEM images obtained before and after washing the PEO content with water. The presence of chitosan on the surface of the composite nanofibers was further supported by XPS studies. The chitosan and PEO compositions in the nanofibrous mats were determined by TGA analysis which were similar to their ratio in the feed solutions. The local compositional homogeneity of the membranes and the efficiency of the washing step to remove PEO were also verified by FTIR. In addition, DSC and XRD were used to characterize the crystalline structure and morphology of the co-electrospun non-woven mats. The prepared co-axial nanofibers (hollow and solid) have several potential applications due to the presence of chitosan on their outer surfaces.

---

3 Published in Biomacromolecules, 13, 2012, 412-421

6.2 Introduction

There has been a growing interest for the fabrication of chitosan nanofibers in recent years due to a wide variety of potential applications such as anti-bacterial films [1], membranes for metal ions removal [2, 3], supports for enzyme immobilization [4], drug delivery systems [5], tissue engineering scaffolds [6, 7] and wound healing dressings.[8] Electrospinning is a simple and continuous process which is used to generate submicron fibers in the form of nonwoven mats. In this process a charged polymer solution flows out of a syringe/needle set-up and accelerates toward a collector, positioned at a fixed distance from the needle. Through electrostatic forces, a driven jet of polymer solution forms, elongates and whips until it is deposited on the collector, resulting in the formation of non-woven random nanofibers.[9] The resulting electrospun membranes exhibit remarkable characteristics such as distinctly high specific surface area (typically 20-100 m^2/g), high porosity and small pore size.[10]

Chitosan is a modified natural polymer derived from chitin, one of the most abundant organic materials in the world. It is very similar to cellulose, except for the amino group replacing the hydroxyl group on the C-2 position The $–NH_2$ groups on the chitosan backbone provide several unique properties such as solubility in acidic aqueous solvents, antifungal and antimicrobial properties and the ability to chelate heavy metal ions.[11] The electrospinnability of chitosan is limited mostly by its polycationic nature in solution, rigid chemical structure and specific inter and intra-molecular interactions.[12-14] The repulsive forces, arising from the protonation of the $–NH_2$ groups, may also restrict the formation of sufficient chain entanglements to allow successful electrospinning.[15, 16]

Neat electrospun chitosan nanofibers have been prepared by dissolving chitosan in trifluoroacetic acid (TFA) [17] and its mixtures with dichloromethane (DCM) and trichloromethane (TCM).[18] TFA forms stable salts with the amino groups of chitosan which can efficiently hinder the intermolecular interactions between chitosan chains and facilitate electrospinning.[17] A highly concentrated aqueous acetic acid solution (80-90%) was also reported by some research groups as another successful solvent for the fabrication of neat chitosan nanofibers, using chitosan grades with degrees of deacetylation (DDA) of 54 [19] and 75-85% .[20] It is believed that decreasing the

surface tension of the solution by increasing the acetic acid content can help the electrospinnability of chitosan.[19]

Applications of electrospun chitosan nanofibers using TFA-based solvents are however limited, as the prepared membranes can easily dissolve in neutral and weak basic aqueous solvents [21], due to the high solubility of the TFA-chitosan salt residues. Additionally, working with toxic and harmful solvents and the possible presence of their residues in the final membranes always raise major concerns.

Blending chitosan with materials that facilitate its processing is another approach to make chitosan electrospinnable. The co-spinning agent should have excellent fiber forming characteristics in order to create entanglements and physical bonds with chitosan, and act as a carrier in the electrospinning process. Synthetic polymers such as polyethylene oxide (PEO) [12, 22-24], polyvinyl alcohol (PVA) [8, 14], polylactic acid (PLA) [25], nylon-6 [26], polycaprolactone (PCL) [27] and proteins such as silk fibroin [28], zein [29] and collagen [30] have been successfully blended with chitosan to produce chitosan-based composite nanofibers. Generally the content of the co-spinning agent varies from 20 to 80 wt%. The presence of this second phase can however affect the properties of the nanofibers by decreasing the chitosan content located at the surface. This influences properties such as biocompatibility and mechanical integrity, and may be hard to rectify by an extraction process.

The co-axial electrospinning method provides an alternative and effective way of fabricating chitosan-based nanofibers. In this technique, two different solutions are spun simultaneously through a spinneret composed of two co-axial capillaries to produce core-shell structured nanofibers. Sun et al. [31] and Jian et al. [32] employed co-axial electrospinning to prepare nanofibers from polymer solutions with limited electrospinnability. They co-electrospun these solutions as the core material, with a readily electrospinnable solution as the shell layer to make core-shell nanofibers of the two components. Previously, Ojha et al. [33] used this method to prepare chitosan nanofibers by co-axial electrospinning of PEO as a template sheath for the chitosan core, and then removal of the shell phase by water washing of PEO to expose the chitosan nanofibers.

In this paper, we demonstrate that chitosan-based nanofibers with chitosan entirely located at the outer surface can be produced by a one-step co-axial electrospinning process, instead of the two-step method reported above. To the best of our knowledge, it is the first time that core-shell

structured PEO-chitosan nanofibers are produced by a one-step co-axial electrospinning process, with chitosan as the shell component (outer layer) and PEO as the core material (inner layer) from aqueous solutions. Therefore any post-treatment required to extract the PEO phase in order to have chitosan on the outer surface is eliminated. The produced nanofibers can have significant potential applications in the biomedical field involving wound care and tissue engineering, due to the biocompatibility of both chitosan and PEO. Moreover, hollow chitosan nanofibers can be obtained by PEO washing of these co-axial nanofibers, which could also be of great interest in applications such as blood purification in hemodialysis.[34] In this work, the morphology and core/shell structure of produced nanofibers are studied by scanning electron microscopy (SEM) and transmission electron microscopy (TEM). The presence of chitosan on the outer layer is also confirmed by X-ray photo electron spectroscopy (XPS) measurements. Bulk and local compositional analysis is performed by thermal gravimetry (TGA) and Fourier transform infra-red spectroscopy (FTIR) techniques. Finally, differential scanning calorimetry (DSC) and X-ray diffraction (XRD) methods are utilized to investigate the crystalline structure of the prepared nanofibrous membranes.

6.3 Experimental section

6.3.1 Materials

A commercial chitosan grade in the form of fine powder was supplied by Marinard Biotech (Rivière-au-Renard, QC, Canada). The weight-average molecular weight of this chitosan was measured by size exclusion chromatography with multi-angle laser light scattering (SEC-MALLS) and was found to be 85 ± 5 kDa. The degree of deacetylation (DDA) (97.5%) was determined from ^{1}H-NMR spectroscopy. More on the characterization of this chitosan grade can be found in reference.[24] PEO with a molecular weight of 600 kDa was obtained from Scientific Polymers Inc. (Ontario, NY, USA). Reagent grade acetic acid (99.7 %, Aldrich, WI, USA) was employed to prepare the aqueous solutions. All the materials were used as received.

6.3.2 Master solutions

The chitosan solution was prepared at a concentration of 4 wt% in 50 wt% aqueous acetic acid. PEO solutions at 2, 3 and 4 wt% of polymer content were prepared in 50 wt% aqueous acetic

acid, and at 4 wt% in water. Solution mixing was performed at room temperature using a laboratory magnetic stirrer (Corning Inc, MA, USA) for 18-24 h to ensure complete dissolution of the polymers and obtain homogeneous solutions. The prepared solutions were left to rest 4 h for degassing and kept in sealed containers at room temperature.

6.3.3 Electrospinning

Co-axial electrospinning was performed using a horizontal set-up containing a variable high DC voltage power supply (Gamma High Voltage Research, FL, USA) and a programmable micro-syringe pump (Harvard Apparatus, PHD 2000, USA). Chitosan and PEO solutions were poured into 10 mL plastic syringes mounted on the pump with a multi-rack grip; hence, the flow rates of the core (PEO solution) and shell (chitosan solution) components were identical during the tests. The syringes were connected by plastic tubes and Luer-Lock connections to the inlets of a co-axial spinneret (Linari Engineering, Pisa, Italy). The co-axial spinneret comprised a 21-gauge (i.d. 0.510 mm, o.d. 0.830 mm) inner needle concentrically mounted on a 15-gauge (i.d. 1.37 mm, o.d. 1.83 mm) outer needle and was grounded by use of an alligator clip. The schematic outline of the co-axial electrospinning set up is shown in Fig. 6-1. Blended chitosan/PEO nanofibers were also produced for comparison purposes. Two chitosan/PEO blend solutions were prepared by mixing the two master solutions at 50/50 and 80/20 chitosan/PEO ratios. The blend solutions were poured into an 8 mL stainless steel syringe (Harvard Apparatus, USA) with a Luer-Lock connection to a 20-gauge blunt tip needle (Cadence Science, NY, USA). The syringe was mounted on the same electrospinning set-up as for the co-axial electrospinning. More details on this procedure have been presented elsewhere.[24] Fiber mats were collected on an aluminum foil attached to a drum collector that could easily be removed for subsequent characterization. A homemade designed drum with both rotational and translational controllable movements was connected to the power supply 15 cm away from the needle. Samples were collected in both static and rotating drum mode, based on the requirements of the subsequent characterization techniques. Flow rates of 0.25 to 0.5 mL/h (in each syringe), and a voltage range of 15-20 kV were used as process parameters. The electrospinning parameters used were chosen based on preliminary tests. All experiments were carried out at ambient temperature and relative humidity of 15-20%.

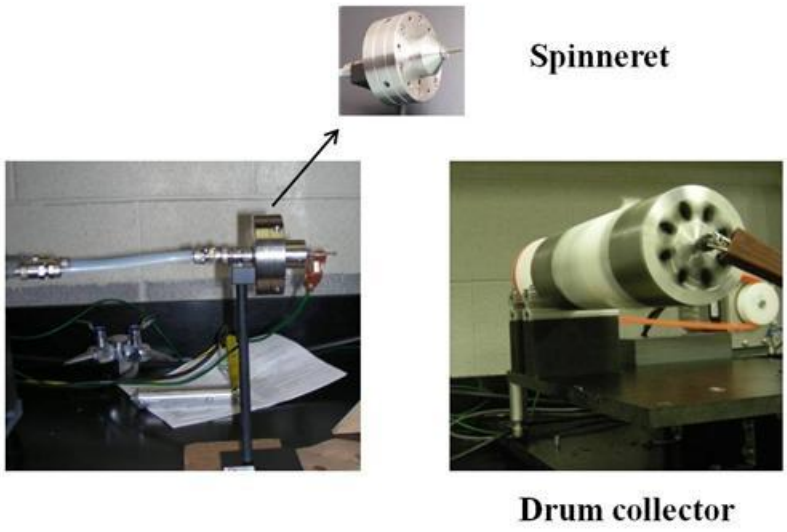

Figure 6-1: Schematic representation of the co-axial electrospinning set-up.

6.3.4 PEO extraction

The prepared electrospun mats were peeled from the aluminum surface of the collector and submerged in water for 24 h. The extracted mats were then vacuum dried at 40 °C overnight to remove the absorbed water, and further kept in a desiccator at room temperature.

6.3.5 Film preparation

For comparison and characterization purposes, chitosan/PEO films were prepared by mixing the two master solutions at different ratio (100/0, 50/50, 80/20 and 0/100). Thin films were prepared by pouring and spreading approximately 10 g of the relevant solutions in plastic Petri dishes. The cast films were vacuum dried at 40 °C overnight to evaporate completely the solvent. The dried films were peeled from the Petri dish and kept in a desiccator at room temperature for subsequent testing.

6.3.6 Characterization

6.3.6.1 Rheological measurements

Dynamic and steady shear rheological properties of the solutions were characterized at 25 ºC, using a stress-controlled rheometer (AR-2000, TA Instruments, DE, USA) with a Couette flow

geometry. Low viscosity silicon oil was used to cover the surface of the sample solutions to prevent evaporation of the solvent during testing. The presence of the oil was shown not to impact the rheological measurements. The stability of the solutions was examined as a function of time in oscillatory shear tests under a low frequency of 1 rad/s and a small deformation of 0.1. Over one hour, the elastic and loss modulus decreased by less than 1 and 3 %, respectively, showing the solutions to be stable. Steady simple shear measurements were carried out by applying shear rates from 0.0625 to 2000 s^{-1}. Possible fluid inertia effects at high shear rates were also examined by looking at values of the Reynolds number R_e. In Couette flow geometry, this number is given by: $R_e = \rho \dot{\gamma} H^2/\eta$, where ρ is the density of the fluid, $\dot{\gamma}$ is the shear rate, H is the flow gap and η is the viscosity of the solution.[35] The calculated R_e values were of the order of 10^{-4} to 1 over the range of shear rates used in these tests, hence the flow conditions were considered inertialess. The zero-shear viscosity of the solutions were estimated by applying the Carreau-Yasuda model [36] to the shear viscosity data.

6.3.6.2 Surface morphology and core-shell structure

The surface morphology of the electrospun nanofibers was characterized using a Hitachi S-4700 field emission scanning electron microscope (FE-SEM) operating at 5-10 kV. Samples were cut from co-electrospun mats collected on aluminum foil. These samples were mounted on aluminum stubs and sputter-coated by an ultrathin layer of platinum. The samples were observed at magnifications between 100 and 40,000 times of their original size to evaluate their electrospinnability through the presence of beads or droplets. Fiber diameters were also determined using Image-J (National Institutes of Health (NIH), http://rsb.info.nih.gov/ij/) image processing software. For each electrospun mat, at least 150 fibers were considered from three different images to calculate the average diameter.

The core-shell structure of the prepared nanofibers was characterized by transmission electron microscopy (TEM, JEOL, JEM 2100 F). For TEM observation, fibers were directly deposited onto a TEM copper mesh. The copper mesh was then submerged in water, dried and observed again by TEM to discriminate the components in the shell and core regions.

6.3.6.3 Thermal analysis

Bulk compositional analysis of the nanofibrous mats was carried out according to the method proposed by Desai et al. [12] using a TA Instruments thermal gravimetric analyzer (TGA, Q 500). Neat PEO, chitosan powder and electrospun mats were weighted (typical weights of 5-10 mg) and heated from room temperature to 1000 °C under a constant heating rate of 10 °C/min. All the TGA tests were performed under a nitrogen atmosphere. The weight loss for chitosan and PEO in the nanofibers was evaluated by taking the first-order derivative of the raw weight loss thermograms. The area under the respective degradation temperature peak is related to the polymer content in the blends.

6.3.6.4 Fourier Transform Infrared Spectroscopy (FTIR)

The local compositional and chemical characteristics of the samples were evaluated by Fourier transform infra red spectroscopy measurements (Perkin Elmer spectrum 65 FTIR-ATR instrument). Transmission and ATR spectra were recorded at room temperature on the as-cast chitosan and PEO films and as-spun nanofibrous mats, at wavelengths in the range of 700-4000 cm^{-1} (resolution 4 cm^{-1}, accumulation of 128 scans). The chitosan to PEO relative ratio in the samples was estimated from the absorbance ratio at 1550 and 1250 cm^{-1} (A_{1550}/A_{1250}), that are characteristic peaks of chitosan and PEO, respectively.[37]

6.3.6.5 Crystalline structure

The crystalline structure of the electrospun nanofibers was investigated using XRD and DSC. Wide angle X-ray diffraction (WAXD) measurements were performed on a diffractometer system (Bruker Discover, D8, 40 kV, 30 mA) equipped with a monochromic Cu Kα (1.542 °A) X-ray source, The XRD patterns were recorded over a diffraction angle (2θ) range from 5° to 40° in 0.02° steps. Differential scanning calorimetry was carried out using a TA Instrument Q 1000 system. Samples of 6 to 10 mg were sealed in aluminum pans and heated under a helium atmosphere from 10 to 200 °C in the DSC instrument at a rate of 10 °C/min.

6.3.6.6 Surface chemistry (XPS)

X-ray photoelectron spectrophotometry (XPS, Thermo Scientific, VG ESCALAB 3 MKII) was used to characterize the surface chemistry of the electrospun mats, in conjunction with a flood

gun to eliminate any charging of the surfaces under study. The chemical composition of the sample surface was determined for all elements contained in the polymers except hydrogen, with a typical sampling thickness of 5-10 nm. An Mg Kα monochromatized X-ray source (1253.6 eV) was used to produce photoelectron emission from the samples. The pressure in the analysis chamber was maintained at 10^{-9} Torr. An area of 2×3 mm^2 (maximum allowable) was used to scan the surface of the samples to account for surface variations and obtain an averaged signal. Survey spectra were taken to identify the chemical species on the sample surface, and a high resolution scan for C, N and O was performed to identify the elemental peaks. XPS data was analyzed using VGS 5000 software to calculate the atom percentage of the various elements found on the mat surface. Peak fitting was performed on the high resolution elemental scans (average of 10 scans) to obtain surface chemistry information. Energy calibration was carried out by placing the hydrocarbon peak in the C1s spectrum at 285 eV.

6.3.6.7 Specific surface area (BET) measurement

The surface area of the electrospun mats was obtained by a Quantachrome instrument BET Autosorb IQ. A gas mixture of nitrogen and helium was continuously fed through the sample cell, which was kept in liquid nitrogen. The total volume of adsorbed nitrogen gas on the surface was measured at different pressures. The volume of gas needed to create an adsorbed monomolecular layer was calculated as follows [38]:

$$\frac{P}{P^0\left[v\left(1-(P/P^0)\right)\right]} = \frac{1}{v_m C} + \frac{C-1}{v_m C}\frac{P}{P^0} \qquad (6\text{-}1)$$

where P is the experimental pressure, P^0 the saturation pressure, ν the volume of the adsorbate, ν_m the volume of gas required to form an absorbed monomolecular layer, and C a constant. The procedure for estimating the surface area from Eq. 6-1 can be found in reference.[39]

6.4 Results and discussion

6.4.1 Rheological behaviour of solutions

The rheological characteristics of chitosan and PEO solutions were measured to gain knowledge of their flow behaviour in the needles during the electrospinning process (Fig. 6-2). The apparent

shear rate at the respective needle walls was approximated by considering the solutions as Newtonian fluids and applying Eq. 6-2:

$$\dot{\gamma} = \frac{4Q}{\pi R^3} \qquad (6\text{-}2)$$

where $\dot{\gamma}$ is the apparent shear rate at the needle wall, Q is the volumetric flow rate and R is the radius of the needle (255 μm for the inner needle, 685 μm for the outer needle, and 415 μm at the annulus). For a typical flow rate of 0.5 ml/h, the calculated shear rates are approximately 11, 0.60 and 2.5 s^{-1} at the three respective needle walls, and these values are illustrated in Fig. 6-2 by dotted lines. The viscosity curves in Fig. 6-2 indicate that the solutions are nearly Newtonian at these operating shear rates in the co-axial needle, which support the use of Eq. 6-2.

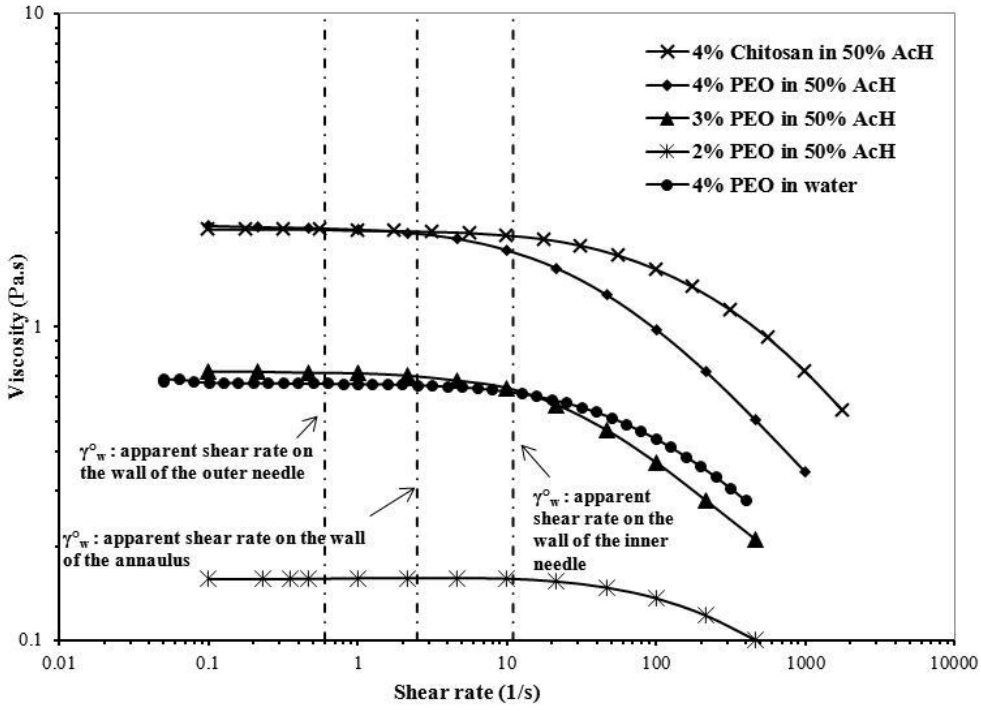

Figure 6-2: Dependence of viscosity on shear rate for PEO solutions (in water and 50 wt% acetic acid) and chitosan in 50 wt% acetic acid (data collected at 25 °C).

All solutions show a well developed zero-shear viscosity plateau. Shear-thinning is observed at higher shear rates, and this behavior is amplified with polymer content due to more disentanglement between polymer chains. The PEO solution show more shear-thinning than chitosan at the same polymer content as well as an earlier onset of shear-thinning, indicative of a larger characteristic time. This can be attributed to the different conformations of their chains in the solution state, i.e. very flexible for PEO and rigid (rod-like) for chitosan. The zero-shear viscosity of 4 wt% PEO in water is nearly the same as 3 wt% PEO in 50 wt% acid (0.7 Pa.s), however this value is much less than (almost one third) that of 4 wt% PEO in 50 wt% acetic acid (2.1 Pa.s). The larger viscosity of PEO in aqueous acetic acid solution, vs. water, could be due to interactions between ether groups in PEO and hydroxyl groups in acetic acid that may expand the polymer conformation in solution.[13]

6.4.2 Morphology and internal structure of the co-axial electrospun nanofibers

Fig. 6-3 shows the SEM images and associated diameter histograms of the nanofibers produced by the co-axial electrospinning of PEO and chitosan solutions in the core and shell streams, respectively. Defect-free, bead-less and geometrically uniform nanofibers could be prepared when 3 and 4 wt% PEO solutions were fed as the core stream (Fig. 6-3-A and 6-3-B, respectively). However, the morphology was changed to beaded fibers when the concentration of PEO was reduced to 2 wt% (Fig. 6-3-C). The same trend was observed for the lower flow rate of 0.25 ml/h (results not shown). The average diameter of the nanofibers decreased from 190 ± 20 nm to 103 ± 24 nm (for the flow rate of 0.5 ml/h) by decreasing the PEO concentration from 4 to 3 wt% in the core solution (Fig. 6-3-A and 6-3-B). It shows that the effect of the core solution concentration in the co-axial electrospinning geometry is similar to that for simple electrospinning, i.e. an increase in solution concentration generally results in a larger fiber diameter.[40] On the other hand, co-axial electrospinning of a 4 wt% PEO in water as the inner stream and chitosan solution as the outer solution did not result in a stable jet and fiber formation (results not shown). Electrospinnability of neat PEO solutions alone (in 50 wt% aqueous acetic acid) in the same set-up has been also studied by removing the outer chitosan stream from the spinneret. It shows that defect-free nanofibers were formed from 3 and 4 wt% PEO concentrations, however, beaded nanofibers and unstable jet were observed for the 2 wt% PEO

solution. Moreover, electrospinning of neat chitosan solution only led to formation of beads and droplets on the collector. This could be due to lack of enough chain entanglements required for a successful electrospinning.[24]

It is believed that in this co-axial setup, the PEO solution serves as a spinning aid to successfully prepare nanofibers from the non-electrospinnable chitosan solution. It is hypothesized that during the co-axial electrospinning process, the core PEO solution carries out the shell chitosan solution through the formation of a stable Taylor cone and continuous jet ejection during the entire process. This could be attributed to a combination of parameters: a) Using the same solvent in the two streams that leads to low interfacial tension between the two solutions is in favor of successful co-axial electrospinning.[32, 41] This is supported by the fact that when the core solvent was changed to water (4 wt% PEO), even though the viscosity is almost the same as the core solution of 3 wt% PEO in 50 wt% acetic acid (Fig. 6-2), no nanofibers were formed. b) Higher conductivity of the shell solution; chitosan is a polyelectrolyte in solution that makes it more conductive than neutral solution of PEO.[24] Yu et al. [32] speculated that higher conductivity in the shell layer compared to that of the core stream can stabilize the co-electrospinning process, probably due to higher shear stress applied on the core material and its subsequent elongational force to form a thinner core. c) Low vapor pressure of the solvent (50 wt% acetic acid solution) that was used to make the core and shell solutions (boiling point of acetic acid = 120 °C). It was shown that high vapor pressure solvents may produce unstable Taylor cones in co-axial electrospinning.[41, 42] Moreover, as we showed in our previous work [24] (chapter 5) specific hydrogen bonds are formed between chitosan and PEO. Those bonds could occur during the co-axial electrospinning process according to Li and Xia [43] results, and would stabilize further the jet.

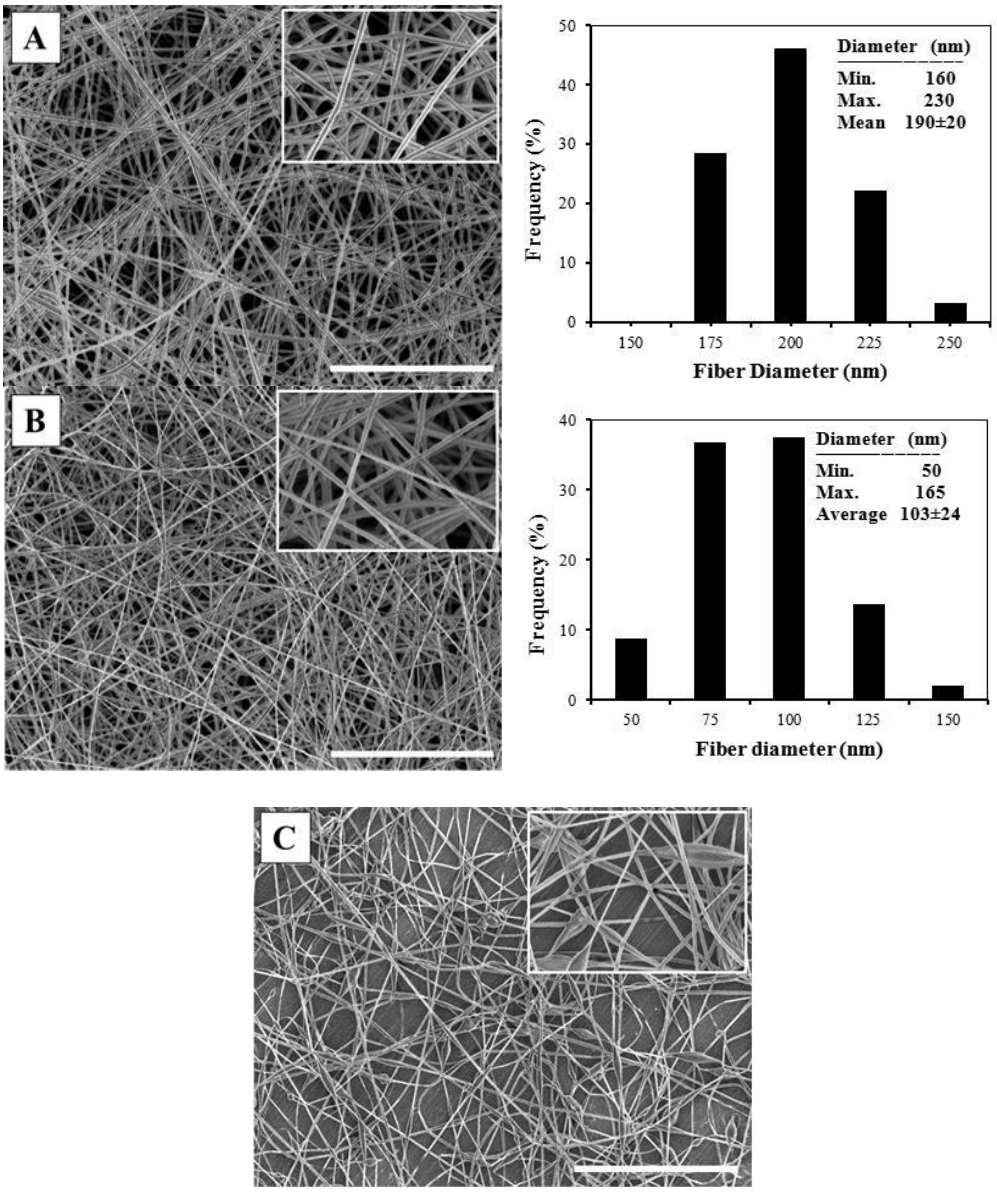

Figure 6-3: SEM micrograph and diameter histogram of co-axial electrospun nanofibers of PEO/chitosan; scale bars represent 10 µm. A) 4 wt% PEO, B) 3 wt% PEO and C) 2 wt% PEO (flow rate 0.5 ml/h, needle to collector distance = 15 cm, voltage = 15 kV).

The detailed morphology of the produced co-axial PEO/chitosan nanofibers is shown in a TEM micrograph in Fig. 6-4. The contrast which is created by electron beam diffraction represents the distinctive phases in the nanofibers. These dark and bright regions represent the core and shell of the nanofiber, respectively. The diameters of the shell and core are approximately 200 and 100

nm, respectively. Complete concentricity is observed for the majority of the produced nanofibers (Fig. 6-4-A), however, eccentricity are noted for some others (Fig. 6-4-B). It is speculated that the nature of the bending instability and whipping motion of the charged jet in the electrospinning process may cause some eccentricity.

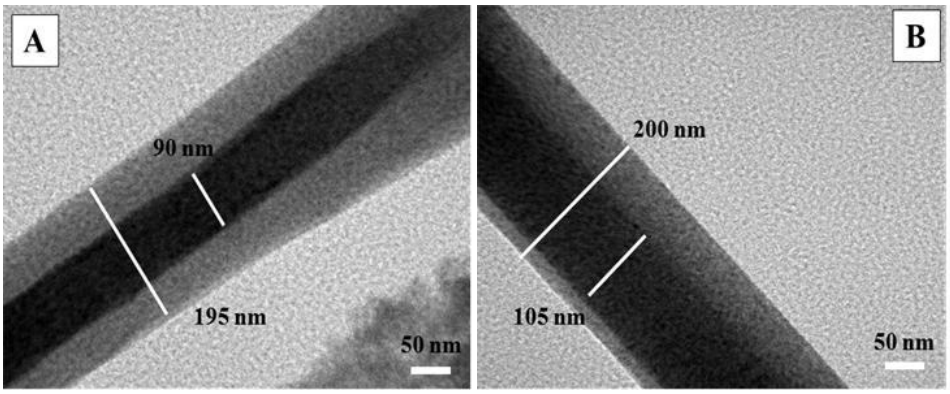

Figure 6-4: TEM micrographs of core-shell structured PEO-chitosan bi-component electrospun nanofibers, showing segments of the nanofibers with sharp boundaries; A) Concentric and B) Eccentric core and shell structures (Flow rate = 0.5 ml/h, needle to collector distance = 15 cm, voltage = 20 kV).

In order to confirm further the formation of the core-shell structure and identify their respective components, the electrospun material deposited on a TEM copper mesh was soaked in water and dried, and examined again. The resulting structure shown in Fig. 6-5 reveals that the core region is completely removed and that a hollow nanofiber is obtained due to the high solubility of PEO in water. Hence, the extraction step reveals that PEO is mainly located in the core while chitosan constitutes the shell of the nanofiber. This is indeed a relatively simple method to produce chitosan hollow nanofibers.

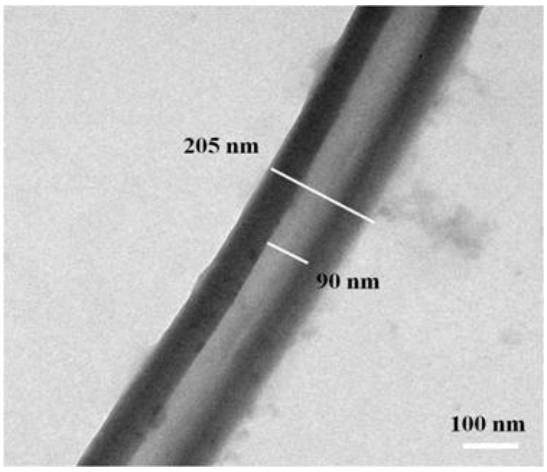

Figure 6-5: TEM micrograph of a hollow chitosan nanofiber obtained after water extraction of the PEO core (Flow rate = 0.5 ml/h, needle to collector distance = 15 cm, voltage = 20 kV).

6.4.3 Structural features of the core-shell nanofibers; Compositional analysis

To determine the PEO content, electrospun mat samples were weighed before and after the extraction by water. A weight reduction of 46 ± 4 wt% was measured, in close agreement with the 50/50 PEO/chitosan flow rates used in the process. The resulting mat also kept its mechanical integrity in the form of a membrane after the soaking in water. A typical SEM image of PEO extracted co-axial electrospun PEO/chitosan nanofibrous mat is shown in Fig. 6-11 in the Supporting Information. To quantify further the bulk composition of chitosan and PEO in the produced co-axial nanofibers, TGA was used. Raw TGA thermograms and their first-order derivative curves for as-spun and PEO extracted co-axial nanofibrous mats, in comparison with neat chitosan and PEO, are shown in Fig. 6-6. The neat chitosan sample in Fig. 6-6-A shows a weight reduction of 6.5 ± 0.5% until 100 °C due to the evaporation of the adsorbed water. In the case of PEO, at 1000 °C there is nearly no residue left, while an ash residue of 28.11 ± 1.16% is observed in the case of chitosan. The neat PEO and chitosan show two separate decomposition temperatures at 414.5 ± 2 °C and 325.8 ± 0.73 °C, respectively (Fig. 6-6-A). As shown in Fig. 6-6-B, the peak temperatures related to PEO and chitosan decomposition were also observed in the co-axial nanofibers, with only a slight shift in their position that has been attributed to the interactions between PEO and chitosan.[24, 44] In addition, in the case of the PEO extracted co-axial mat, the PEO peak disappears as expected and only the chitosan peak is observed, with a

curve quite similar to that of the neat chitosan (Fig. 6-6-B). These results also reveal that the extraction step is quite efficient in removing PEO from the nanofibers core. The data obtained from the TGA thermograms is used to determine the content of PEO and chitosan in the produced co-axial nanofibers, considering the humidity and residue level in the mats. This is achieved by measuring the related area under the peaks in the first-order derivative of the TGA curves (Fig. 6-6-B). Using this method the chitosan content is calculated to be 52 ± 3% for the co-axial electrospun mats, which agrees with the value obtained from the extraction method (~54 wt%).

To evaluate the local compositional homogeneity of the membranes, FTIR analysis has been performed on the samples. Figure 6-7 shows the ATR-FTIR spectra of as-spun and PEO extracted co-axial electrospun nanofibers. Neat chitosan and PEO cast films were also characterized for comparison. Neat chitosan exhibits a broad band around 3100-3500 cm^{-1} and another one at 1550 cm^{-1}, which are commonly attributed to the N-H and O-H stretching of the primary amino groups (due to hydrogen bonds with O-H groups) and N-H stretching of the secondary amides (known as Amide II), respectively.[14, 45, 46] Very weak peaks for the stretching of the carbonyl (C=O-NHR) groups at 1650 cm^{-1} (known as Amide I) and C-H stretching at 2880 cm^{-1} also appear. The neat PEO shows its FTIR absorption feature bands around 2880, which are assigned to the CH_2 stretching; however this band overlap with that detected for chitosan. Other feature bands of PEO are observed at 1150, 1110 and 1060 cm^{-1} as triplet peaks related to C-O-C stretching vibrations, and sharp peaks at 1360, 1340, 1275 and 1250 cm^{-1} attributed to CH deformation of the methyl groups.[13, 46] The absorbance intensity ratio at 1550 cm^{-1} and 1250 cm^{-1} (A_{1550}/A_{1250}) is used as an indication of the chitosan to PEO ratio.[37] Therefore, local compositions of chitosan and PEO are determined by evaluating this ratio in different areas of the co-axial nanofibers by recording the transmission FTIR spectra for that region. It is found that the A_{1550}/A_{1250} ratio does not vary significantly for various locations of the samples, confirming the uniformity and homogeneity of the prepared nanofibers and the stability of the electrospinning process. A chitosan content of 55 ± 1.6 % was calculated based on this ratio, and is again in close agreement with the values obtained from bulk compositional analysis, i.e. the extraction test (~54%) and TGA (52 ± 1.6%). In addition, after washing the co-axial electrospun mat with water, the feature peaks of PEO disappear and the spectra obtained is that of neat chitosan (Fig. 6-7). Therefore it can be concluded that after PEO washing, a nanofibrous mat exclusively made of chitosan can be obtained.

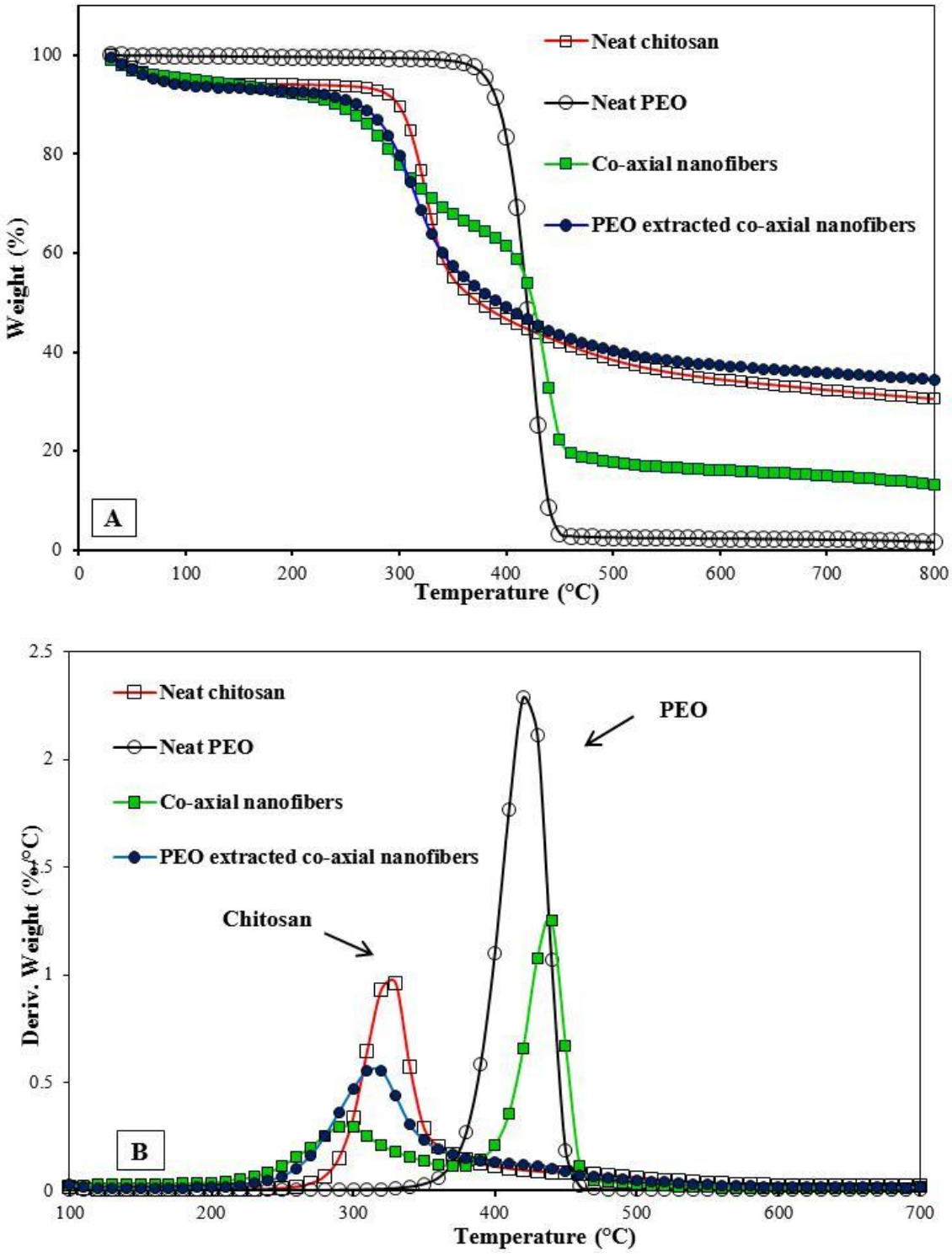

Figure 6-6: TGA curves of as-spun and PEO extracted co-axial electrospun PEO/chitosan mats compared with neat chitosan and PEO powder A) raw TGA curves, and B) first-order derivative of TGA curves.

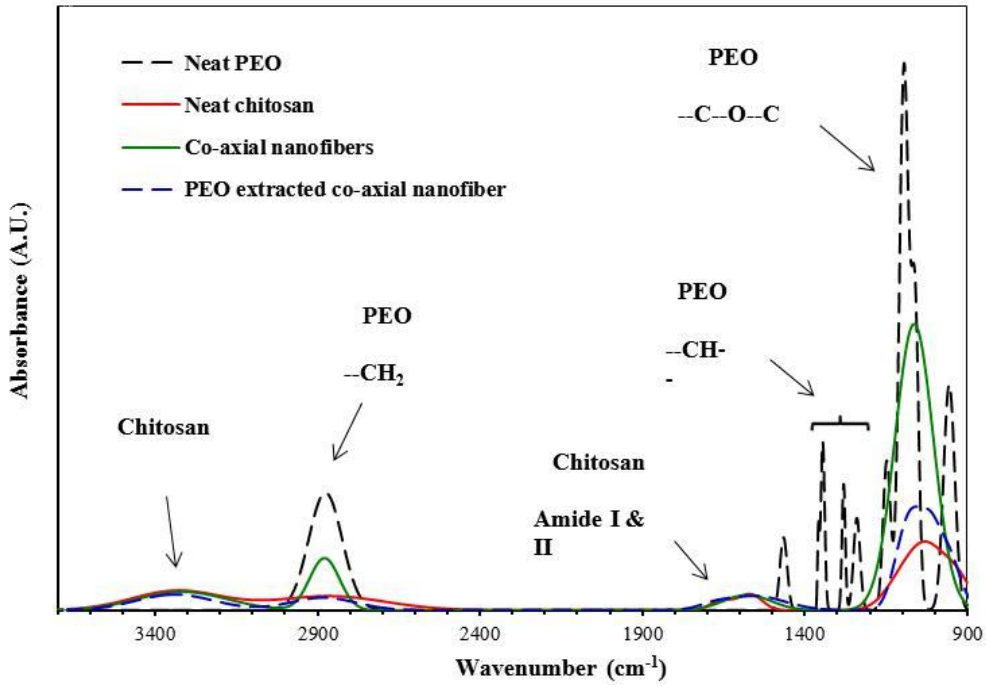

Figure 6-7: ATR-FTIR spectra of neat chitosan and PEO powder, and co-axial electrospun PEO/chitosan nanofibers: as-spun and after extracting PEO by water.

6.4.4 Crystalline structure of the nanofibers

To evaluate the crystalline structure, DSC and XRD tests have been performed on chitosan/PEO electrospun nanofibers and compared with results for neat chitosan and PEO. DSC thermograms of as-spun and washed co-axial electrospun nanofibers, and nanofibers prepared from a 50/50 chitosan/PEO blend solution are presented in Fig. 6-8. DSC curves of neat chitosan and PEO powder are also shown for comparison purposes. The broad endothermic peak in the chitosan curve is attributed to the evaporation of bound water from chitosan.[13] For the neat PEO powder, a sharp endothermic melting peak around 71 °C is observed. On the other hand, the co-axial PEO-chitosan nanofibers show a melting transition at 62.1 °C. This peak disappears after PEO extraction and the DSC curve become similar to that of the neat chitosan powder (Fig. 6-8). The nanofibers from the 50/50 chitosan/PEO blend solution also exhibit an endothermic melting transition, closely located to that of the co-axial nanofibers. Table 6.1 shows melting point and enthalpy of fusion for neat PEO powder and nanofiber in comparison with co-axial electrospun

nanofibers and 50/50 blended chitosan/PEO nanofibers. It shows that the melting point and enthalpy of fusion (hence crystallinity) in the PEO nanofibers decrease as compared to that of the neat powder. This is attributed to the very fast evaporation of the solvent in the electrospinning process that may prevent the crystals to form completely.[47, 48] In the case of nanofibers based on blend (50/50), interactions between chitosan and PEO chains in the nanofibers may also hinder the crystallization of PEO.[46]

Table 6.1: Melting point and enthalpy of fusion of neat PEO powder and electrospun nanofibers

Sample	Tm (°C)	ΔH (J/g; PEO)
PEO powder	69.0 ± 1.0	180.8
PEO nanofiber	64.5 ± 1.7	165.5
Co-axial nanofibers	62.1 ± 2.0	158.7
50/50 blend nanofibers	62.0 ± 1.6	157.1

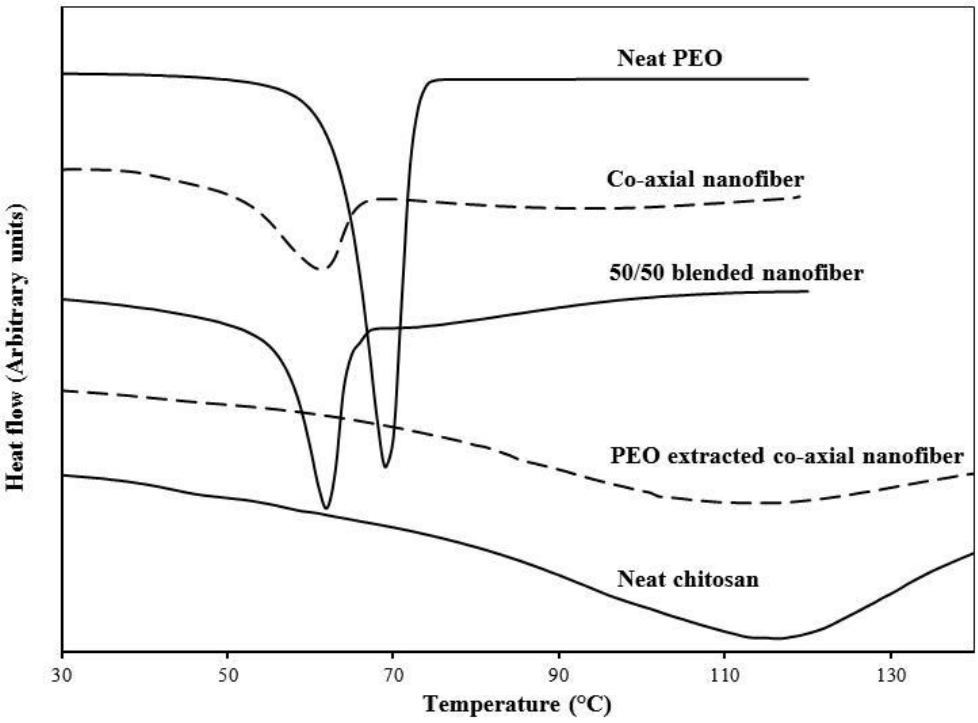

Figure 6-8: DSC thermograms of neat chitosan and PEO powder, as-spun and washed co-axial electrospun PEO/chitosan nanofibers, and 50/50 blend chitosan/PEO nanofibers.

In order to further illustrate the differences in crystalline content and morphology of the nanofibers and neat materials, X-ray diffraction patterns were obtained. Figure 6-9 presents the XRD patterns of neat chitosan and PEO powder, co-axial PEO-chitosan nanofibers before and after washing and 50/50 and 80/20 blend chitosan/PEO nanofibers. The neat PEO powder show two sharp feature peaks around $2\theta=19.1°$ and $2\theta=23.2°$.[47] The peak appearing around $2\theta = 20.1°$ is characteristic of chitosan and has a much lower intensity than those of PEO, indicating that the crystalline ordering in chitosan is significantly less than in PEO.[11] The two peaks related to the PEO crystals also appear in the XRD patterns of the co-axial nanofibers and the 50/50 blended chitosan/PEO nanofibers, however the peak around $2\theta = 23.2°$ is weaker than for the neat PEO powder. Nevertheless it depicts the existence of the same PEO crystalline structure in the electrospun nanofibers, with a crystallinity degree slightly lower than in the neat material, as indicated previously by the DSC results. The difference between the intensity of the main peaks in the neat PEO powder as compared to its electrospun counterparts may be related to the orientation of the PEO crystals according to the strong elongational field in the electrospinning process, and possibly also to less crystals formed.[49] No peak is observed after PEO washing from the co-axial mats, which reveals once more the complete removal of PEO and a remaining chitosan amorphous structure. This indicates that the crystalline microstructure of chitosan cannot build up as well as PEO in the electrospinning process, most probably due to the fast evaporation of the solvent in this process. Additionally, in the case of the 80/20 blend chitosan/PEO nanofibers, the low amount of PEO and the presence of chitosan-PEO interactions hinder crystal formation and lead to an almost amorphous structure.

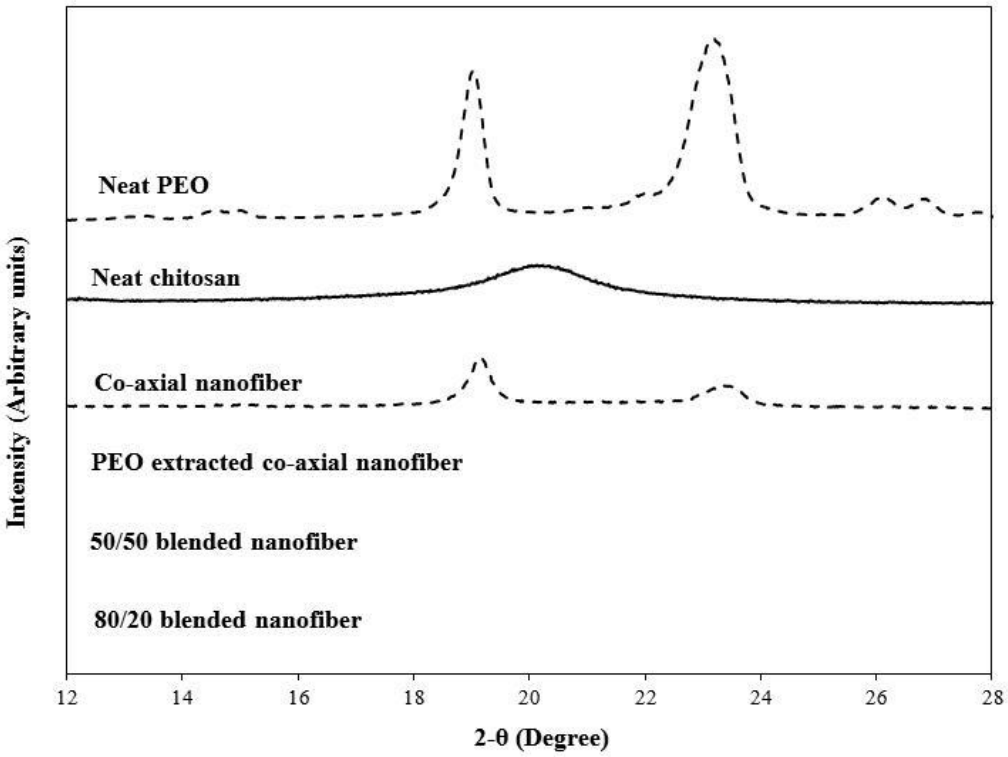

Figure 6-9: XRD diffraction pattern of neat chitosan and PEO powder, co-axial electrospun PEO-chitosan nanofibers: as-spun and after extracting the PEO by water, and blended chitosan/PEO nanofibers (80/20 and 50/50 chitosan/PEO blend ratios).

6.4.5 Surface properties of core-shell nanofibers

X-ray photo electron spectroscopy (XPS) analysis was performed to quantify the surface composition of the co-axial electrospun nanofibers. The XPS survey spectra (data not shown here) and the surface elemental content of carbon, oxygen and nitrogen of the co-axial and blended chitosan/PEO electrospun nanofibers, as well as cast films of the neat components, were analysed by the XPS technique. Chitosan contains nitrogen in its amine and acetylamine groups on its backbone; however PEO has only oxygen and carbon in its structure. Figure 6-10 shows the surface nitrogen composition in electrospun nanofibers and cast films vs. chitosan content in the blend (or feed) solutions. The theoretical nitrogen composition for a 97.5% DDA chitosan, calculated from the chemical structure and ratios of the repeating units in chitosan,[2] is calculated to be 9 % and is shown as the dashed line in Fig. 6-10. It can be observed from Fig. 6-10 that this value is not in close agreement with the surface nitrogen composition of neat chitosan film

measured by XPS, i.e. 5.2% (shown as dotted line in Fig. 6-10). This discrepancy between the theoretical nitrogen composition and the surface nitrogen composition measured by XPS has been previously reported[2, 50] for surface analysis of chitosan containing films. This can be attributed to a contaminating overlayer on the surface or the film surface composition is not necessarily the same as its expected theoretical stoichiometric bulk composition. As expected, the surface nitrogen composition increases with chitosan content, and for the 90/10 chitosan/PEO blend the nitrogen composition is close to that of neat chitosan (cast film). In the 50/50 chitosan/PEO blend, the surface nitrogen content is very low (~ 1%), however in co-axial electrospun nanofibers this value increases to 4.6 ± 0.6%, a value very close to that of the neat chitosan cast film. This is another indication of the successful formation of a core/shell nanostructure, with a chitosan shell.

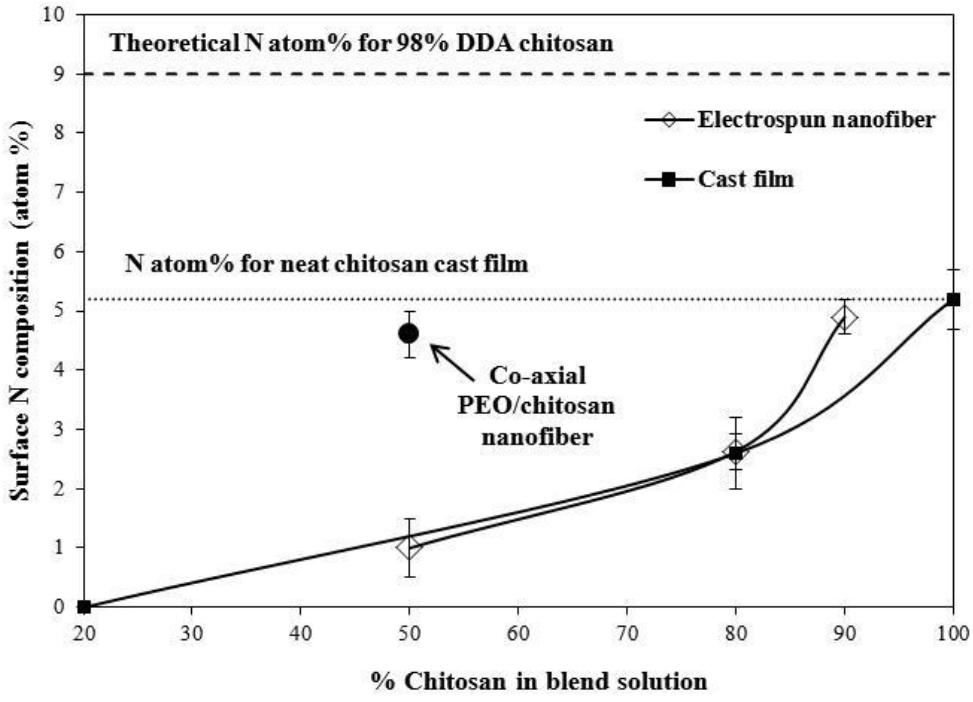

Figure 6-10: Surface nitrogen composition of the blended chitosan/PEO electrospun nanofibers and their cast films. The point represents the co-axial PEO/chitosan electrospun mats.

The actual specific surface area of the electrospun co-axial nanofibers, neat chitosan powder and chitosan cast film were obtained through conventional N_2 adsorption measurements based on the Brunauer-Emmett-Teller (BET) theory.[38] A specific surface area of 15 ± 1.5 m^2/g was calculated for the co-axial nanofibers prepared from a 0.5 ml/h flow rate, a value which is much higher than that of chitosan powder (less than 1 m^2/g) and most probably film. The specific surface area of the nanofibers was also calculated theoretically by considering the fibers as cylinders and neglecting the area of the cross sections, based on Eq. (6-3):

$$A = \frac{4000}{D \times \rho} \qquad (6\text{-}3)$$

where A is the specific surface area in g/m^2 and D and ρ denote the diameter (in nm) and density (in g/cm^3) of the nanofibers, respectively. The theoretical surface area of the co-axial nanofibers was calculated to be 16.7 m^2/g, considering 190 nm as the average diameter and 1.26 g/cm^3 for the density of the nanofibers (detailed on page 2 of the Supporting Information). This value is in good agreement with the experimental result (15 ± 1.5 m^2/g).

6.5 Conclusions

Chitosan is a cationic biopolymer that is challenging to electrospin. In this work we were able to produce fairly uniform sized core/shell structured PEO/chitosan nanofibers using a co-axial electrospinning technique. PEO and chitosan solutions were fed as core and sheath materials to a co-spinneret, respectively. Core-shell structure of the nanofibers was observed by TEM images. Presence of chitosan on the shell was confirmed by TEM images of hollow nanofibers obtained after extracting the PEO content. The obtained mats after the washing step were comprised of nearly 100% chitosan in the form of hollow nanofibers. The presence of chitosan on the surface was also confirmed by XPS analysis as further evidence of core/shell formation. Bulk and local compositional analysis of chitosan and PEO in the electrospun nanofibers showed that the ratio of chitosan to PEO in the nanofibers was similar to that in the feed streams, and also that the local composition of the prepared nanofibers was homogeneous, indicating the stability of the electrospinning process. Due to a shell layer entirely made of chitosan, this processing method has several advantages such as the simplicity of a one-step production without any

post-treatment, with the possibility of producing chitosan hollow nanofibers through a subsequent PEO water washing. These nanofibers have interesting potential applications in the biomedical field such as purification of the blood in hemodialysis and wound dressings.

6.6 Acknowledgements

The authors gratefully acknowledge the financial support of NSERC (National Science and Engineering Research Council of Canada) and FQRNT (Fonds québécois de la recherche sur la nature et les technologies). We are also thankful to Mesdames Weawkamol Leelapornpisit and Suzie Poulin for their great help in the morphological and XPS studies. Messrs. Daniel Dumas and Robert Delisle are appreciated for the design and fabrication of the nanofibers collecting system and great gratitude to Mrs. Melina Hamdine for her coordination in assembling the electrospinning set up.

6.7 Associated content

6.7.1 Supporting Information

SEM micrograph of a PEO extracted nanofibrous mat; density calculation of the co-axial nanofibers. This material is available free of charge via the Internet at http:// pubs.acs.org.

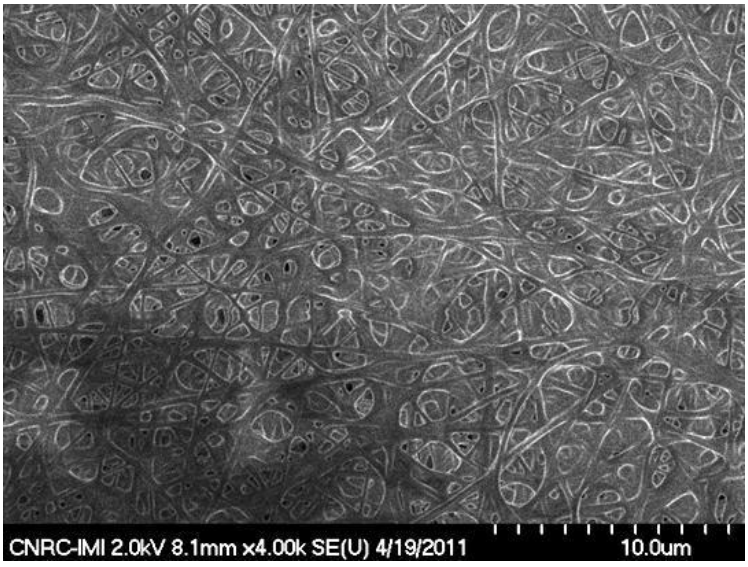

Figure 6-11: SEM image of PEO extracted co-axial PEO/chitosan nanofibrous mat

6.7.2 Calculation of co-axial nanofibers density

Density of PEO (typically 70% crystalline) = 1.20 (g/cm^3)[4]

Density of chitosan = 1.33 (g/cm^3) [5]

Weight percent of chitosan in co-axial nanofibers ≅ 52 wt% (TGA results)

Density of the co-axial nanofibers = $1/ (\Sigma w_i/d_i) = 1 / ((0.52/1.33) + (0.48/1.2)) = 1.26$ g/cm^3

where w_i and d_i are weight fraction and density of component i in the mixture, respectively.

6.8 References

1. An, J.; Zhang, H.; Zhang, J. T.; Zhao, Y. H.; Yuan, X. Y. Colloid and Polymer Science 2009, 287, (12), 1425-1434.
2. Desai, K.; Kit, K.; Li, J. J.; Davidson, P. M.; Zivanovic, S.; Meyer, H. Polymer 2009, 50, (15), 3661-3669.
3. Haider, S.; Park, S. Y. Journal of Membrane Science 2009, 328, (1-2), 90-96.
4. Ye, P.; Xu, Z. K.; Wu, J.; Innocent, C.; Seta, P. Biomaterials 2006, 27, (22), 4169-4176.
5. Ignatova, M. G.; Manolova, N. E.; Toshkova, R. A.; Rashkov, I. B.; Gardeva, E. G.; Yossifova, L. S.; Alexandrov, M. T. Biomacromolecules 2010, 11, (6), 1633-1645.
6. Wang, W.; Itoh, S.; Konno, K.; Kikkawa, T.; Ichinose, S.; Sakai, K.; Ohkuma, T.; Watabe, K. Journal of Biomedical Materials Research Part A 2009, 91A, (4), 994-1005.
7. Cooper, A.; Bhattarai, N.; Zhang, M. Q. Carbohydrate Polymers 2011, 85, (1), 149-156.
8. Zhou, Y. S.; Yang, D. Z.; Chen, X. M.; Xu, Q.; Lu, F. M.; Nie, J. Biomacromolecules 2008, 9, (1), 349-354.
9. Li, D.; Xia, Y. N. Advanced Materials 2004, 16, (14), 1151-1170.
10. Greiner, A.; Wendorff, J. H. Angewandte Chemie-International Edition 2007, 46, (30), 5670-5703.
11. Rinaudo, M. Progress in Polymer Science 2006, 31, (7), 603-632.
12. Desai, K.; Kit, K.; Li, J.; Zivanovic, S. Biomacromolecules 2008, 9, (3), 1000-1006.
13. Duan, B.; Dong, C. H.; Yuan, X. Y.; Yao, K. D. Journal of Biomaterials Science-Polymer Edition 2004, 15, (6), 797-811.
14. Li, L.; Hsieh, Y. L. Carbohydrate Research 2006, 341, (3), 374-381.
15. McKee, M. G.; Wilkes, G. L.; Colby, R. H.; Long, T. E. Macromolecules 2004, 37, (5), 1760-1767.

---

[4] Lin, H.; Freeman, B. D. *Journal of Membrane Science* **2004,** 239, (1), 105-117.

[5] Musale, D. A.; Kumar, A. *Journal of Applied Polymer Science* **2000,** 77, (8), 1782-1793.

16. McKee, M. G.; Hunley, M. T.; Layman, J. M.; Long, T. E. Macromolecules 2006, 39, (2), 575-583.
17. Ohkawa, K.; Minato, K. I.; Kumagai, G.; Hayashi, S.; Yamamoto, H. Biomacromolecules 2006, 7, (11), 3291-3294.
18. Schiffman, J. D.; Schauer, C. L. Biomacromolecules 2007, 8, (2), 594-601.
19. Geng, X. Y.; Kwon, O. H.; Jang, J. H. Biomaterials 2005, 26, (27), 5427-5432.
20. Homayoni, H.; Ravandi, S. A. H.; Valizadeh, M. Carbohydrate Polymers 2009, 77, (3), 656-661.
21. Sangsanoh, P.; Supaphol, P. Biomacromolecules 2006, 7, (10), 2710-2714.
22. Klossner, R. R.; Queen, H. A.; Coughlin, A. J.; Krause, W. E. Biomacromolecules 2008, 9, (10), 2947-2953.
23. Bhattarai, N.; Edmondson, D.; Veiseh, O.; Matsen, F. A.; Zhang, M. Q. Biomaterials 2005, 26, (31), 6176-6184.
24. Pakravan, M.; Heuzey, M. C.; Ajji, A. Polymer 2011, 52, 4813-4824.
25. Ignatova, M.; Manolova, N.; Markova, N.; Rashkov, I. Macromolecular Bioscience 2009, 9, (1), 102-111.
26. Zhang, H. T.; Wu, C. Y.; Zhang, Y. L.; White, C. J. B.; Xue, Y.; Nie, H. L.; Zhu, L. M. Journal of Materials Science 2010, 45, (9), 2296-2304.
27. Shalumon, K. T.; Anulekha, K. H.; Girish, C. M.; Prasanth, R.; Nair, S. V.; Jayakumar, R. Carbohydrate Polymers 2010, 80, (2), 413-419.
28. Park, W. H.; Jeong, L.; Yoo, D. I.; Hudson, S. Polymer 2004, 45, (21), 7151-7157.
29. Torres-Giner, S.; Ocio, M. J.; Lagaron, J. M. Carbohydrate Polymers 2009, 77, (2), 261-266.
30. Chen, Z. G.; Mo, X. M.; Qing, F. L. Materials Letters 2007, 61, (16), 3490-3494.
31. Sun, Z. C.; Zussman, E.; Yarin, A. L.; Wendorff, J. H.; Greiner, A. Advanced Materials 2003, 15, (22), 1929-1932.
32. Yu, J. H.; Fridrikh, S. V.; Rutledge, G. C. Advanced Materials 2004, 16, (17), 1562-1566.
33. Ojha, S. S.; Stevens, D. R.; Hoffman, T. J.; Stano, K.; Klossner, R.; Scott, M. C.; Krause, W.; Clarke, L. I.; Gorga, R. E. Biomacromolecules 2008, 9, (9), 2523-2529.
34. Modrzejewska, Z.; Eckstein, W. Biopolymers 2004, 73, (1), 61-68.
35. Yosick, J. A.; Giacomin, J. A.; Stewart, W. E.; Ding, F. Rheologica Acta 1998, 37, (4), 365-373.
36. Carreau, P. J.; De Kee, D.; Chabra, P. R., Rheology of polymeric systems: principles and applications. Hanser Publishers: Munich, 1997.
37. Kriegel, C.; Kit, K. M.; McClements, D. J.; Weiss, J. Polymer 2009, 50, (1), 189-200.
38. Brunauer, S.; Emmett, P. H.; Teller, E. Journal of American Chemical Society 1938, 60, (2), 309-319.
39. Li, J.; Favis, B. D. Polymer 2001, 42, (11), 5047-5053.
40. Fridrikh, S. V.; Yu, J. H.; Brenner, M. P.; Rutledge, G. C. Physical Review Letters 2003, 90, (14).
41. Li, D.; Babel, A.; Jenekhe, S. A.; Xia, Y. N. Advanced Materials 2004, 16, (22), 2062-2066.
42. Moghe, A. K.; Gupta, B. S. Polymer Reviews 2008, 48, (2), 353-377.
43. Li, D.; Xia, Y. N. Nano Letters 2004, 4, (5), 933-938.
44. Lewandowska, K. Thermochimica Acta 2009, 493, (1-2), 42-48.
45. Jia, Y. T.; Gong, J.; Gu, X. H.; Kim, H. Y.; Dong, J.; Shen, X. Y. Carbohydrate Polymers 2007, 67, (3), 403-409.

46. Zivanovic, S.; Li, J. J.; Davidson, P. M.; Kit, K. Biomacromolecules 2007, 8, (5), 1505-1510.
47. Deitzel, J. M.; Kleinmeyer, J.; Harris, D.; Tan, N. C. B. Polymer 2001, 42, (1), 261-272.
48. Son, W. K.; Youk, J. H.; Lee, T. S.; Park, W. H. Polymer 2004, 45, (9), 2959-2966.
49. Zhang, J. F.; Yang, D. Z.; Xu, F.; Zhang, Z. P.; Yin, R. X.; Nie, J. Macromolecules 2009, 42, (14), 5278-5284.
50. Matienzo, L. J.; Winnacker, S. K. Macromolecular Materials and Engineering 2002, 287, (12), 871-880.

CHAPITRE 7

GENERAL DISCUSSION

In spite of different studies that reported the fabrication of chitosan nanofibers with varying degrees of success, there are many aspects to be improved and clarified, especially for the production of electrospun chitosan-based nanofibers from harmless aqueous solutions that are significantly more suitable for biomedical applications. Several methods have been used to prepare porous structures of chitosan previously. Among them, the electrospining technique has gained a lot of attention lately since it can produce microporous non-woven three dimensional structures of sub-micrometer fibers that are more advantageous for applications such as wound healing dressings, anti-bacterial packaging films, drug delivery systems, scaffolds for tissue engineering and membrane filters for air and water purification.

The first part of this work is aimed at understanding the miscibility and phase behaviour of chitosan/PEO solutions. Since electrospinning is carried out through a polymer solution, precursor and PEO is added to chitosan to improve its processability. A rheological approach was introduced as a sensitive method to evaluate the liquid-liquid phase separation of polymer solutions. In this method, the phase separation behavior of polymer solutions was investigated using small amplitude oscillatory shear measurements. Binodal decomposition temperatures were determined from the sudden changes in the slope of the storage modulus or loss tangent versus dynamic temperature sweep plots. The spinodal decomposition temperatures were also evaluated by using a mean field theoretical approach. This technique was first applied on a well-known PEO/water solution and then it was used to study the solutions of our interest, aqueous acetic acid solutions of PEO, chitosan and their blends. Comparing the obtained critical points with those reported from other experimental techniques, revealed that rheological measurements can detect the early stages of phase separation.

Subsequently the method was applied to 50 wt% aqueous acetic acid solutions of PEO, chitosan and their blends at different ratios which previously showed incoherent results in the elecctrospinning process at elevated temperatures. These solutions showed a lower critical solution temperature (LCST) phase diagram that was attributed to the existence of hydrogen bonds between ether groups on PEO and hydroxyl, acetylamine and amino groups on chitosan

molecules and the solvent. Critical decomposition temperatures for binodal and spinodal points were estimated from isochronal temperature sweep experiments. It was conceded that chitosan and PEO solutions are miscible and stable up at moderate temperatures of 25-65 °C. Therefore, blending chitosan with PEO at this range of temperature lead to a one phase stable solution that can be used in the electrospinning process.

Afterwards, a systematic quantitative analysis was conducted to investigate the solution properties that resulted in successful electrospinning. Various characteristics such as surface tension, conductivity, shear viscosity and acid concentration were considered to shed light on the electrospinnability of chitosan. The effect of PEO on the improvement of the electrospinnability of chitosan solutions was examined. The different behaviour of these two solutions in the electrospinning process indicated that the polyelectrolyte nature of chitosan and its chain stiffness in solution, which leads to lower chain entanglements, limits its electrospinnability as compared to PEO. However, elongational viscosity is another characteristic feature of solutions that can play role in electrospinnability of chitosan and PEO solutions, especially because it was shown that PEO chains have more entanglements in solution that could lead to more elasticity and higher elongational viscosity.

A transmission FTIR study performed on chitosan/PEO spun nanofibers from solution blends confirmed the presence of hydrogen bonding between chitosan and PEO at room tempearture. These strong polar bonds form between the ether groups of PEO and hydroxyl and amino groups of chitosan. Hence, the success of chitosan PEO-assisted electrospinning was ascribed to the consequence of these bonds. It is speculated that PEO may act as a carrier of chitosan in the electrospinning process via these physical hydrogen bonds. In a successful effort, a new designed set up was utilized to electrospin at moderate temperatures. Defect free nanofibers with diameters of 60-120 nm and high chitosan content as high as 90 wt% were prepared by using this set up. The success of this technique was related to lowering the surface tension and shear viscosity of the solutions in the electrospinning process. However, further increase in temperature (more than 70-80 °C) resulted in unstable jet in the electrospinning process and beaded fibers morphology was obtained. This observation was attributed to the phase separation of the polymer solutions in the vicinity of this range of temperature. Since the rheological measurements evaluated the same range of temperature for phase separation of these precursor electrospinning solutions.

It was also found that higher chitosan content in the precursor blend solution led to a significant reduction in nanofibers diameters. After finding the optimized conditions for electrospinning of chitosan/PEO solutions, continuous electrospinning was performed and nanofibrous mats were collected on a drum with both rotational and translational movements. Fabrication of these defect free nanofibrous membranes with high chitosan content from aqueous acetic acid solutions via a completely stable electrospinning process is very promising for further applications.

In the last part of this work, novel core-shell structured PEO/chitosan nanofibers were prepared through a coaxial electrospinning set up. Due to a shell layer entirely made of chitosan, this approach had several advantages over the conventional approach of blending chitosan with a readily electrospinnable polymeric phase. In addition to the simplicity of a one-step production without blending and any post treatment, the amount of required chitosan to prepare the nanofibers of the same size will be reduced as well.

To fabricate those nanofibers, a co-axial electrospinning technique was employed and for the first time a core-shell structured PEO-chitosan nanofibers from aqueous solutions were produced, in which chitosan is located at the shell (outer layer) and PEO at the core (inner layer). Uniform sized defect-free nanofibers of 100-190 nm diameter were produced. The core-shell nanostructure and presence of chitosan on the shell layer were suggested by TEM images obtained before and after extracting the PEO content by water. The obtained electrospun mats after the PEO washing step were nearly 100% chitosan in the form of hollow nanofibers. The presence of chitosan on the surface of the composite nanofibers was supported by XPS studies. Bulk PEO and chitosan compositions in the electrospun mats were determined by TGA analysis, which were similar to their ratio in the feed solution, indicating homogeneity and uniformity of the prepared nanofibers. In addition, the local compositional homogeneity of the prepared membranes and the efficiency of washing step to remove PEO were verified by transmission FTIR analysis. It was shown that the crystalline microstructure of chitosan as well as PEO cannot build up in the electrospinning process, most likely due to the fast evaporation of the solvent in this process. The prepared coaxial nanofibers (hollow and solid) prepared by this technique have several potential applications due to the presence of chitosan on their outer surfaces.

CHAPITRE 8

CONCLUSIONS AND RECOMMENDATIONS

8.1 Conclusions

In this dissertation, chitosan-based nanofibrous mats were successfully fabricated from aqueous solutions using two approaches: blending and co-axial electrospinning of chitosan solution with a readily electrospinnable polymeric solution, i.e. an aqueous acetic acid solution of polyethylene oxide (PEO). A fundamental study was performed to shed light on the electrospinning of chitosan/PEO solutions and the phase behaviour of these solutions was investigated using isochronal dynamic temperature sweep experiments. The following conclusions are drawn from this work:

1- Defect free beadless nanofibers of 60-120 nm can be obtained from an aqueous acetic solution of chitosan in the presence of a small amount of PEO (10 wt%).

2- Positive charges on the chitosan molecules and its chain stiffness are considered as the main limiting factors for the electrospinnability of chitosan solutions.

3- Electrospinning at moderate temperatures (40-70 °C) helps to obtain beadless nanofibers with higher chitosan content of 90 wt%.

4- Higher chitosan content in the precursor solutions of its blend with PEO reduces significantly the diameter of resulting electrospun nanofibers (from 123 to 63 nm for 50/50blend and 90/10 chitosan/PEO blends, respectively).

5- Rheological measurements provide a sensitive tool to determine the phase behaviour of polymer solutions.

6- Binodal decomposition points of polymer solutions are estimated from dynamic temperature sweep experiments and spinodal points are quantitatively calculated on the basis of a mean field theory.

7- Core-shell structured PEO/chitosan nanofibers are prepared by a one-step coaxial electrospinning process, with chitosan as the shell component (outer layer) and PEO as the core material (inner layer) from aqueous solutions.

8- Hollow chitosan nanofibers can be obtained from core-shell structured chitosan/PEO nanofibers after washing the PEO content with water.

8.2 Recommandations

The following aspects are recommended for more exploration in future work:

1- To investigate the effect of molecular weight and concentration of the PEO component on the electrospinnability of chitosan/PEO blend solutions to find out the minimum PEO molecular weight and concentration that leads to a stable electrospinning conditions.

2- To explore the efficiency of chitosan-based microporous mats in applications for heavy metal ions removal from drinking water, stability of the membranes in contact with water, clean water permeation and fouling behaviour.

3- To investigate the anti-bacterial characteristics of the fabricated membranes for applications in anti-bacterial film packaging and wound healing dressings.

4- To compare the properties of the chitosan membranes prepared by the electrospinning process in this work by other conventional techniques such as thermal induced phase separation (TIPS), cryogenic induced phase separation temperature (CIPS) and selective salt extraction.

5- To investigate the effect of surfactants and salts on the electrospinnability of chitosan/PEO solutions and their final resulting nanofibrous membranes.

6- To study the possibility of fabrication of three-dimensional chitosan-based structures by the electrospinning technique.

7- To conduct a systematic investigation to minimize the thickness of chitosan in the core-shell structured coaxial nanofibers of PEO/chitosan by changing the molecular weight, concentration and flow rate ratio of the two feeding streams.

APPENDICES

Appendix A

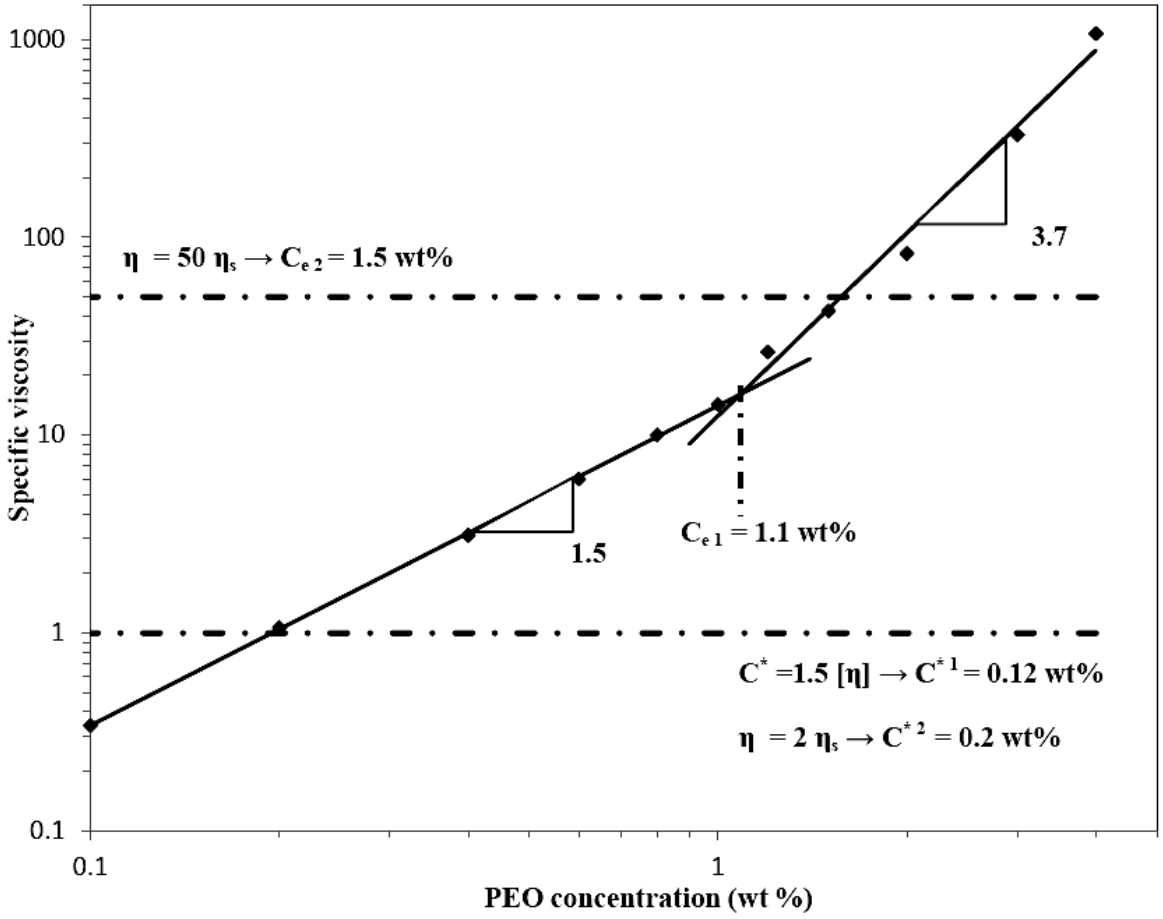

Dependence of specific viscosity on concentration for PEO dissolved in 50% acetic acid

REFERENCES

Ajji, A. and L. Choplin (1991). "Rheology and dynamics near phase-sepatation in a polymer blend: model and scaling analysis." Macromolecules **24**(18): 5221-5223.

Ajji, A., L. Choplin, et al. (1991). "Rheology of polystyrene/poly(vinyl methyl ether) blends near the phase transition." Journal of polymer science: Part B: polymer physics **29**: 1573-1578.

An, J., H. Zhang, et al. (2009). "Preparation and antibacterial activity of electrospun chitosan/poly(ethylene oxide) membranes containing silver nanoparticles." Colloid and Polymer Science **287**(12): 1425-1434.

Bae, Y. C., S. M. Lambert, et al. (1991). "Cloud-point curves of polymer-solutions from thermooptical measurements " Macromolecules **24**(15): 4403-4407.

Baumgarten, P. K. (1971). "Electrostatic spinning of acrylic microfibers." Journal of colloid interface and science **36**: 71-79.

Begin, A. and M. R. Van Calsteren (1999). "Antimicrobial films produced from chitosan." International Journal of Biological Macromolecules **26**(1): 63-67.

Bhattarai, N., D. Edmondson, et al. (2005). "Electrospun chitosan-based nanofibers and their cellular compatibility." Biomaterials **26**(31): 6176-6184.

Bousmina, M., A. Lavoie, et al. (2002). "Phase segregation in SAN/PMMA blends probed by rheology, microscopy, and inverse gas chromatography techniques." Macromolecules **35**(16): 6274-6283.

Brugnerotto, J., J. Desbrieres, et al. (2001). "Overview on structural characterization of chitosan molecules in relation with their behavior in solution." Macromolecular Symposia **168**: 1-20.

Cai, Z. X., X. M. Mo, et al. (2010). "Fabrication of Chitosan/Silk Fibroin Composite Nanofibers for Wound-dressing Applications." International Journal of Molecular Sciences **11**(9): 3529-3539.

Cooley, J.F. (1902). "Apparatus for electrically dispersing fluids." US patent, **692,631**.

Cooley, J.F. (1903). "Electrical method of dispersing fluids." US patent, **745,276**.

Cooper, A., N. Bhattarai, et al. (2011). "Fabrication and cellular compatibility of aligned chitosan-PCL fibers for nerve tissue regeneration." Carbohydrate Polymers **85**(1): 149-156.

Desai, K., K. Kit, et al. (2008). "Morphological and surface properties of electrospun chitosan nanofibers." Biomacromolecules **9**(3): 1000-1006.

Desai, K., K. Kit, et al. (2009). "Nanofibrous chitosan non-wovens for filtration applications." Polymer **50**(15): 3661-3669.

Dormidontova, E. E. (2002). "Role of competitive PEO-water and water-water hydrogen bonding in aqueous solution PEO behavior." Macromolecules **35**(3): 987-1001.

Doshi, J. and D. H. Reneker (1995). "Electrospinning process and applications of electrospun fibers." Journal of Electrostatics **35**(2-3): 151-160.

Duan, B., C. H. Dong, et al. (2004). "Electrospinning of chitosan solutions in acetic acid with poly(ethylene oxide)." Journal of Biomaterials Science-Polymer Edition **15**(6): 797-811.

Dutta, P. K., J. Dutta, et al. (2004). "Chitin and chitosan: Chemistry, properties and applications." Journal of Scientific & Industrial Research **63**(1): 20-31.

Dutta, P. K., S. Tripathi, et al. (2009). "Perspectives for chitosan based antimicrobial films in food applications." Food Chemistry **114**(4): 1173-1182.

Fischer, V. and W. Borchard (2000). "Thermodynamic properties of poly(ethylene glycol)/water systems. 2. Critical point data." Journal of Physical Chemistry B **104**(18): 4463-4470.

Fischer, V., W. Borchard, et al. (1996). "Thermodynamic properties of poly(ethylene glycol) water systems .1. A polymer sample with a narrow molar mass distribution." Journal of Physical Chemistry **100**(39): 15992-15999.

Fong, H., I. Chun, et al. (1999). "Beaded nanofibers formed during electrospinning." Polymer **40**(16): 4585-4592.

Formhals, A. (1934). "Process and apparatus for preparing artificial threads" US patent, **1,975,504**.

Formhals, A. (1943). "Production of artificial fibers from fiber forming liquids" US patent, **2,323,025**.

Fredrickson, G. H. and R. G. Larson (1987). "Viscoelasticity of homogeneous polymer melts near a critical point." Journal of chemical physics **86**(3): 1553-1560.

Geng, X. Y., O. H. Kwon, et al. (2005). "Electrospinning of chitosan dissolved in concentrated acetic acid solution." Biomaterials **26**(27): 5427-5432.

Greiner, A. and J. H. Wendorff (2007). "Electrospinning: A fascinating method for the preparation of ultrathin fibres." Angewandte Chemie-International Edition **46**(30): 5670-5703.

Gu, Z. Y., P. H. Xue, et al. (2001). "Preparation of the porous chitosan membrane by cryogenic induced phase separation." Polymers for Advanced Technologies **12**(11-12): 665-669.

Haider, S. and S. Y. Park (2009). "Preparation of the electrospun chitosan nanofibers and their applications to the adsorption of Cu(II) and Pb(II) ions from an aqueous solution." Journal of Membrane Science **328**(1-2): 90-96.

Hamdine, M., Heuzey, M.C., Begin, A. (2005). "Effect of Organic and Inorganic Acids on Concentrated Chitosan Solutions and Gels." International Journal of Biological Macromolecules, **37**(3):134-142.

Hamdine, M., Heuzey, M.C., Bégin, A. (2006). "Viscoelastic Properties of Phosphoric and Oxalic Acid-Based Chitosan Hydrogels." Rheologica Acta, **45**(5): 659-675.

Hammouda, B., D. Ho, et al. (2002). "SANS from poly(ethylene oxide)/water systems." Macromolecules **35**(22): 8578-8585.

Hammouda, B., D. L. Ho, et al. (2004). "Insight into clustering in poly(ethylene oxide) solutions." Macromolecules **37**(18): 6932-6937.

He, M. J., Y. M. Liu, et al. (1991). "Spinodal decomposition in a hydrogen-bonded polymer blend." Macromolecules **24**(2): 464-473.

Han, T., A. L. Yarin, et al. (2008). "Viscoelastic electrospun jets: Initial stresses and elongational rheometry." Polymer **49**(6): 1651-1658.

Homayoni, H., S. A. H. Ravandi, et al. (2009). "Electrospinning of chitosan nanofibers: Processing optimization." Carbohydrate Polymers **77**(3): 656-661.

Horzum, N., E. Boyaci, et al. (2010). "Sorption Efficiency of Chitosan Nanofibers toward Metal Ions at Low Concentrations." Biomacromolecules **11**(12): 3301-3308.

Huang, Z. M., Y. Z. Zhang, et al. (2003). "A review on polymer nanofibers by electrospinning and their applications in nanocomposites." Composites Science and Technology **63**(15): 2223-2253.

Hudson, S. and D. W. Jenkins (2001). Chitin and chitosan. Encyclopedia of polymer science and technology H. F. Mark and N. J. Hoboken. New York, Wiley Interscience**:** 569-580.

Ignatova, M., N. Manolova, et al. (2009). "Electrospun Non-Woven Nanofibrous Hybrid Mats Based on Chitosan and PLA for Wound-Dressing Applications." Macromolecular Bioscience **9**(1): 102-111.

Ignatova, M., K. Starbova, et al. (2006). "Electrospun nano-fibre mats with antibacterial properties from quaternised chitosan and poly(vinyl alcohol)." Carbohydrate Research **341**(12): 2098-2107.

Ignatova, M. G., N. E. Manolova, et al. (2010). "Electrospun Nanofibrous Mats Containing Quaternized Chitosan and Polylactide with In Vitro Antitumor Activity against HeLa Cells." Biomacromolecules **11**(6): 1633-1645.

Jayakumar, R., D. Menon, et al. (2010). "Biomedical applications of chitin and chitosan based nanomaterials-A short review." Carbohydrate Polymers **82**(2): 227-232.

Jayakumar, R., M. Prabaharan, et al. (2010). "Novel chitin and chitosan nanofibers in biomedical applications." Biotechnology Advances **28**(1): 142-150.

Jia, Y. T., J. Gong, et al. (2007). "Fabrication and characterization of poly (vinyl alcohol)/chitosan blend nanofibers produced by electrospinning method." Carbohydrate Polymers **67**(3): 403-409.

Kang, Y. O., I. S. Yoon, et al. (2010). "Chitosan-Coated Poly(vinyl alcohol) Nanofibers For Wound Dressings." Journal of Biomedical Materials Research Part B-Applied Biomaterials **92B**(2): 568-576.

Kapnistos, M., A. Hinrichs, et al. (1996). "Rheology of a lower critical solution temperature binary polymer blend in the homogeneous, phase-separated, and transitional regimes." Macromolecules **29**(22): 7155-7163.

Klossner, R. R., H. A. Queen, et al. (2008). "Correlation of Chitosan's Rheological Properties and Its Ability to Electrospin." Biomacromolecules **9**(10): 2947-2953.

Knaul, J. Z., S. M. Hudson, et al. (1999). "Crosslinking of chitosan fibers with dialdehydes: Proposal of a new reaction mechanism." Journal of Polymer Science Part B-Polymer Physics **37**(11): 1079-1094.

Koombhongse, S., W. X. Liu, et al. (2001). "Flat polymer ribbons and other shapes by electrospinning." Journal of Polymer Science Part B-Polymer Physics **39**(21): 2598-2606.

Kumar, M. (2000). "A review of chitin and chitosan applications." Reactive & Functional Polymers **46**(1): 1-27.

Kumar, M., R. A. A. Muzzarelli, et al. (2004). "Chitosan chemistry and pharmaceutical perspectives." Chemical Reviews **104**(12): 6017-6084.

Larrondo L. and R. S. J. Manley (1981). "Electrostatic fiber spinning from polymer melts. I. Experimental observations on fiber formation and properties." Journal of Polymer Science: Polymer Physics Edition **19**: 909-920.

Li, D. and Y. N. Xia (2004). "Electrospinning of nanofibers: Reinventing the wheel?" Advanced Materials **16**(14): 1151-1170.

Li, L. and Y. L. Hsieh (2006). "Chitosan bicomponent nanofibers and nanoporous fibers." Carbohydrate Research **341**(3): 374-381.

Li, W. J., Z. Y. Gu, et al. (1999). "Cryogenic induced phase separation of chitosan solution - A novel method for preparation of membrane with high porosity." Chinese Science Bulletin **44**(20): 1887-1891.

McKee, M. G., T. Park, et al. (2005). "Electrospinning of linear and highly branched segmented poly(urethane urea)s." Polymer **46**(7): 2011-2015.

McKee, M. G., G. L. Wilkes, et al. (2004). "Correlations of solution rheology with electrospun fiber formation of linear and branched polyesters." Macromolecules **37**(5): 1760-1767.

Mi, F. L., S. S. Shyu, et al. (2001). "Fabrication and characterization of a sponge-like asymmetric chitosan membrane as a wound dressing." Biomaterials **22**(2): 165-173.

Mi, F. L., Y. B. Wu, et al. (2003). "Asymmetric chitosan membranes prepared by dry/wet phase separation: a new type of wound dressing for controlled antibacterial release." Journal of Membrane Science **212**(1-2): 237-254.

Min, B. M., S. W. Lee, et al. (2004). "Chitin and chitosan nanofibers: electrospinning of chitin and deacetylation of chitin nanofibers." Polymer **45**(21): 7137-7142.

Morton, W.J., (1903). US, **705,691**.

Niu, Y. H. and Z. G. Wang (2006). "Rheologically determined phase diagram and dynamically investigated phase separation kinetics of polyolefin blends." Macromolecules **39**(12): 4175-4183.

No, H. K., S. P. Meyers, et al. (2007). "Applications of chitosan for improvement of quality and shelf life of foods: A review." Journal of Food Science **72**(5): R87-R100.

Ohkawa, K., D. I. Cha, et al. (2004). "Electrospinning of chitosan." Macromolecular Rapid Communications **25**(18): 1600-1605.

Ohkawa, K., K. I. Minato, et al. (2006). "Chitosan nanofiber." Biomacromolecules **7**(11): 3291-3294.

Ojha, S. S., D. R. Stevens, et al. (2008). "Fabrication and characterization of electrospun chitosan nanofibers formed via templating with polyethylene oxide." Biomacromolecules **9**(9): 2523-2529.

Pillai, C. K. S., W. Paul, et al. (2009). "Chitin and chitosan polymers: Chemistry, solubility and fiber formation." Progress in Polymer Science **34**(7): 641-678.

Polic, W. F. and W. Burchard (1983). "Static light scattering from aqueous solutions poly (ethylene oxide) solutions in the temperature range 20-90 C." Macromolecules **16**: 978-982.

Prabhakaran, M. P., L. Ghasemi-Mobarakeh, et al. (2011). "Electrospun Composite Nanofibers for Tissue Regeneration." Journal of Nanoscience and Nanotechnology **11**(4): 3039-3057.

Ramakrishna, S., K. Fujihara, et al. (2005). An introduction to electrospinning and nanofibers. Singapore, World scientific.

Reneker, D. H. and I. Chun (1996). "Nanometre diameter fibres of polymer, produced by electrospinning." Nanotechnology **7**(3): 216-223.

Reneker, D. H. and A. L. Yarin (2008). "Electrospinning jets and polymer nanofibers." Polymer **49**(10): 2387-2425.

Reneker, D. H., A. L. Yarin, et al. (2000). "Bending instability of electrically charged liquid jets of polymer solutions in electrospinning." Journal of Applied Physics **87**(9): 4531-4547.

Rinaudo, M. (2006). "Chitin and chitosan: Properties and applications." Progress in Polymer Science **31**(7): 603-632.

Rinaudo, M., G. Pavlov, et al. (1999). "Influence of acetic acid concentration on the solubilization of chitosan." Polymer **40**(25): 7029-7032.

Sangsanoh, P. and P. Supaphol (2006). "Stability improvement of electrospun chitosan nanofibrous membranes in neutral or weak basic aqueous solutions." Biomacromolecules **7**(10): 2710-2714.

Schiffman, J. D. and C. L. Schauer (2007). "Cross-linking chitosan nanofibers." Biomacromolecules **8**(2): 594-601.

Shalumon, K. T., K. H. Anulekha, et al. (2010). "Single step electrospinning of chitosan/poly(caprolactone) nanofibers using formic acid/acetone solvent mixture." Carbohydrate Polymers **80**(2): 413-419.

Sharma, J. and N. Clarke (2004). "Miscibility determination of a lower critical solution temperature polymer blend by rheology." Journal of Physical Chemistry B **108**(35): 13220-13230.

Shenoy, S. L., W. D. Bates, et al. (2005). "Role of chain entanglements on fiber formation during electrospinning of polymer solutions: good solvent, non-specific polymer-polymer interaction limit." Polymer **46**(10): 3372-3384.

Shetty, A. M. and M. J. Solomon (2009). "Aggregation in dilute solutions of high molar mass poly(ethylene) oxide and its effect on polymer turbulent drag reduction." Polymer **50**(1): 261-270.

Shin, Y. M., M. M. Hohman, et al. (2001). "Experimental characterization of electrospinning: the electrically forced jet and instabilities." Polymer **42**(25): 9955-9967.

Sionkowska, A. (2011). "Current research on the blends of natural and synthetic polymers as new biomaterials: Review." Progress in Polymer Science **36**(9): 1254-1276.

Son, B., B. Y. Yeom, et al. (2009). "Antibacterial Electrospun Chitosan/Poly(vinyl alcohol) Nanofibers Containing Silver Nitrate and Titanium Dioxide." Journal of Applied Polymer Science **111**(6): 2892-2899.

Sun, Z. C., E. Zussman, et al. (2003). "Compound core-shell polymer nanofibers by co-electrospinning." Advanced Materials **15**(22): 1929-1932.

Taylor, G.I. (1964). "Disintegration of water drops in an electric field." Proceedings of the Royal Society of London Series A, **280:** 383-397.

Theron, S. A., E. Zussman, et al. (2004). "Experimental investigation of the governing parameters in the electrospinning of polymer solutions." Polymer **45**(6): 2017-2030.

Thompson, C. J., G. G. Chase, et al. (2007). "Effects of parameters on nanofiber diameter determined from electrospinning model." Polymer **48**(23): 6913-6922.

Torres-Giner, S., M. J. Ocio, et al. (2008). "Development of active antimicrobial fiber based chitosan polysaccharide nanostructures using electrospinning." Engineering in Life Sciences **8**(3): 303-314.

Torres-Giner, S., M. J. Ocio, et al. (2009). "Novel antimicrobial ultrathin structures of zein/chitosan blends obtained by electrospinning." Carbohydrate Polymers **77**(2): 261-266.

Vlassopoulos, D., A. Koumoutsakos, et al. (1997). "Rheology and phase separation in a model upper critical solution temperature polymer blend." Journal of Rheology **41**(3): 739-755.

Wang, W., S. Itoh, et al. (2009). "Effects of Schwann cell alignment along the oriented electrospun chitosan nanofibers on nerve regeneration." Journal of Biomedical Materials Research Part A **91A**(4): 994-1005.

Wang, Z. G., L. S. Wan, et al. (2009). "Enzyme immobilization on electrospun polymer nanofibers: An overview." Journal of Molecular Catalysis B-Enzymatic **56**(4): 189-195.

Woerdeman, D. L., S. Shenoy, et al. (2007). "Role of chain entanglements in the electrospinning of wheat protein-poly(vinyl alcohol) blends." Journal of Adhesion **83**(8): 785-798.

Yang, D. Z., Y. Jin, et al. (2008). "Fabrication and Characterization of Chitosan/PVA with Hydroxyapatite Biocomposite Nanoscaffolds." Journal of Applied Polymer Science **110**(6): 3328-3335.

Yarin, A. L., S. Koombhongse, et al. (2001). "Bending instability in electrospinning of nanofibers." Journal of Applied Physics **89**(5): 3018-3026.

Yarin, A. L., S. Koombhongse, et al. (2001). "Taylor cone and jetting from liquid droplets in electrospinning of nanofibers." Journal of Applied Physics **90**(9): 4836-4846.

Ye, P., Z. K. Xu, et al. (2006). "Nanofibrous poly(acrylonitrile-co-maleic acid) membranes functionalized with gelatin and chitosan for lipase immobilization." Biomaterials **27**(22): 4169-4176.

Yeganeh, J. K., F. Goharpey, et al. (2010). "Rheology and Morphology of Dynamically Asymmetric LCST Blends: Polystyrene/Poly(vinyl methyl ether)." Macromolecules **43**(20): 8670-8685.

Yu, J. H., S. V. Fridrikh, et al. (2004). "Production of submicrometer diameter fibers by two-fluid electrospinning." Advanced Materials **16**(17): 1562-1566.

Zeng, M. F., Z. P. Fang, et al. (2004). "Novel method of preparing microporous membrane by selective dissolution of chitosan/polyethylene glycol blend membrane." Journal of Applied Polymer Science **91**(5): 2840-2847.

Zhang, H. T., C. Y. Wu, et al. (2010). "Elaboration, characterization and study of a novel affinity membrane made from electrospun hybrid chitosan/nylon-6 nanofibers for papain purification." Journal of Materials Science **45**(9): 2296-2304.

Zhang, Y., J. R. Venugopal, et al. (2008). "Electrospun biomimetic nanocomposite nanofibers of hydroxyapatite/chitosan for bone tissue engineering." Biomaterials **29**(32): 4314-4322.

Zhang, Y. Z., J. Venugopal, et al. (2005). "Characterization of the surface biocompatibility of the electrospun PCL-collagen nanofibers using fibroblasts." Biomacromolecules **6**(5): 2583-2589.

Zhou, Y. S., D. Z. Yang, et al. (2008). "Electrospun water-soluble carboxyethyl chitosan/poly(vinyl alcohol) nanofibrous membrane as potential wound dressing for skin regeneration." Biomacromolecules **9**(1): 349-354.

Zivanovic, S., J. J. Li, et al. (2007). "Physical, mechanical, and antibacterial properties of chitosan/PEO blend films." Biomacromolecules **8**(5): 1505-1510.